Spring 2012

Comparison and evaluation of global publicly available bathymetry grids in the Arctic

Anastasia S. Abramova
University of New Hampshire, Durham

Follow this and additional works at: https://scholars.unh.edu/thesis

COMPARISON AND EVALUATION
OF GLOBAL PUBLICLY AVAILABLE
BATHYMETRY GRIDS IN THE ARCTIC

BY

ANASTASIA S. ABRAMOVA

Master's Degree in Geography: Geomorphology and Paleogeography,

Lomonosov Moscow State University, 2008

THESIS

Submitted to the University of New Hampshire

in Partial Fulfillment of

the Requirements for the Degree of

Master of Science

in

Earth Sciences

May, 2012

UMI Number: 1518001

UMI

Dissertation Publishing

UMI 1518001

ProQuest®

This thesis has been examined and approved.

Thesis Director, Dr. David Monahan,
Adjunct Professor of Geography and Geodesy and Geomatics
Engineering

Dr. Larry Mayer,
Professor of Ocean Engineering and Marine Sciences and Earth
Sciences

Dr. Thomas Lippmann,
Research Associate Professor of Earth Sciences and Ocean
Engineering

Dr. Brian Calder,
Research Associate Professor

05/04/12
Date

DEDICATION

I dedicate the body of this work to my mother, sister and brother, and to all those who set my life path to science.

ACKNOWLEDGMENTS

TABLE OF CONTENTS

LIST OF TABLES

LIST OF FIGURES

FIGURES IN APPENDICES

ACRONYMS

BODC --- British Oceanographic Data Centre

BSH --- The German Hydrographic Office

CCOM --------------------- Center For Coastal and Ocean Mapping, University of New Hampshire

CHS -- Canadian Hydrographic Service

DCDB -- IHO Data Centre for Digital Bathymetry

GDA --- GEBCO Digital Atlas [BODC, 2003]

GEBCO --- General Bathymetric Chart of the Oceans

GIN RAS -- Geological Institute Russian Academy of Sciences

GINA--- Geographic Information Network of Alaska

GMRT--- Global Multi-Resolution Topography

GMT----------------------------------Generic Mapping Tools software package [Wessel and Smith, 1998]

HDNO---------- Head Department of Navigation and Oceanography, Russian Ministry of Defense

IBCAO-- International Bathymetric Chart of the Arctic Ocean

IFREMER ------------------------------------- French Research Institute for Exploitation of the Sea

IHB --- International Hydrographic Bureau

INT --- International Nautical Charts

JAMSTEC --------------------------------- Japan Agency for Marine-Earth Science and Technology

KMS --- Danish National Survey and Kadastre

LDEO-------------------------------------- Lamont Doherty Earth Observatory, Columbia University

MGDS --- Marine Geoscience Data System

NAVO --- US Naval Oceanographic Office

NERC -- UK Natural Environment Research Council

NGA --- US National Geospatial-Intelligence Agency

NGDC --- US National Geophysical Data Center

NOAA --- US National Oceanic and Atmospheric Administration

NRL --- US Naval Research Laboratory

NSF ---US National Science Foundation

RDANH ----------------------------- Royal Danish Administration of Navigation and Hydrography

S&S--- Smith and Sandwell bathymetry grid

SCAR -------------- Scientific Committee on Antarctic Research [British Antarctic Survey, 1993]

SCICEX --- SCientific ICe EXercise program

SIO --- Scripps Institution of Oceanography

SOEST -- School of Ocean and Earth Science and Technology

SOHO -- Swedish Hydrographic Office

UKHO --- UK Hydrographic Office

UNH --- University of New Hampshire

WHOI -- Woods Hole Oceanographic Institution

ABSTRACT

COMPARISON AND EVALUATION OF GLOBAL PUBLICLY AVAILABLE BATHYMETRY GRIDS IN THE ARCTIC

By

Anastasia S. Abramova
University of New Hampshire, May, 2012

In this study we evaluate the differences between six publicly available bathymetry grids in different regions of the Arctic. The independent, high-resolution and accuracy multibeam sonar derived grids are used as a ground truth against which the analyzed grids are compared. The specific bathymetry grids assessed, IBCAO, GEBCO 1 minute, GEBCO_08, ETOPO1, SRTM30_Plus, and Smith and Sandwell, are separated into two major Types: Type A, grids based solely on sounding data sources, and Type B, grids based on sounding data combined with gravity data. The differences were evaluated in terms of source data accuracy, depth accuracy, internal consistency, presence of artifacts, interpolation accuracy, registration issues and resolution of the coastline. These parameters were chosen as quality metrics important for the choice of the grid for any given purpose. We find that Type A bathymetry grids (in particular GEBCO_08) perform better than Type B grids in terms of internal consistency, and have higher accuracy in the different morphological provinces, especially the continental shelf, mainly due to the better source data coverage. Type B grids, on the other hand, have pronounced artifacts and have low accuracy on the shelf due to the scarcity of source data in the region and, in general, the poor performance of gravity prediction in shallow areas and high latitudes. Finally, we propose qualitative metrics that are important when choosing a bathymetry grid and support these metrics with a quality model to guide the choice of the most appropriate grid.

CHAPTER I

INTRODUCTION

1.1 State of the art of ocean mapping problem

Knowledge of sea floor topography is essential to understanding most earth processes ranging from global to small scales. The bathymetry map serves as the base map for any geological, geophysical, environmental or oceanographic investigation as the shape of the seafloor is a key to understanding processes and dynamics [Laughton, 2001]. Beyond fundamental research, applications for mapping in shallow waters vary from mapping for navigation purposes to studies of coastal erosion and environmental issues. Mapping in the off-shore continental shelf zones are of particular interest to coastal states' resource sovereignty, exploration for natural resources, providing data for fisheries management, predicting landslides and modeling tsunami impact.

Most maps of the oceans appear to be finished creations. Global scale maps particularly show the roughness of the seafloor with its ridges, planes and trenches, spanning from shallows to deeps and then back to shallows. It is painful to open the secrets, but the truth should be known – our deep ocean is mapped less than many planets of our solar system. Our knowledge of sea floor topography comes from sparse and irregularly located acoustic data about ocean depths acquired from ship-board measurements. According to the optimistic estimates of Becker et al. [2009], only about 10 percent of the ocean depths are those actually measured at 1 minute resolution, and most of the measurements are of questionable accuracies, randomly distributed all over the globe. In the deep ocean, and especially in hard to reach regions like the Arctic and Southern Seas, the density of ship tracks leaves areas as large as 10,000 km^2 unsurveyed [Marks and Smith, 2006] (Figure 1-1). Information about the remaining 90 percent of the ocean floor is obtained

from indirect measurement methods like satellite altimetry, as well as from geological interpretations and assumptions.

There have been attempts to organize a systematic program to acoustically survey the deep ocean such as the Global Ocean Mapping Project (GOMaP) [Vogt et al., 2001]. According to the estimates of Becker et al. [2009], it will take at least 120 ship-years to complete mapping of the ocean deeper than 500 m (at a spatial resolution of 100 m). The estimated cost of the project (16 billion US dollars) is an order of magnitude less than money spent on space exploration [Vogt et al., 2001]. Although the project is not impossible to realize if international organizations and institutions were coordinated and the exploration of shallow regions was left to the coastal countries, progress has not been apparent. We are still at the beginning of a very long way to the day when the ocean is totally mapped, seamlessly, to fine resolution.

The history of ocean mapping dates back at least 4000 years. However, not until the beginning of the 20th century did we start to get a better feeling of the shape of the ocean floor. The development of ocean mapping over the years has been tightly related to the development of technology. Until the 20th century the most commonly used instruments to measure depths were lead and a rope; this method was extremely slow, with sparse measurements of limited positioning accuracy. The first bathymetric contour charts were based on sparse spot depths, and the shape of the sea floor features were mostly guessed by cartographers (Figure 1-2a).

Echo sounding methods were developed in the 20th century and provided the ability to obtain more accurate depth measurements in a profile form. Maps created using single beam echosounder data depicted a more accurate shape of the ocean floor, although most of the features depicted on maps were the result of geological interpretation (Figure 1-2b). The multibeam echosounder was introduced in the late 1970s. It provided full coverage and allowed the production of high resolution, accurate images of the ocean floor. The development of the multibeam echosounder was a real revolution that brought us closer to the reality of seamlessly mapping the ocean floor. At the same time multibeam sonar techniques introduced the problem of
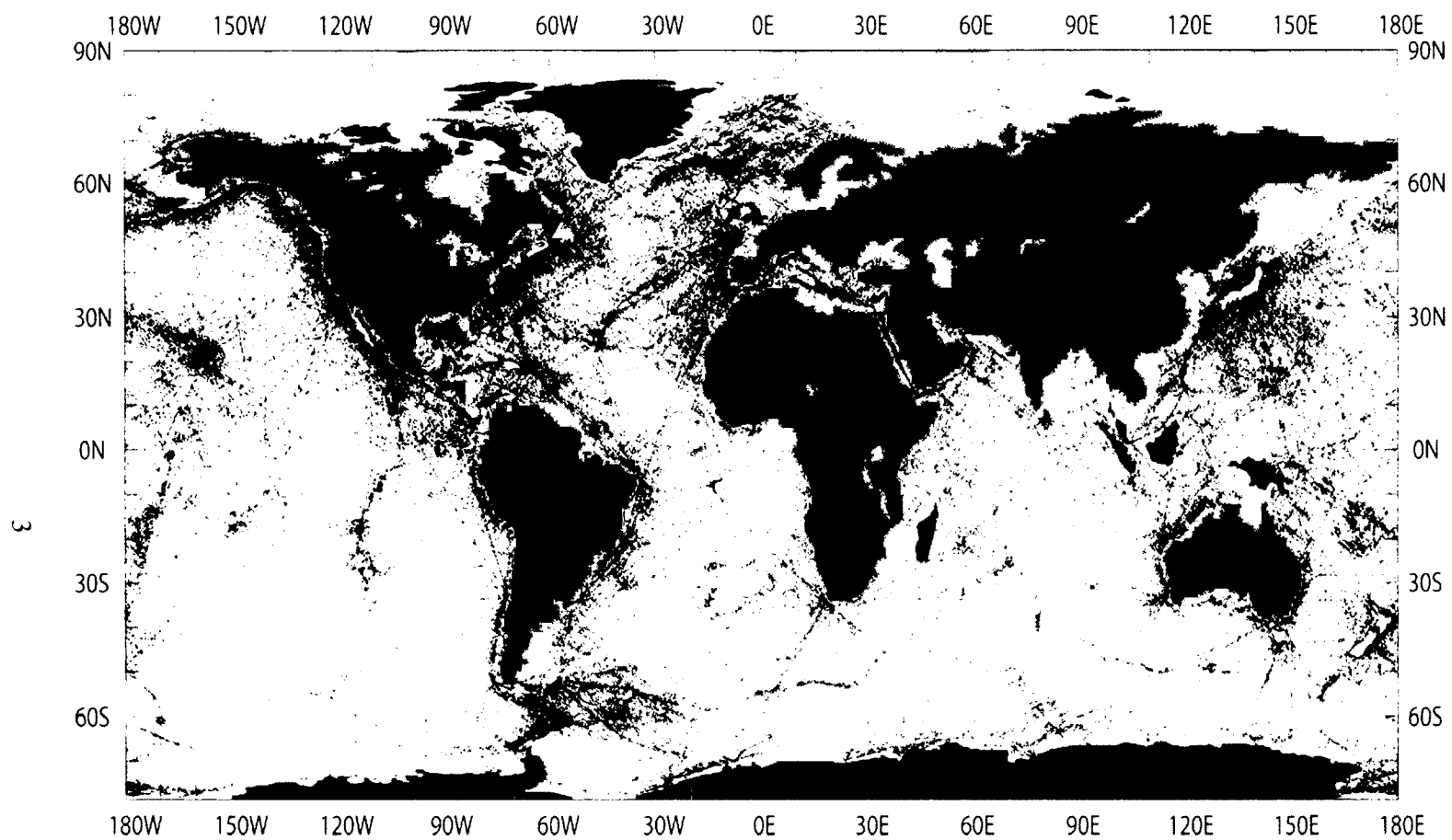
Figure 1-1: Total trackline coverage including bathymetry, gravity and magnetics data as of 2009 available from GEODAS, Ver. 5.0.13 [NGDC, 2009].

Figure 1-2: Comparison of three maps depicting three eras in ocean mapping: (a) fragment of Sir John Murray's map of the world ocean for the Indian Ocean published in 1912 [NOAA Photo Library]: the features seen on this map are far from 'truth'; (b) fragment of the physiographic diagram of the world's ocean by Heezen B. and Tharp M. (1977) [LDEO]: although the position of major features is almost correct, the portrayal of morphology of mid-oceanic ridges is based on the author's imagination and is misleading; (c) fragment of Smith and Sandwell ver. 12.1 satellite-derived predicted bathymetry combined with depth soundings [Smith and Sandwell, 1997]: on this map we can delineate the orientation of previously undetected tectonic features as well as see middle scale ocean morphology.

data processing that requires substantial time, labor and storage capacity.

In the 1990s satellite altimetry was introduced as an alternative way of estimating the ocean depths from sea surface height anomalies [Smith and Sandwell, 1994]. Although altimetry-predicted bathymetry provides resolution not comparable with that acquired from acoustic measurements, it provides global coverage with redundant measurements. Satellite altimetry allowed previously unknown features to be mapped (Figure 1-2c).

1.2 History of bathymetry: from contour maps to digital elevation models

Traditionally bathymetry was depicted on paper charts with contours drawn by hand. The contours were drawn by cartographers and geologists based on sounding information available from paper sounding sheets. The first series of global bathymetry charts started with the initiation of the GEBCO organization in 1903. 'La Carte generale bathymetrique des oceans'- the General Bathymetric Chart of the Oceans - depicted ocean morphology on maps at 1:10 million scale with hand-drawn contours at intervals of 500 m [Carpine-Lancre et al., 2003]. GEBCO series of charts went through five editions. The incredible increase in the amount of data acquired in the curiosity-driven expeditions of the 1970's, together with development of computer technology, created a need to develop high-capacity digital means of storing and representing bathymetry.

The Digital Bathymetric Data Base 5 (DBDB-5) [NGDC, 1988], released by the U.S. Naval Oceanographic Office in the early 1980's, was the first digital elevation model of global bathymetry with 5 arc minute resolution (~10 km). It evolved later into the ETOPO-5 digital data base of land and seafloor elevations [NGDC, 1988]. This digital dataset was based on bathymetric data from numerous sources compiled into digitized contours and interpolated onto a 5 minute grid. The large node spacing, minimum curvature spline gridding method [Briggs, 1974] and interpolation from contour maps rather than original data resulted in large artifacts and statistical bias in the depth distribution. For those reasons DBDB-5 was assessed as of a limited use for scientific purposes [Smith, 1993].

By the 1990's, several digital bathymetry databases were released due to the

5

improvement in computer technology, increase in bathymetry data acquired with multibeam sonars and declassification of altimeter mission data. In 1993 the IHO Data Centre for Digital Bathymetry (DCDB), operated by US NGDC, released the two-volume CD-ROM of the GEODAS database, containing a worldwide collection of acoustic and geophysics data [NGDC, 2002]. By 1994 GEBCO released the GEBCO Digital Atlas (GDA) containing all source data such as soundings, coastlines and contours in digital form [Jones, 1994].

In 1996 Smith and Sandwell released a global bathymetry model predicted from satellite-derived gravity (Geosat and ERS-1 and Topex/Poseidon altimetry missions) and calibrated with available acoustic soundings [Smith and Sandwell, 1997]. The Smith and Sandwell bathymetry model revealed previously unmapped features and large scale morphology for the whole world ocean, except at high latitudes. The gravity–derived bathymetry was at that time an entirely new and untested product awaiting acceptance from the scientific community [Goodwillie, 2003].

Despite the various limitations of, and assumptions taken in production of bathymetry from satellite-derived altimetry [Smith and Sandwell, 1994, 1997, 2001], it has became increasingly apparent that satellite altimetry is the future of large scale bathymetry and possibly the only method to portray the seafloor morphology other than to measure depths acoustically. Today most global bathymetric products incorporate the Smith and Sandwell model, including GEBCO_08 30 arc seconds grid [BODC, 2008], GMRT multi-resolution synthesis [Ryan et al., 2009], SRTM30_Plus [Becker et al., 2009], GINA [Lindquist, 2004], ETOPO1 [Amante and Eakins, 2009] and Google Ocean [Google, 2009]. All of the above-listed products are publicly available through the internet.

1.3 Objectives

The large number of available global bathymetry datasets and countless number of applications in which bathymetry information is used presents a choice for a scientist: which bathymetry grid to use. In addition, most of the datasets are being updated regularly and require reevaluation from time to time. This study follows Marks and Smith's [2006] evaluation of

6

publicly available bathymetry datasets and is directed towards the assessment of differences between publicly available bathymetry datasets with particular focus in the Arctic, where limited evaluation has been done. The IBCAO grid [Jakobsson et al., 2000, 2008] is considered to be the most authoritative representation of the Arctic bathymetry even though in some areas it is based on digitized contours from published maps. Besides IBCAO, the following global bathymetry grids that provide Arctic coverage are evaluated: GEBCO 1 min, ver. 2.00 [BODC, 2003], GEBCO_08 30 arc seconds [BODC, 2008], SRTM30_Plus ver. 6.0 [Becker et al., 2009], Smith and Sandwell ver. 13.1 [Smith and Sandwell, 1997], and ETOPO1 [Amante and Eakins, 2009] and the regional grid IBCAO [Jakobsson et al., 2000, 2008].

The choice of a bathymetry grid for a given purpose is complicated by the fact that there is not enough comprehensive supplementary information on their quality. Quality is an imprecise term, since there is no single measure of quality. In addition, the quality of any bathymetry model varies in space, since the factors affecting it are space dependent [Veregin, 1999; Bernhardsen, 2002]. The following factors affect quality of the final gridded model [modified after Li, 1990]:

- main attributes of source data: accuracy, density, distribution and resolution
- complexity of the modeled surface
- interpolation method used for model construction
- resolution of derived surface

Some of the analyzed datasets even lack source data coverage information used for construction of the grids in a usable form. For example, IBCAO [Jakobsson et al., 2008] publicly provides source data coverage only as an image file. Some of the datasets do not even provide sufficient documentation to understand the compilation procedures undertaken. For example, Smith and Sandwell have released a number of undocumented updated versions of their bathymetry grid since the initial published papers [Smith and Sandwell, 1994, 1997]. Also, differences between the construction of SRTM30_Plus [Becker et al., 2009] and Smith and Sandwell datasets is not well documented.

7

The metadata, as a primary quality information, should be provided with any bathymetry grid, including source data coverage, uncertainty levels associated with varying accuracies of data sources, as well as uncertainties of the final bathymetry grid which account for the uncertainties of the gridding algorithm [Li and Chen, 1999; Li and Gold, 2005]. Ideally a "reliability grid" should be provided together with any dataset [Jakobsson et al., 2002].

There are existing approaches of addressing uncertainties accumulated in the input data [Hare et al., 1995; Jakobsson et al., 2002; Elmore et al., 2009], and there are models of estimating the uncertainties of interpolation [Wechsler and Kroll, 2006; Amante et al., 2011]. The major reasons why such "reliability" grids will not be provided in the near future are: 1) they require well documented metadata for each data source, and 2) they are computationally intensive, especially on the global scale, since they require use of original soundings. Historical data, which comprises a large portion of the source data, lack any adequate metadata [Jakobsson et al., 2002]. The minimum information necessary includes the year of collection, positioning and acoustic instrumentation, and sound speed corrections; finding this kind of information is a very time-consuming task to complete.

Being an active member of the GEBCO Organization and a recent GEBCO scholar (2008-2009), my thesis objectives fall within the GEBCO Organization main objective, which is providing *"the most authoritative, publicly available bathymetry data sets"* by constantly updating and improving global bathymetry grids. The specific objectives of this study include the following:

1. Define quality metrics important for the choice of the most appropriate grid.

2. Quantitatively and qualitatively assess differences between current existing bathymetry grids in the Arctic in terms of defined quality metrics and determine the reasons for those differences.

3. Report problems identified in the grids to facilitate improvement of current versions of bathymetry models.

8

The main goal of the study is to provide the guidance on the choice of the bathymetry grid in the Arctic.

1.4 Methods and approach

As noted before, in this study the following bathymetry grids (see also Table 2.1) which provide Arctic coverage are compared: the global bathymetry grids GEBCO 1 min, ver. 2.00, GEBCO_08 30 arc seconds, SRTM30_Plus ver. 6.0, Smith and Sandwell ver. 13.1, and ETOPO1, and one regional dataset, IBCAO.

The analyzed datasets were separated into two major Types: Type A datasets, based solely on acoustic data sources and interpolated with digitized contours in the areas of no data; and Type B datasets, based on a combination of acoustic sounding data combined with gravity-predicted bathymetry (Table 2.1). The datasets of Type A include IBCAO, GEBCO 1 minute, GEBCO_08 and ETOPO1. The datasets of Type B include Smith and Sandwell (S&S) and SRTM30_Plus. Since the grids within each Type are very similar, the major part of the analyses was performed on a representative dataset from each Type, namely GEBCO_08 and S&S grids.

The study is made possible by the availability of recently acquired high resolution multibeam sonar grids provided by the Geological Institute Russian Academy of Sciences (GIN RAS) [Peyve et al., 2009; Zayonchek et al., 2009; Zayonchek et al., 2010]. The location of the GIN RAS multibeam sonar surveys defined the study area for this work. The comparison is focused on the region of the Svalbard archipelago and the adjacent Barents and Norwegian-Greenland Seas. The GIN RAS multibeam sonar grids provide wide spatial coverage and are not incorporated into any of the analyzed datasets. The GIN RAS grids were used in this study as a ground truth against which analyzed grids are evaluated.

The differences between analyzed grids are assessed in terms of quality metrics which were defined as important when choosing a bathymetry grid. The defined quality metrics include the following: source data accuracy, depth accuracy, internal consistency (presence and magnitude of artifacts), interpolation accuracy, registration issues and resolution of the coastline.

9

The differences between the analyzed grids and GIN RAS multibeam sonar grids is used as the measure of accuracy. The *source data accuracy* is assessed by comparison between source data values used for the construction of analyzed grids and the GIN RAS multibeam gridded values. The *depth accuracy* of the grids is assessed by comparison between depth values in the grids and the averaged GIN RAS multibeam gridded values at the corresponding locations. *Internal consistency* is measured by the presence and magnitude of artifacts in the bathymetry grids. The internal consistency is assessed qualitatively by visual inspection of the bathymetry grids for the presence of artifacts as well as quantitatively by comparison of the depth values in the grids to the surrounding depth values. The *interpolation accuracy* is measured by how well the bathymetry grids represent values in the areas distant from source data. *Registration* issues are tested by comparison of contours produced from the bathymetry of analyzed grids. *Resolution of the coastline* is visually assessed by comparison between bathymetry values in the analyzed grids to the GEBCO shoreline.

1.5 General concepts behind the GMT grid format

A grid is used to represent mathematically continuous phenomena using a finite number of data points. It is a convenient form of storing and manipulating data and is commonly used by many disciplines. In the case of the analyzed digital bathymetry models, the bathymetry surface is represented as a grid of uniformly spaced depth values. These models have constant cell size over the entire grid (Table 2.1). The analyzed bathymetry grids are available in GMT (Generic Mapping Tools) [Wessel and Smith, 1991, 1998] netCDF grid format. The GMT grid format is described below.

The grid cell is defined at the intersection of X and Y coordinates (Figure 1-3). Data is stored in rows going from top (north) to the bottom (south) and data within each row is stored from left (west) to right (east). The *corner coordinates* are the coordinates of the top left corner; they define the starting point from where the data is ordered. The distance between intersections in X and Y direction defines the *grid size*, and therefore the *resolution* of the grid. The grid cell

10

has one value that represents the average value over the cell of grid dimensions. *Registration method* defines what area each data point represents: in *gridline* registration - nodes are centered on the gridline intersect, while in *pixel* registration - nodes are located at the center of each grid cell (Figure 1-3) [Wessel and Smith, 1991, 1998].

The values in the grid are derived from irregularly distributed acoustic sounding data employing some interpolation function. Figure 1-4 illustrates hypothetical data points that need to be gridded over the chosen resolution. In order to perform gridding, the grid cells with more than one data point need to be replaced by one median value of all the input data points. The subsampling procedure is important in order to eliminate erratic values, avoid aliasing, and shorten the computation time [Smith and Wessel, 1990; Goodwillie, 2003]. The grid cells with no data values are filled with interpolated values obtained by applying a mathematical surface fitted to the input values and calculating the values at empty cells.

The interpolation algorithm used for the construction of the analyzed grids is the continuous curvature spline in tension [Briggs, 1974; Smith and Wessel, 1990]. A surface with continuous second derivatives and total squared curvature defined by the tension factor is fitted to the observations. Spline in tension is an exact interpolant, where the surface fits to the data points exactly. The interpolated values in the grid are estimated from the weighted average of values of nearby data points. The tension parameter defines the weights given to the surrounding data points in the value estimation: the higher the tension the more weight closer data point values will have over the further points. Therefore the tension factor defines the curvature of the surface: the lower the tension, the more data points will influence the solution at each node; the higher the tension, the less data points will influence the solution allowing high curvature (oscillations) only at the locations of data points.

An alternative method of filling the data gaps in bathymetry was introduced by Smith and Sandwell. In their method they fill the data gaps with predicted bathymetry, derived from

11
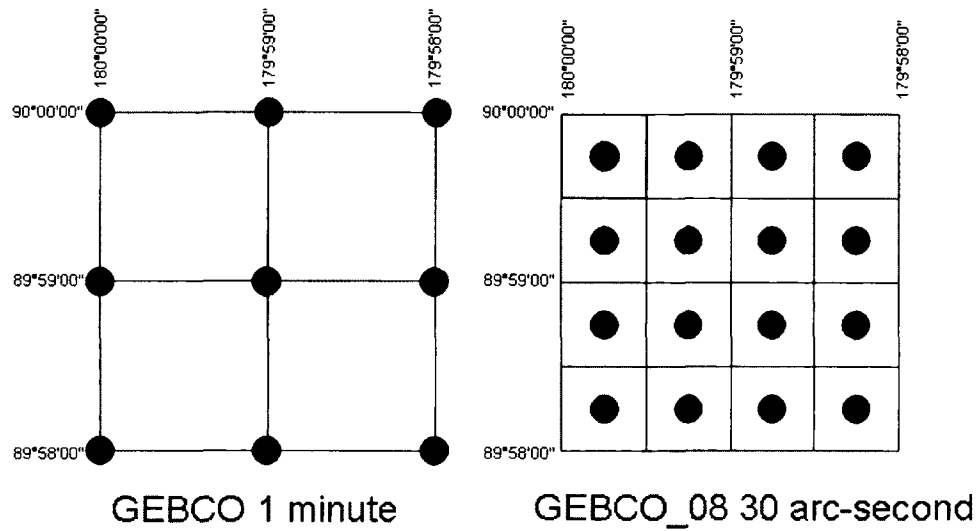
Figure 1-3: Difference between gridline registration in GEBCO 1 minute grid (left) and pixel registration in GEBCO_08 30 arc seconds grid (right). The colored area represents the area of the data point value.
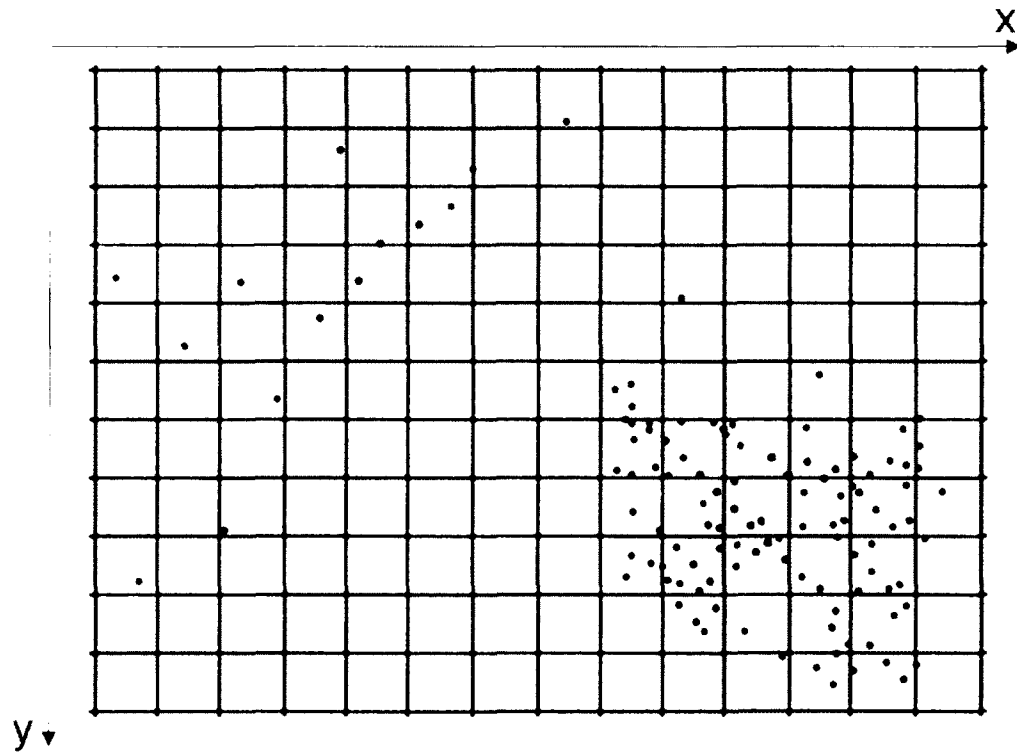
Figure 1-4: Example of hypothetical input data points (blue) overlain by grid mesh of chosen resolution. The grey cells will have values defined by the input data. The white cells will be filled by interpolation algorithm.

gravity data [Smith and Sandwell, 1997]. The correlation between large-scale bathymetry and satellite-observed gravity defines the regional scaling factor to apply to the gravity to obtain predicted bathymetry. The predicted bathymetry is combined with sounding information afterwards. This method is not really interpolation, but rather filling the data gaps with an alternative data source. In this work we refer to Smith and Sandwell's method as interpolation with satellite-derived gravity data.

To conclude, there are several fundamental limitations of any gridded bathymetry dataset which should be kept in mind before making any scientific interpretations. These include:

1) A bathymetry grid is calculated from an assemblage of information with fragmented distribution and irregular geographic density;

2) A variety of data sources are assembled into the grid, these include hand drawn contour maps, singlebeam measurements, point soundings, multibeam soundings, and indirect information such as marine gravity models. These types of sources feature a wide range of accuracies and resolutions, while often all of them are included into the grid as being equally accurate;

3) A bathymetry grid represents the equidistant estimates of depth; in order to produce those estimates a mathematical algorithm is used. The real bathymetry surface is more complex than the grid surface constructed from the source data.

CHAPTER II

DATASETS USED

This chapter describes the datasets used in this study. The first part gives a description of the publicly available global bathymetry grids evaluated in the study and the procedures followed to create them; the second part gives a description of the gridded multibeam bathymetry datasets provided by GIN RAS and used as a ground truth in the evaluation.

As mentioned earlier, the following datasets are compared in the Arctic: IBCAO, GEBCO_08, GEBCO 1 minute, SRTM30_Plus, S&S and ETOPO1. These datasets usually share common sounding data sources, since there is a limited amount of bathymetry data available for the Arctic. All of the data is usually incorporated into the IBCAO database as soon as it becomes available. At the same time, there are differences among the datasets, due to:

- major differences in the compilation process, especially the interpolation method;

- different post-processing methods applied to the source data, including data cleaning and sound speed corrections;

- data thinning (block-median) over different grid cell sizes that have different physical areas covered;

- misregistration errors through reprojection and resampling (for datasets based on reprojecting previously gridded data)

Using the compilation process as the major difference between these datasets, the grids can be separated into two major Types (Figure 2-1):

- Type A bathymetry grids – based solely on acoustic sounding data sources (singlebeam, multibeam and single soundings) and interpolated with digitized contours from published charts in areas that lack data.

14

- Type B bathymetry grids – based on acoustic sounding data sources (singlebeam, multibeam and single soundings) and interpolated with satellite-derived gravity data.

a)

```
┌─────────┐
│ Source  │   Gridding on PS              Resampling to Geo
│ data    │ ──────────────▶  IBCAO  ──────────────────▶
└─────────┘
```
GEBCO 1 minute
GEBCO_08
ETOPO1

b)

```
┌─────────┐   Gridding on Mercator
│ Source  │ ──────────────────▶  Smith and Sandwell
│ data    │
│         │   Gridding on Geo
└─────────┘ ──────────────────▶  SRTM30_Plus
```
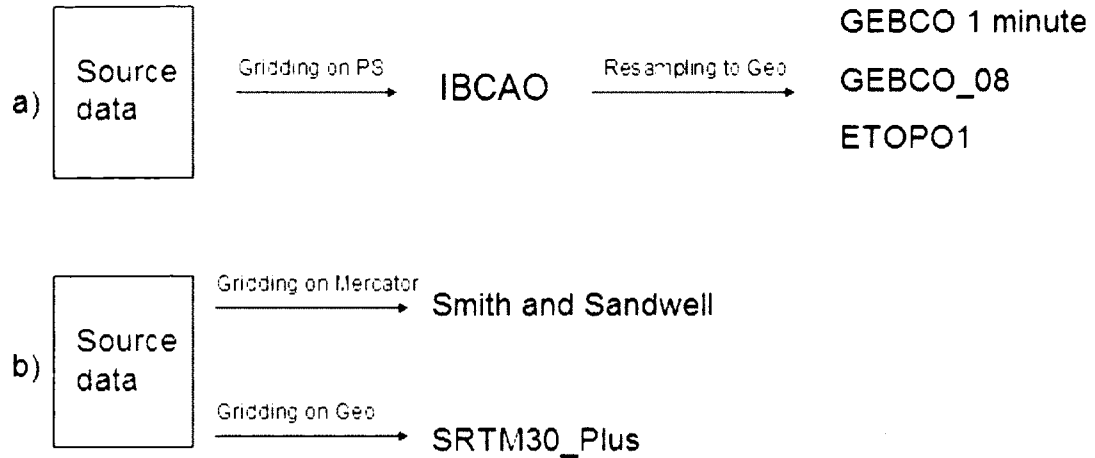
Figure 2-1: Scheme representing two Types of datasets and defining primary and secondary grids within each group: (a) Type A grids; (b) Type B grids.

In this study, the main analysis is performed on the representative grid from each Type. For the Type A datasets, IBCAO in polar stereographic projection (PS) is the primary grid created from the sounding data sources (Figure 2-1a). GEBCO 1 minute, GEBCO_08 and ETOPO1 grids are resampled versions of the IBCAO grid in a geographic coordinate system (Geo). Since GEBCO datasets and ETOPO1 were reprojected from IBCAO independently, these datasets are expected to be slightly different due to possibly different reprojection and resampling methods. GEBCO_08 was selected to be used in this study as the Type A dataset with the highest resolution.

For the Type B datasets, S&S and SRTM30_Plus are the grids in which depths are predicted from gravity and are calibrated with acoustic sounding sources. These two datasets share similar data sources which are gridded using different projections: S&S uses Mercator projection with 1 minute resolution and SRTM30_Plus uses a geographic coordinate system with 30 arc seconds resolution (Figure 2-1b). Also, the SRTM30_Plus is a global grid, and it includes values from the IBCAO grid north of 80.7°N, while S&S provides coverage only up to 80.7°N.

S&S will be the main interest of this study, as it is the original dataset which provides predicted bathymetry from gravity, and this information is used to create SRTM30_Plus.

Additionally, it needs to be noted that some of the grids are provided in several data formats (Table 2.1). As an example, IBCAO is provided in two different projections and formats: polar stereographic 2 km and geographic 1 minute, each in GMT netCDF and ESRI ASCII formats. The main difference between the two formats is the registration method, and whether they can be utilized in a particular software (see Section 1.5). The conversion from one to another format usually causes slight differences and misregistrations. For example, conversion from netCDF grid-registered format to the ArcMap pixel-registered format will cause smoothing and might cause scaling issues due to reduction of the grid size in one pixel. Other differences between the datasets could result from reprojections.

2.1 Short description of compilation procedure for each grid Type

2.1.1 Type A grids

The IBCAO bathymetry grid version 2.23 is the original grid on which other datasets of Type A are based in the Arctic region. The IBCAO is an assemblage of all publicly available sounding sources for the Arctic Ocean, north of 64°N. The sources include single and multibeam ship track data, declassified submarine depth measurements, historic point soundings from ice camps and hydrographic charts, gridded datasets and hand-drawn digitized contours [Jakobsson et al., 2000]. The majority of the data sources are single beam soundings obtained from the following archives: US National Geophysical Data Center, US Naval Research Laboratory, US Geological Survey, Norwegian Hydrographic Service and Royal Danish Administration of Navigation and Hydrography (Table 2.1) [Jakobsson et al., 2008]. The multibeam data covers approximately 6% of the IBCAO grid area and is based on the data collected during recent ice-breaker cruises [Jakobsson et al., 2008]. In the areas outside of available multibeam surveys, digitized isobaths from bathymetry maps of the Head Department of Navigation and

Oceanography (HDNO), Russian Ministry of Defence, and contours from the GEBCO Digital Atlas are used [Jakobsson et al., 2008].

The main steps involved in the construction process of IBCAO are depicted in Figure 2-2. In order to produce the final IBCAO bathymetry grid the following steps were taken [Jakobsson and Macnab, 2008]:

1) Cleaning the input data: sound speed corrections are applied, soundings are cleaned of outliers, cross-track errors are minimized and input contours are adjusted to fit bathymetry acoustic measurements.

2) Data thinning: track subsampling along the track, block-median filter the input data over the grid cell size.

3) Interpolation: the depth values for all grid nodes are computed by a continuous curvature spline in tension algorithm with tension 0.35 [Smith and Wessel, 1990].

4) Quality control: the intermediate output grid is checked for artifacts; discrepancies between the original data and the output surface are highlighted. The systematic errors found are corrected. In some areas additional information such as support contours are added to constrain gridding.

5) Gridding and interpolation on corrected input data. Steps (1) through (4) are repeated until the errors in the output grids are minimized.

6) The final smoothing is applied by running a weighted average filter. At this step the final IBCAO grid is constructed.

In order to produce the geographic version of the IBCAO grid for inclusion in the global GEBCO 1 minute, GEBCO_08 and ETOPO1 grids, the IBCAO grid was sampled over the geographic matrix of corresponding resolutions [Macnab and Jakobsson, 2001; Amante and Eakins, 2009].

17
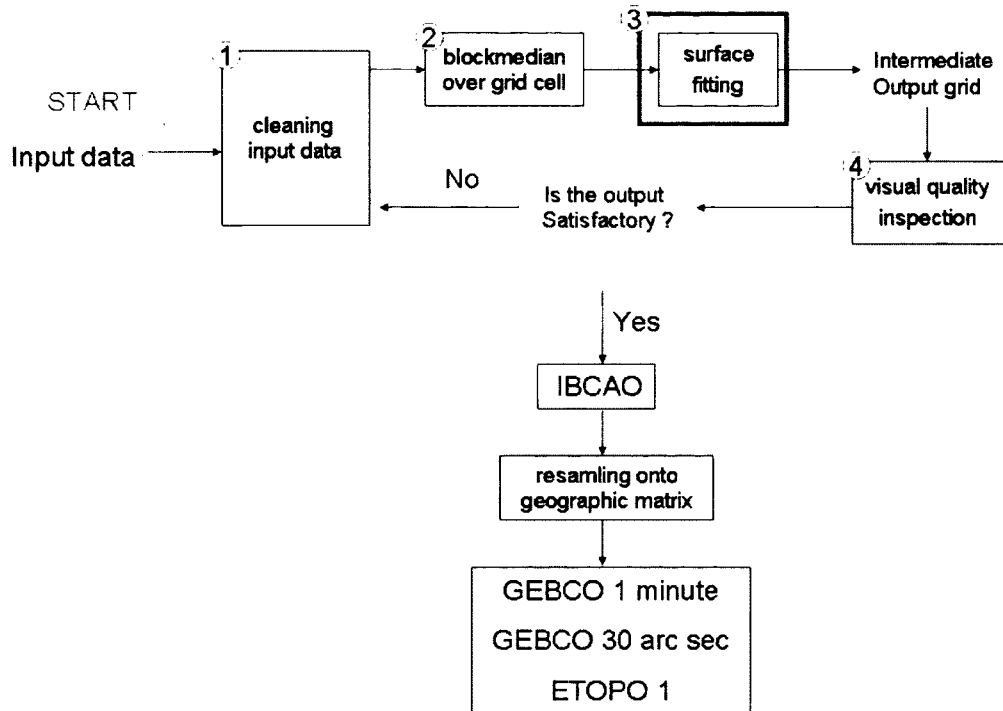
Figure 2-2: Flow diagram giving the scheme used for construction of Type A grids (modified after Goodwillie, 2003). The green box defines the interpolation step, see Figure 2-3 for comparison. The plain yellow box defines intermediate output.

2.1.2 Type B grids

S&S is the global bathymetry grid which is based on a satellite-derived gravity model combined with acoustic soundings from a variety of sources. The gravity model is based on ocean topography data derived from Geosat, ERS-1 and Topex/Poseidon altimetry missions [Smith and Sandwell, 1997, 2001]. The sounding sources include single and multibeam ship track data, point soundings from hydrographic charts and gridded multibeam datasets. Major sounding sources are National Geophysical Data Center (NGDC), Lamont Doherty Earth Observatory (LDEO) archives, Scripps Institution of Oceanography (SIO) database, National Geospatial Intelligence Agency (NGA), and more (see Table 2.1) [Becker et al., 2009].

Under certain geophysical assumptions and geologic conditions, there is a correlation between gravity and bathymetry within a 20 to 160 km horizontal wavelength band [Smith and Sandwell, 1994, 2001]. In order to predict bathymetry from the gravity information, the scaling

18

factor, or ratio between gravity and bathymetry, is determined for the regions where they are correlated. The determined scaling factor is used to convert gravity to bathymetry, resulting in a "predicted bathymetry", which is then combined with the measured acoustic sounding information available to provide final bathymetry. A more detailed description of the method can be found in Smith and Sandwell [1994, 1997, 2001]. Here we provide a summary of compilation procedure steps used to construct the grid.

The description of the following steps is based on published procedures for the S&S [1994, 1997, 2001] and SRTM30_Plus grids [Becker et al., 2009]. Becker et al. gives a more current description of the procedures than do Smith and Sandwell. Both datasets share similar procedures (personal correspondence with D. Sandwell, 2011). The following steps describe the compilation flow (Figure 2-3):

1) Data cleaning of outliers, the predicted bathymetry surface from S&S is used for identifying major outliers and to flag bad data sources.

2) Thinning the data. The data is block-medianed over 500 m by 500 m cells. This step removes major outliers (erroneous values are eliminated by taking the median of the input values).

3) Creating the predicted bathymetry grid. The predicted bathymetry grid is created in the following way:

   1.   The cleaned and thinned soundings are gridded onto a bathymetry grid of defined resolution.

   2.   The derived bathymetry is band pass-filtered into high (<160 km wavelength) and the low frequency components (>160 km wavelength).

   3.   The correlation and scaling factor between high pass filtered bathymetry and high pass filtered (and downward continued) gravity grids are estimated for each region of 160 x 160 km on the globe.

   4.   For the areas where there is a strong correlation, the high pass filtered

19

gravity is scaled by the coefficient estimated in step 3 to provide predicted depth.

5. The total predicted bathymetry grid is derived from the sum of scaled high pass filtered gravity and long-wavelength component of bathymetry.

4) Cleaning step 2: the created predicted bathymetry grid is used to automatically compare against the soundings, correct errors where possible and flag suspicious cruises. The flagged cruises are not used in the next iteration of creating predicted bathymetry. Steps 2, 3 are repeated.

5) At this step the values of the nonflagged soundings are restored into the predicted bathymetry grid.

6) The predicted bathymetry grid "polishing" step. Transition between the predicted surface and measured depth values is made by a "polishing" procedure [Smith and Sandwell, 1997]. The depth difference between the predicted bathymetry and known depths is interpolated using a continuous curvature spline with tension 0.75 [Smith and Wessel, 1990]. Afterwards the difference is added back to the prediction grid [Smith and Sandwell, 2001; Becker et al., 2009].

7) Quality control step. At this step the inspection for outliers and suspicious tracklines is carried out. The bad tracklines are identified by computing residuals and the deviation between the predicted bathymetry surface and the measured depths on a cruise-by-cruise basis. If the deviation is too high, the cruise is flagged unless it is possible to identify the sources of errors and to correct them [Smith and Sandwell, 1999].

8) All flagged cruises are excluded from the process, and the whole process starting from step 1 is repeated again.

START

1   2
7   3
6   4
5   1
3   2

(3)

gravity
anomaly
grid

bathymetry
grid

Highpass
filter
gravity

3.
Estimate scaling
factor **S** from
gravity / bathy
ratio

4. Scale
highpass
gravity
By **S**

5.
Sum highpass
scaled
gravity and
lowpass
bathymetry

2a. Highpass filter
bathymetry

2b. Lowpass filter
bathymetry

1. Gridding/
interpolation

(2) blockmedian
over grid cell

Total predicted
bathymetry

(1)

(4) 1st

2nd

START

**Input bathy
data**

Cleaning/
flagging

(5)
Reset original
Source values

No Is the output
Satisfactory ?

(7)
Visual/statistical
Quality inspection

Polished
predicted
bathymetry

(6)
Polish grid

Yes

**Smith and Sandwell
SRTM30_Plus**

Figure 2-3: Flow diagram giving the scheme used for construction of Type B datasets. The green box defines the interpolation stage for Type B datasets, compare to the green box for Type A datasets in Figure 2-2.

Summarizing, six steps are defined for the process of constructing the bathymetry grids analyzed in this thesis: (1) input data cleaning; (2) input data thinning; (3) interpolation step; (4) quality control of the output surface; (5) repetition of the steps (1) through (4) without flagged data; (6) creation of a final output surface. It can be seen from Figures 2-2 and 2-3 that there are similar construction steps involved in the creation of both dataset Types. At the same time, for Type A datasets it is easier to create a linear flow diagram than for the Type B with its very nonlinear process. Within each step, differences are significant for the data cleaning step and interpolation step, which is marked as a green box on Figures 2-2 and 2-3.

Grid name	Date released	Coverage	Resolution	Format	Projection	Regist.	Based on	Sources
IBCAO ver. 2.23	2001, updated 2008	64°-90° N	2 km 1 min	netCDF, Arc ascii, pdf map	Polarstereographic, true scale at 75°N WGS 1984 Geographic WGS 1984	grid pixel	soundings derived from hydrographic charts, ice camps, single and multibeam surveys and declassified sumbarine measurements interpolated on contours in the areas that lack data	ship track data NGDC, NRL, CHS, RDANH, icebreakers, RV Polarstern (Germany), RV Oden (Sweden), SCICEX program nuclear submarine: contour maps HDNO maps, NRL charts, GEBCO DGA [Jakobsson, 2008]
GEBCO 1 min ver. 2.00	2003, updated 2008	global	1 min	netCDF	Geographic WGS 1984	grid	soundings derived from hydrographic, contour and sounding charts and single and multibeam surveys, interpolated on digitized hand drawn contours; includes IBCAO grid for latitudes 64°N-90°N	BSH, UKHO, SOHO, Norwegian, British, USSR, German, INT nautical charts, Norwegian, Soviet and USA unpublished and public contour charts and bathymetric maps (sources are given only for GEBCO Sheet 5.01) [Goodwillie, 2003]
GEBCO_08 ver. 20091120	Feb. 2009	global	30 arc sec	netCDF	Geographic WGS 1984	pixel	soundings interpolated with satellite-derived gravity data from SRTM30_Plus, includes IBCAO grid for latitudes 64°N-90°N	GEBCO, IHB, NGA, NOAA, NAVO, SIO, NERC [The GEBCO_08 documentation, 2008]
ETOPO 1	2009	global	1 min	netCDF, GRD98, binary, xyz, geotiff	Geographic WGS 1984	grid pixel	soundings interpolated with satellite-derived gravity data from S&S, includes IBCAO grid for latitudes 64°N-90°N	JODC, NGDC, CEP, CIESM [Amante & Eakins, 2009]
Smith and Sandwell ver.13.1	Aug. 2010	80.738°S-80.738°N	1 min longitude	binary, gif image	GMT Spherical Mercator	pixel	high resolution marine gravity model ver. 18.1 combined with available depth soundings [Smith and Sandwell, 1997]	NGDC, MGDC, GEOMAR, NSF, SOEST, WHOI, SIO, NGA, JAMSTEC, NOAA, IFREMER, CCOM, GEBCO, NAVO, IBCAO [Becker, et al., 2009]
SRTM30_Plus ver.6.0	Nov. 2009	global	30 arc sec	netCDF, xyz	Geographic WGS 1984	pixel	high resolution marine gravity model ver. 18.1 combined with available depth soundings, includes IBCAO database for latitudes north 80°N [Becker, et al., 2009]	same as Smith and Sandwell ver 12.1

Table 2.1: Main differences between the analyzed grids. See the translation of abbreviations in the Acronyms Section.

23

2.2 Multibeam datasets

In the current study, GIN RAS multibeam sonar gridded bathymetry not incorporated into any of the evaluated gridded datasets is used as a ground truth. The bathymetry grids are based on the multibeam sonar data acquired during cruises 24, 25 and 26 of RV *Akademik Nikolai Strakhov* carried out in the Norwegian-Greenland and Barents Seas during the period of 2006-2008 [Peyve et al., 2009; Zayonchek et al., 2009; Zayonchek et al., 2010].
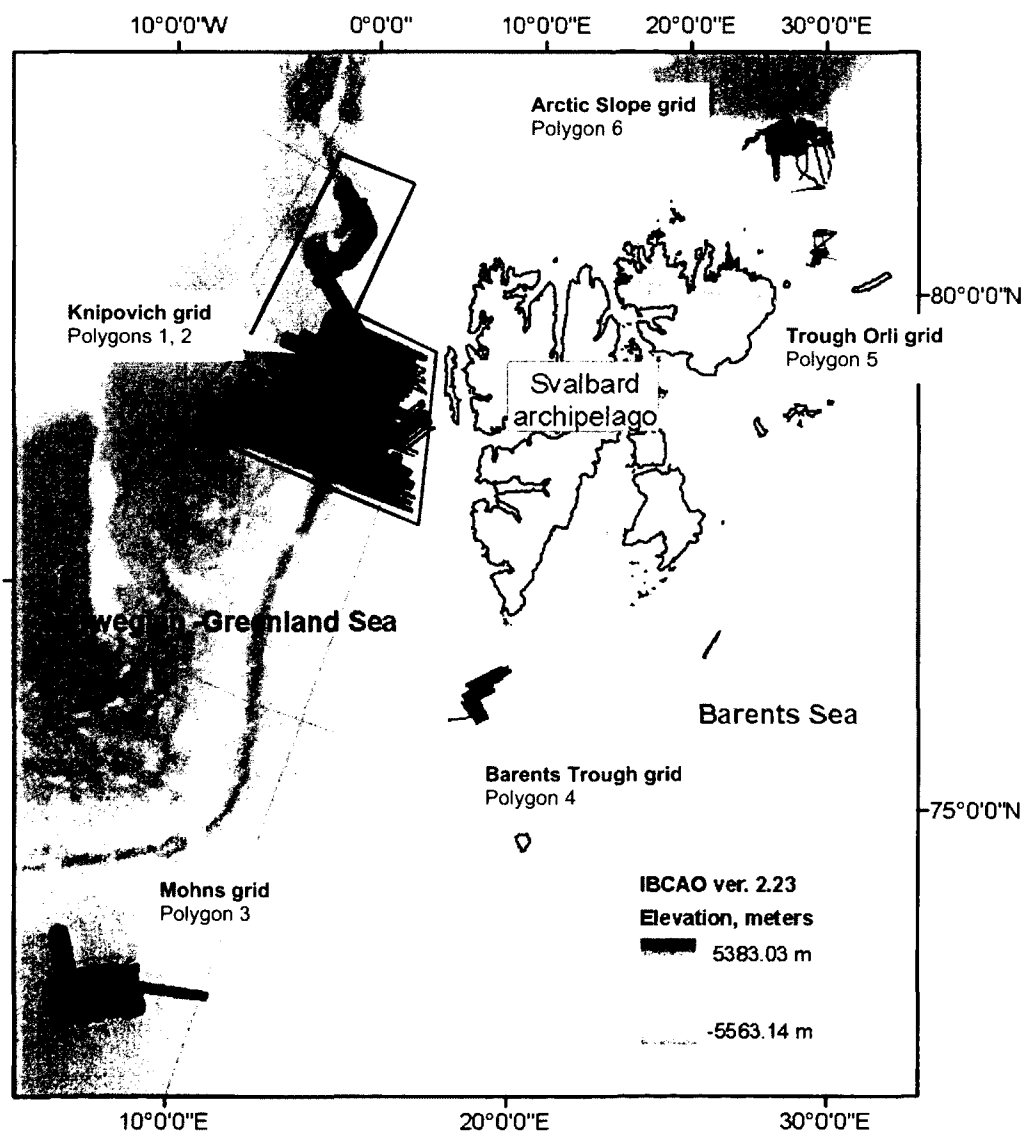
Figure 2-4: Overview map of the location of GIN RAS multibeam grids (in black) and corresponding study polygons. Polygons 1 and 2 are outlined in blue and red.

24

Five GIN RAS bathymetry grids provide wide spatial coverage and capture the variety of seafloor features (Figure 2-4, Table 2.2). The covered areas include the Norwegian - Greenland Sea in the area of Knipovich and Molloy mid-oceanic ridges (Knipovich grid, Figure 2-4) and abyssal plain in the vicinity of Mohns mid-oceanic ridge (Mohns grid). Two grids provide coverage on the Barents Sea continental shelf (Trough Orli and Barents Trough grids). One grid covers the Arctic continental slope (Arctic slope grid). Five GIN RAS bathymetry grids were separated into six study polygons (Figure 2-4). The polygons have distinct differences in morphology, water depth and source data used for the construction of the analyzed bathymetry datasets, summarized in Table 2.2. In the further analyses study polygons 1 through 6 will be used.

The multibeam sonar data collection, post processing and gridding were performed by the GIN RAS. The data was collected with RESON sonar multibeam systems, which included shallow (SeaBat-8111, 100 kHz) and deep water (SeaBat-7150, 12 kHz) multibeam echo sounders. The sound speed data was acquired during the cruises with SVP-25 RESON Sound Velocity Probe. The data was corrected for the sound speed and cleaned of the outliers using RESON PDS2000 Software. The edited multibeam data was gridded using Golden Software Surfer with inverse distance to power interpolation (power = 0.5). The resolution of GIN RAS multibeam grids varies depending on the area (Table 2.2).

The worst case uncertainty of GIN RAS multibeam data was estimated using the CARIS uncertainty model, adopted from Hare et al. [1995]. Accuracy of GIN RAS multibeam is assessed by comparison with independent multibeam datasets acquired by RV/Icebreaker *Oden* and USCGC *Healy*. See Chapter IV for the worst case estimates of uncertainty and accuracy of GIN RAS multibeam data.

GIN RAS grid name	polygon No	projection of GIN RAS grid	resolution of GIN RAS grid	depth range meters	morphologic province	roughness of seafloor	source data type	source data density
Knipovich	1	utm zone 32N	100 m	1200-5400	mid-oceanic ridge	very rough	RV Polarstern MBES grid	dense
Knipovich	2	utm zone 32N	100 m	110-3600	mid-oceanic ridge	very rough	Norwegian single soundings + NGDC singlebeam + **contours**	relatively dense
Mohns	3	utm zone 32N	100 m	1700-3000	abyssal plain	smooth	Norwegian MBES	dense
Barents Trough	4	utm zone 37N	50 m	150-400	shelf (trough)	smooth	Norwegian single soundings	sporadic
Trough Orli	5	utm zone 37N	10 m	50-500	shelf (trough)	rough/smooth	**contours** + MBES tracks + Norwegian single soundings +NGA single soundings + **MBES**	poor
Arctic Slope	6	utm zone 37N	50 m	60-2900	continental slope	smooth sloped	contours + MBES tracks + Norwegian single soundings + **MBES**	sporadic

Table 2.2: Description of GIN RAS multibeam bathymetry grids and main information for the study polygons depicted in Figure 2-4. The source data type column describes data sources incorporated into GEBCO_08 (IBCAO) and S&S grids, given in color are additional data sources included only into IBCAO grid (blue) and S&S grid (red).

CHAPTER III

METHODS

In this chapter methods used to assess the differences between analyzed grids are discussed. The differences are assessed in terms of quality metrics. These quality metrics reflect principal quality components that often play an important role in the choice of the most appropriate grid. Quality is an imprecise term, is application dependent, and for geographically based data varies in space and time. Since there is no single measure of quality, several criteria for assessing quality of bathymetry datasets were chosen. Metrics chosen are defined as [modified after Hutchinson and Gallant, 1999, 2000; Veregin, 1999; Lin et al., 1999; Karel et al., 2006]:

- *Source data accuracy* used for construction of the analyzed bathymetry grids, measured by the accuracy of source data values against an independent GIN RAS multibeam sonar data of higher accuracy;

- *Depth accuracy* of analyzed bathymetry grids, measured by how well the depth values in the grids fit values from an independent GIN RAS multibeam sonar data of higher accuracy;

- *Internal consistency* of the bathymetry grids, measured by the presence of artifacts in the grids and smoothness of the bathymetry surface for visualization purposes;

- *Interpolation accuracy*, measured by how well the bathymetry grids represent values in areas distant from source data;

- *Registration issues* are tested by comparison between contours produced from the bathymetry of analyzed grids;

- *Resolution of the coastline* is tested by fitness of depth values in analyzed bathymetry grids to the GEBCO shoreline.

27

The methods described below are used to assess accuracy of the source data used for the grids construction, the accuracy of analyzed grids, internal consistency and interpolation accuracy.

As discussed in Chapter 2, datasets are separated into two Types: Type A datasets, based on sounding source data, and Type B datasets, based on sounding source data combined with gravity information. Datasets within each Type have common characteristics, since they use similar procedures for their compilation (Chapter II). Since consistency and interpolation performance depend primarily on the modeling process used, these two criteria are assessed for one dataset in each Type (GEBCO_08 and S&S) and not for each individual dataset. Since S&S and SRTM30_Plus are gridded using different projections (Chapter II), some differences between these grids are expected. Therefore, the depth accuracy is assessed for GEBCO_08, S&S and SRTM30_Plus.

3.1 Primary method for accuracy assessment

The depth accuracy of the bathymetry grids is assessed by taking the difference between the GIN RAS multibeam grids and the analyzed bathymetry grids. The accuracy is measured by the means and standard deviations of the differences distribution. Depth difference computation was performed separately for each study polygon to address the regional accuracy of each grid depending on the main accuracy-defining parameters.

The primary method of comparison between the bathymetry grid and gridded multibeam bathymetry involves a difference computation between the values at corresponding locations. Ideally the depth difference between compared datasets would be calculated for each grid cell and not involve any alteration of original values. The challenge lies in the fact that the test datasets and gridded multibeam bathymetry are created in different coordinate systems, with different resolutions and registration methods (Table 2.1 and Table 2.2). The multibeam grids are in UTM projection with resolution varying from 50 m to 100 m, S&S is in GMT spherical Mercator projection with ≈ 1853 m cell size and IBCAO is in polar stereographic projection with 2 km

SS and multibeam grid   SS and IBCAO grid   SS and GEBCO_08 grid
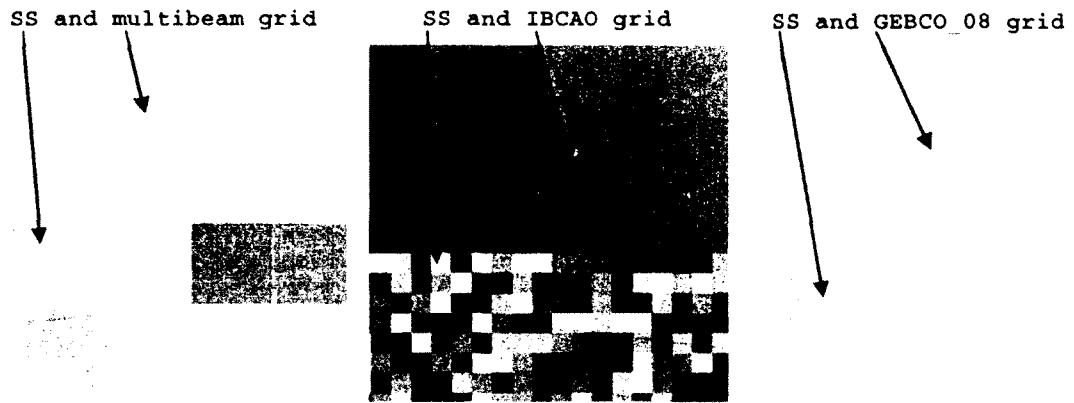
Figure 3-1: Visual representation of differences in orientation and size of grid cells for analyzed grids. Colored cells represent the S&S grid (Mercator 1850 m grid) which is compared to the GIN RAS multibeam grid (UTM 100 m grid), IBCAO grid (polar stereographic 2 km grid) and GEBCO_08 grid (geographic coordinate system 30 arc second grid). The noticeable difference in the size of S&S (1850 m) grid cells compared to IBCAO (2 km) grid cells is caused by the projection difference: true scale in S&S Mercator grid is on the equator, and true scale in IBCAO polar stereographic grid is at 75°N. ArcMap view: the projection view is set to the Mercator.

$\bar{Z}_B$-Z_{A1}

Z_{A1} Z_{A2}

Z_{A3} Z_{A4}

Z_{B1} Z_{B2} Z_{B3} Z_{B4} Z_{B5}
Z_{B6}

Z_{Bn}

[a]   [b]   [c]
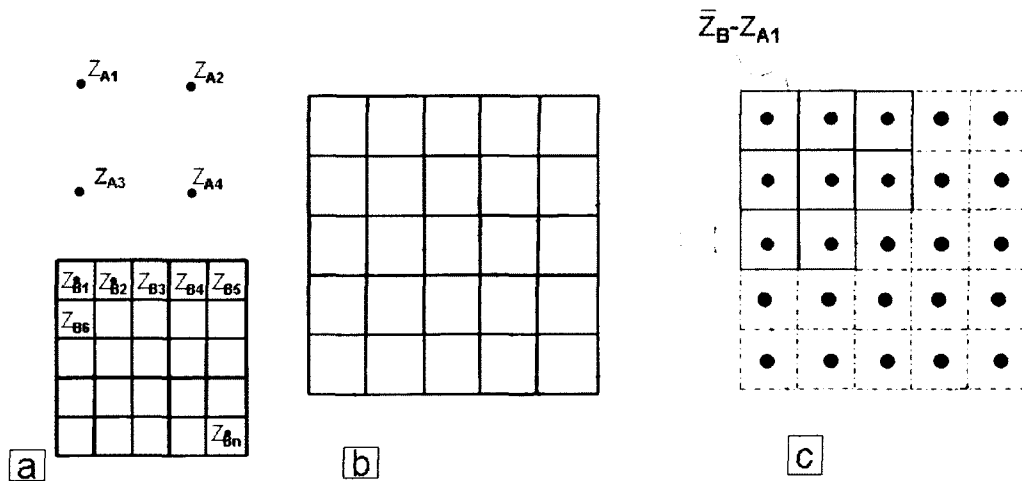
Figure 3-2: Method of depth difference computation for datasets of different resolutions: (a) illustrates schematically two grids A and B of different projections and resolutions. Each cell has some depth value Z_A or Z_B respectively; (b) illustrates overlaid grids in some projected space, mismatch between cells makes it impossible to calculate the difference between two datasets; (c) while representing grid B as point depth values rather than grid cells, it can be reprojected into the new projection. Multibeam data points B are averaged (Z_B) over the grid cell in dataset A. The difference between two datasets is computed as the difference between Z_B and Z_A at corresponding locations.

resolution. The rest of the analyzed grids are in geographic coordinate system: SRTM30_Plus and GEBCO_08 are 30 arc second grids, ETOPO1 and GEBCO 1 minute are 1 minute grids. A visual representation of how grid cell sizes differ is presented in Figure 3-1.

The GMT software package [Wessel and Smith, 1998] was used for computation. GMT was chosen since most of the analyzed datasets were created using GMT, and GMT can handle the projection and format in which the S&S dataset is provided (GMT spherical Mercator projection, binary format).

The method chosen for depth difference computation does not involve extra interpolation of original values in the analyzed datasets, and follows the method used by Marks et al. [2010]. The following procedure was carried out in order to compute the difference between values in bathymetry grid A and multibeam grid B (Figure 3-2):

1. The values in the multibeam grid B are converted into xyz data points.

2. The GMT routine mapproject is used to reproject grid B to the projection of grid A.

3. The multibeam grid B values are averaged over each grid cell of dataset A.

4. Dataset A grid values are sampled at each averaged multibeam data point B using GMT routine grdtrack.

5. The difference for each grid cell in grid A is computed by subtracting the dataset A value from multibeam B averaged value.

The method described above was used to assess the accuracy of the analyzed grids, source data accuracy and the interpolation accuracy.

3.2 Method of internal consistency assessment

For some applications the absolute accuracy of the model is not as important as the consistency in the relative change of values. Any operation on the neighborhood values such as aspect, slope and other local derivatives will be affected by the inconsistencies (or artifacts) in the surface [Gallant and Wilson, 2000]. This section describes the methods used to assess the

30

consistency of the datasets. Assessment of consistency includes a qualitative part involving

inspection of the grids for the artifacts and a quantitative part involving statistical analyses.

3.2.1 Qualitative assessment of internal consistency (inspection for artifacts)

In order to assess the consistency of datasets qualitatively, visual inspection of the

GEBCO_08 and S&S grids for the presence of artifacts was carried out. The bathymetry grids

were inspected in Fledermaus IVS 3D. Artifacts can be misinterpreted as real features and are not

easy to identify automatically. Different types of artifacts are caused by different types of

sounding source data (singlebeam, multibeam, single soundings, contours) or by interpolation

method (e.g. filling data gaps with gravity, spline interpolation). Three regions were chosen for

inspection in order to cover all types of source data. Also, it was important to cover several types

of geologic conditions which affect correlation between gravity and bathymetry [Smith and

Sandwell, 1997].
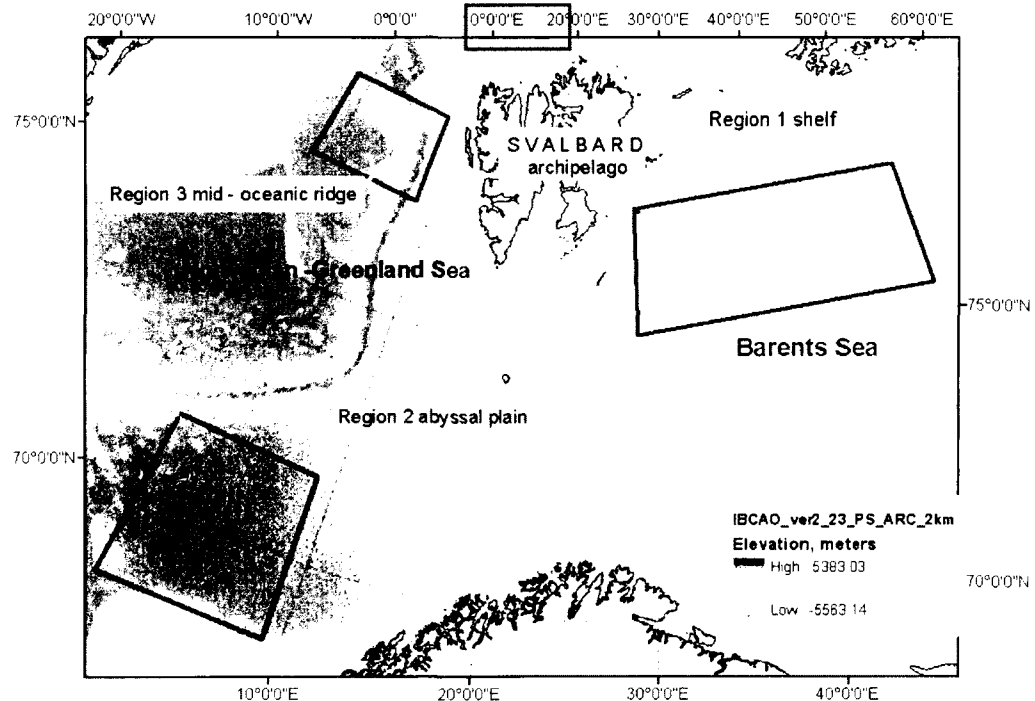
Figure 3-3: Location of three regions used for inspection of presence of artifacts in the bathymetry of the S&S and GEBCO_08 datasets (the blue polygon outlines the location for Figure 4-19 in Chapter IV).

31

The types of source data usually correlate with different morphologic provinces. The following regions were chosen (Figure 3-3):

Region 1: Shelf area - mainly singlebeam soundings and historic single soundings; correlation of gravity with bathymetry is poor because of assumed crustal density and sediment thickness;

Region 2: Abyssal plain - singlebeam soundings and multibeam coverage; correlation of gravity with bathymetry is poor because of the great sediment thickness;

Region 3: Mid-oceanic ridge - multibeam combined with singlebeam and hydrographic soundings; correlation of gravity with bathymetry is good because sediment thickness is low (depending on the local geologic conditions).

A classification of artifacts based on the source data causing them was made for Types A and B datasets. This classification is based on the source data types causing them and morphology of the artifacts. The full classification table of artifact types observed in the grids is provided in Chapter IV.

3.2.2 Quantitative assessment of internal consistency

This section describes the method chosen to quantify differences in consistencies of the two Types of datasets. A simple area was chosen to assess consistency (Region 1 in Figure 3-3) – a shelf area with smooth morphology. The area chosen is also simple in terms of the data sources used to construct bathymetry models: only historical singlebeam soundings and digitized contours are available sounding data sources for this area.

From visual inspection of the data it was found that high frequency artifacts are usually associated with the location of source data points. An edge detection filter was run on the bathymetry values of S&S and GEBCO_08 datasets to confirm the observation that the highest variations occur at the locations of the input data. Figure 3-4 and Figure 3-5 illustrate edge detection maps for S&S and GEBCO_08 datasets.
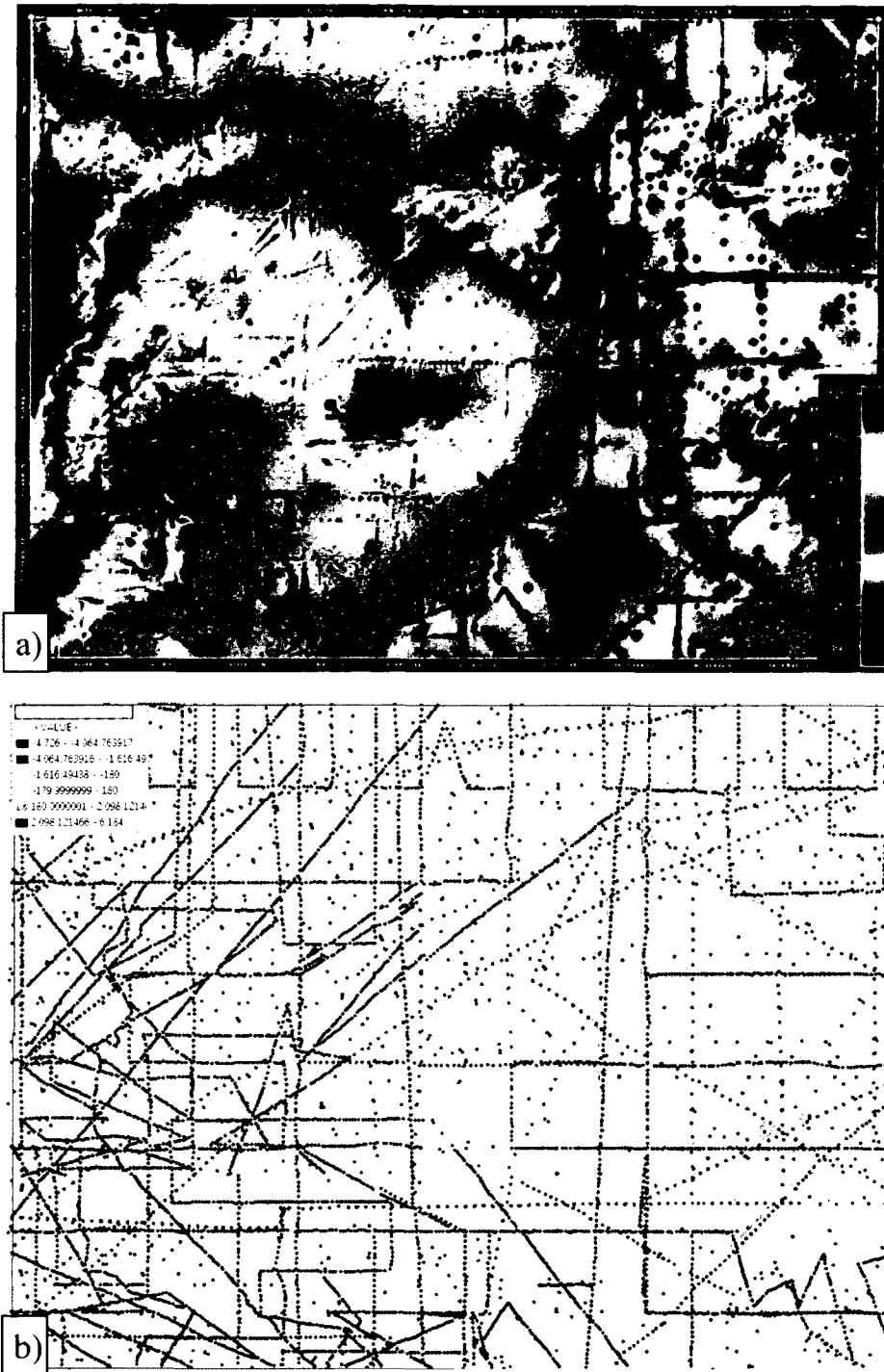
Figure 3-4: (a) Bathymetry in S&S grid for Region 1 in Figure 3-3 (depth in meters); (b) edge detection map produced by running 7x7 edge detection filter on the bathymetry values in Region 1. The map is overlaid by source data to show correlation between location of input data and high edge detection values.
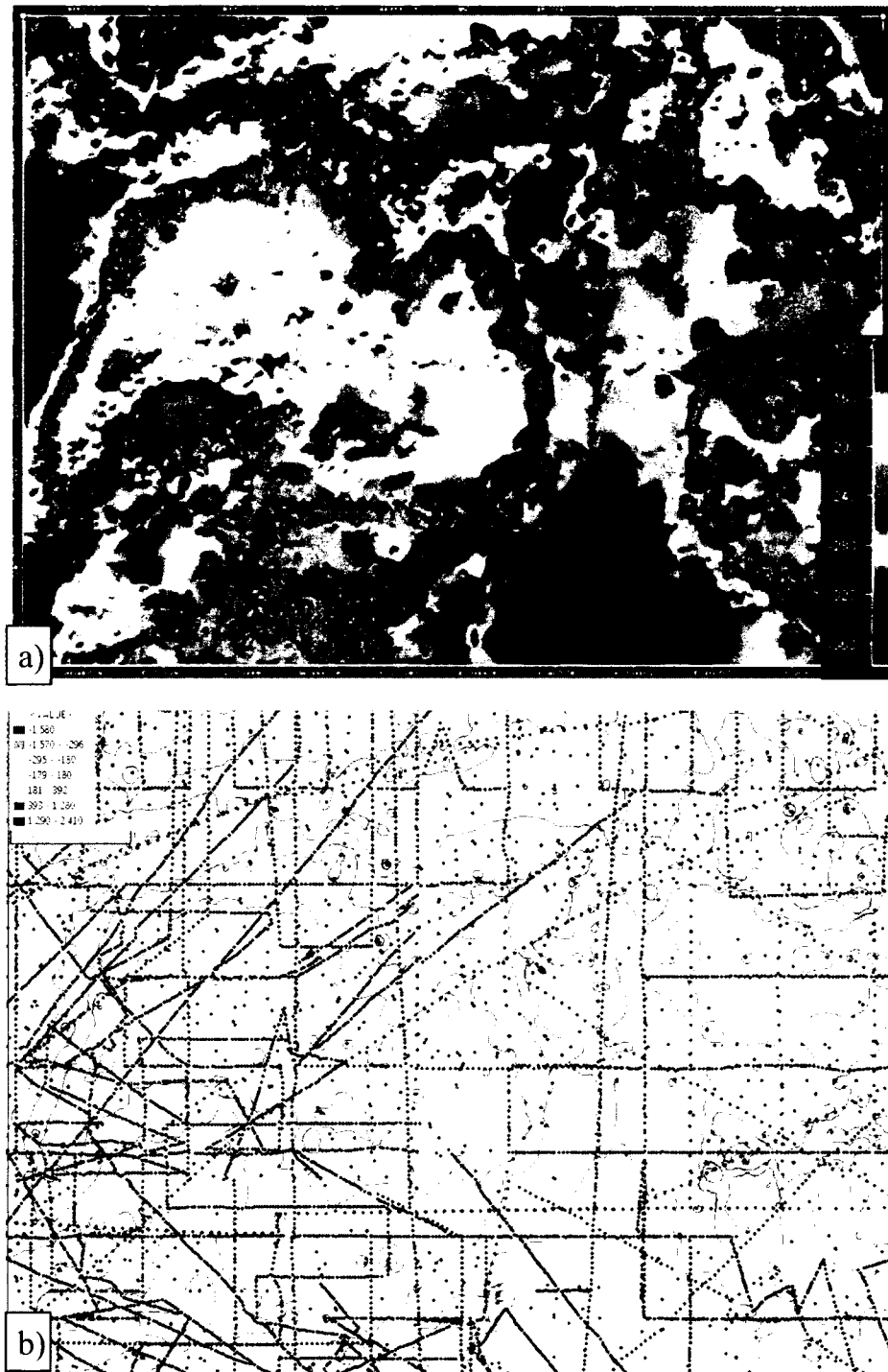
Figure 3-5: (a) Bathymetry in GEBCO_08 grid for the same area as Figure 3-4 (depth in meters); (b) edge detection map produced by running 7x7 edge detection filter on the bathymetry values in Region 1. The map is overlaid by source soundings and contours. High edge detection values correlate with the location of input data, especially in the areas where contours do not agree with sounding values.

While comparing the bathymetry in Figure 3-4a with that in Figure 3-5a, it is easy to separate visually which of the datasets is more consistent. S&S bathymetry has a lot of artifacts around the input data points, while GEBCO_08 fits the input values smoothly. These differences are due to the differences in construction procedures for the grids (discussed in Chapter II). At the same time, the S&S bathymetry model is expected to be more reliable in the areas of no soundings, since interpolation is based on additional gravity information, while GEBCO_08 interpolation is based on digitized hand-drawn contours.

The chosen method of consistency assessment is based on comparison of *variability* around source data points in the two datasets to the *"true" variability*. Figure 3-6 illustrates "morphology" observed around the source soundings for the two datasets. As can be seen from Figure 3-6, the bathymetry surface fits input soundings more smoothly in the GEBCO_08 grid than in the S&S grid. We expect the surface around input soundings to be smooth to some extent, and beyond some smoothness/roughness value the surface becomes inconsistent. Here the area which is influenced by the values of input source soundings will be referred to as a *source data area of influence* (SDAI) (Figure 3-6b). The area in the bathymetry surface outside of the sounding influence in the S&S grid will be referred to as a *"true" variability area* (TVA) (Figure 3-6b). The *"true" variability* is observed in the S&S grid in the areas where the bathymetry values are predicted from gravity information. The assumption is made that the gravity-predicted bathymetry surface reflects the true behavior of the bathymetry surface.
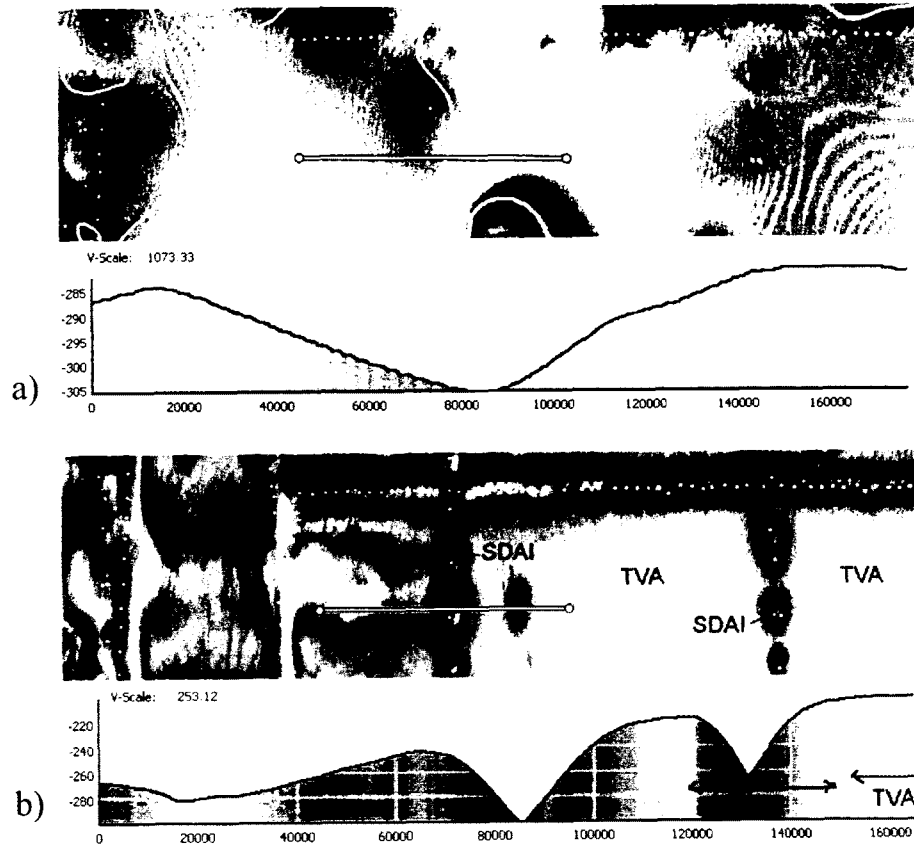
Figure 3-6: (a) Fragment of GEBCO_08 bathymetry overlaid by input source soundings (white dots) and contours (white lines). Profile is taken across the bathymetry in the area of source soundings; (b) Fragment of S&S bathymetry overlaid by source soundings. Profile is taken across the bathymetry in the same location as the profile across GEBCO_08. GEBCO_08 fits smoothly into input soundings, while S&S has "holes" in the bathymetry surface at the locations of source data points. The value of the source sounding is also influencing values in the surrounding area, here referred to as a *source data area of influence* (SDAI). The area outside of SDAI in S&S bathymetry is referred to as *the "true" variability area* (TVA).

High variability around source soundings is not always an artifact of the gridding process. In some cases, high roughness can be result of natural seafloor variability. The method chosen is meant to avoid confusing natural with artificial roughness. It is expected that in the case of large depth variation within the source data area of influence and low variation in the areas of "true" variability, these differences will be due to inconsistencies in the surface. If similar high variability is observed both within the area of the soundings influence and within the area of "true" variability, then the surface will not be misinterpreted as being inconsistent.

36
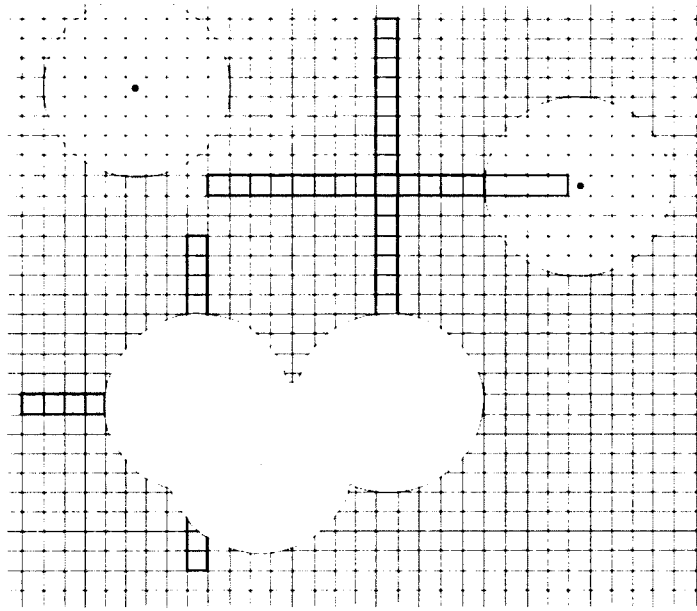
Figure 3-7: Illustrates method of assessing variability at the location of source data points (cells with black dots) and outside, where the "true" variability is assumed. Purple cells show cells used for variability computation at the locations of source data points. Grey cells show cells used for "true" variability computation. Yellow circles outline SDAI. Cells outside the yellow buffer are those used to estimate the "true" variability. Note that if the cells within a window used for assessing "true" variability fall in an SDAI, they are not used in the computation. Method is explained in text.

In order to assess consistency of GEBCO_08 and S&S datasets the following procedure was used for both datasets. The method is illustrated in Figure 3-7. The computations are carried out in MATLAB.

1. Variability is computed at each grid cell which is based on the source data (cells with black dots in Figure 3-7). Variability is estimated by taking the difference between the depth value within grid cell at the location of source data and the median grid cell value calculated over the narrow Y direction window surrounding the grid cell (not including the center grid cell in the median computation). The same difference is computed in the X direction window (purple cells in Figure 3-7 indicate cells used in computation). The maximum of the two differences values is taken as a variability value. After that, the distribution of all variability values is plotted for each dataset (Figure 4-20).

2. "True" variability is computed at each grid cell in the S&S bathymetry model inside the area

37

of assumed "true" variability. The cells that might fall inside the SDAI are buffered and not included in any computation (yellow cells in Figure 3-7). A similar procedure is carried out in order to calculate a variability value for each grid cell: Y and X direction variability values are compared and the larger of the two is used (grey cells in Figure 3-7 indicate cells used in the computation). After the variability is computed for each grid cell within the TVA, the distribution of all variability values is plotted (Figure 4-20).

3. The variability for each dataset is compared to the "true" variability. The results are provided in Chapter IV.

The challenge lies in the choice of the buffer size of the SDAI and the window size for variability computation. Ideally the buffer should exclude all the grid points influenced by the source data point. The horizontal range of any depth artifact (diameter of the SDAI, Figure 3-6b) depends on the type of the data source which is causing it and can vary with a range of scales. The buffer size chosen was taken from the edge detection map of Figure 3-4b. The maximum radius of source data influence was taken as 10 grid cells.

The window chosen for variability computation should be big enough to capture the values from the area of true variability. The choice of the window is dictated by the inherent resolution of the source data in the area. It is known that in areas where no high-resolution multibeam data is available, the horizontal resolution of the gravity–based S&S product is 20 - 25 km [Smith and Sandwell, 1997]. Therefore, according to the most conservative statement of gravity resolution of 25 km, no variations shorter than 12.5 km (or half wavelength of gravity resolution) are expected to be real in the S&S grid in the areas of no multibeam coverage. (That might not be the case for GEBCO_08, but only in the case when the along-track singlebeam survey is capturing variations shorter than 12.5 km).

The distance of 12.5 km corresponds to approximately 25 pixels in the S&S grid at latitude of 75°N (study area). Therefore the window chosen for S&S is 1x25 pixels in the X and 25x1 in the Y direction. The window chosen for the GEBCO_08 dataset is 1x53 pixels in the X

38

direction and 1x13 pixels in the Y direction. The different window size was chosen to assess variability of GEBCO_08 compared to S&S in order to account for the differences in the physical areas covered by grid cells in different projections (Figure 3-8).
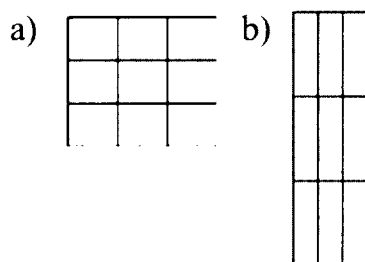
Figure 3-8: Comparison of 3x3 window for two datasets: (a) S&S grid cells in Mercator projection and (b) GEBCO_08 grid cells in geographic coordinate system. For the area of study (75°N) one cell of geographic grid covers approximately two grid cells of the Mercator grid cell in the Y direction, and covers approximately half of a Mercator grid cell in the X direction. In order to adjust the window to cover a similar area in both datasets, in the X direction 53 pixels of GEBCO_08 are used versus 25 pixels in S&S, and in the Y direction 13 pixels of GEBCO_08 are used versus 25 pixels in S&S.

3.3 Assessment of interpolation accuracy

Interpolation accuracy is assessed by considering whether there are correlations between the difference of GIN RAS multibeam grids and analyzed grids versus the distance to the closest source data point. The distance to the nearest source data point grid is created following the method used by Marks et al. [2010]. As noted before, the interpolation accuracy is tested for the S&S and GEBCO_08 grids. The distance grids are created with the same resolution as the original analyzed datasets. As discussed in Section 3.2.2 (Figure 3-8), S&S and GEBCO_08 grid cells have different dimensions. In order to make interpolation analyses performed on grids created in different resolutions and projections comparable, distances to the nearest source point are measured in pixels. Therefore, the distances in the real world covered by S&S and GEBCO_08 grid cells will not be the same, as well as distances in the real world covered by GEBCO_08 grid cell in X and Y directions. For interpolation accuracy assessment it is important to measure distance in pixels, since the source data is block-medianed over the grid resolution

before the interpolation is performed. The distance grids for S&S and GEBCO_08 are provided in Appendix F. An example distance grid is depicted in Figure 3-9.

For the reason of computational efficiency, a slightly different procedure was carried out in order to create a distance grid for the two analyzed datasets. The distance grid for S&S was calculated in GMT. The GMT routine img2grd is provided to extract the locations of grid cells based on source soundings. Source tracklines were extracted separately for each polygon. The GMT routine grdmath was used to create a distance grid with resolution of 1 minute (pixel registration) on a spherical Mercator projection for each polygon.
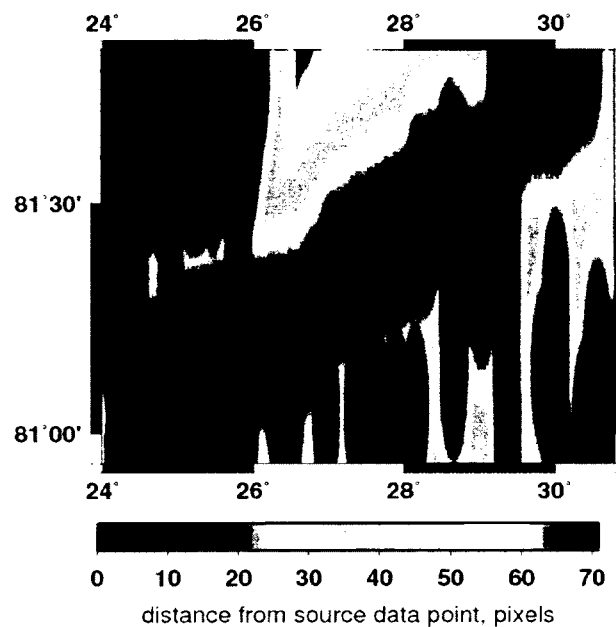
Figure 3-9: Example of a distance grid for the GEBCO_08 dataset, polygon 5. Black points locate source data points used for construction of GEBCO_08 dataset.

A distance grid for the GEBCO_08 grid was calculated in ESRI ArcMap. The source data coverage for the IBCAO grid, and therefore GEBCO_08 grid, was obtained from David Sandwell (personal communication) who used the source data from the IBCAO database in the construction of SRTM30_Plus. The GEBCO_08 source data was provided in xyz format and was extracted separately for each polygon using the GMT routine gmtselect. The distance was calculated using the ArcMap Spatial Analyst Toolbox (Distance > Euclidean Distance). The corner

40
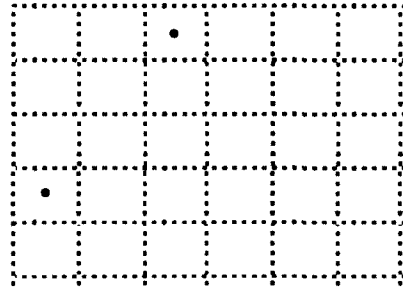
Figure 3-10: Illustrates solution for edge problem. Grey grid illustrates original GEBCO_08 grid. Blue grid illustrates distance grid created in ArcMap based on xyz source data points (black points). In order to provide an exact match between the distance grid and the original grid, as well as to cover the same area of interest, an artificial data point (red) was added in the upper left corner of the xyz trackline file (center of upper left grid cell), so that the location of it will define the exact same grid as the original GEBCO_08 grid.

coordinates for the ArcMap grid are defined by the most northern point and most western points in the extracted trackline dataset (or upper left corner) (Figure 3-10). Exact coincidence between grid cells in the original grid and distance grid is needed for interpolation assessment. In order to provide exact alignment of grid cells in the distance grid with grid cells in the GEBCO_08 grid, an artificial data point was added in the upper left corner of each polygon. Coordinates for the data point were taken from polygon corner coordinates, the same registration as in the original grid was used – the data point was located in the center of the grid cell (Figure 3-10). A distance grid with a resolution of 30 arc seconds in geographic coordinates was created for each polygon. After that, it was exported to GMT for further computation.

In order to assess interpolation accuracy, differences between GIN RAS multibeam grids and analyzed grids versus distance to the nearest source data point plots were created for S&S and GEBCO_08 grids. The GMT routine grdtrack was used to sample distance values from the created distance grids at each location and the depth difference with GIN RAS multibeam grid. Difference with GIN RAS multibeam grid versus distance plots are provided in Chapter IV.

41

CHAPTER IV

RESULTS

4.1 General comparison between the analyzed grids in the region: expected and unexpected differences.

Visual comparison of bathymetry for six analyzed grids confirms the expected similarity between datasets of Type A (Figure 4-1b) and some differences in Type B datasets (Figure 4-1a). As can be seen from Figure 4-1, Type A datasets portray a smoother appearance as compared to Type B datasets which have artificially rough morphology on shelf areas caused by trackline artifacts (red arrows, Figure 4-1a). At the same time, grids based on satellite altimetry resolve seamounts unresolved by grids based solely on acoustic sounding data sources (red circles, Figure 4-1a). Figure 4-2 shows the ship trackline coverage used for construction of the grid. Ship trackline artifacts and resolved seamounts can be seen to be a direct result of source coverage.

The depth difference maps depicted in Figure 4-3 reveal similarities between GEBCO 1 minute and GEBCO_08 (Figure 4-3d) and unexpected discrepancies between SRTM30_Plus and S&S in the Greenland shelf north of 79°N (Figure 4-3a). The difference map between SRTM30_Plus and GEBCO_08 (Figure 4-3b) reveals that this difference is due to the "patching in" of GEBCO_08 into the SRTM30_Plus in Area 1. Another noticeable patch is observed in Area 2 (Figure 4-3b), where GEBCO_08, SRTM30_Plus and S&S have the same values and (consequently) zero differences. Difference maps also show that in Area 3 there is a step in the bathymetry of both SRTM30_Plus and S&S datasets (Figure 4-3(b, c)). This "patching" causes artifacts in other regions as well, which can be seen in Figure 4-1a (blue arrow).

The histogram of depth distribution for the analyzed datasets (Figure 4-4) shows that Type B datasets have more continuous depth distribution than Type A, while Type A distribution

42

exhibits spikes at the IBCAO contour values. As can be seen from Figure 4-4a, the shape of all three distributions of Type A datasets is similar, with the counts changing according to the resolution, a consequence of all datasets being based on the IBCAO source data.

The Type B datasets show similar depth distribution. Spikes in the shallow 0 to 250 m water depths for these two datasets might be explained by adopting IBCAO contours for the shallow regions (Figure 4-5).

Grids of Type A visually have a smoother appearance compared to the grids of Type B owing to the large number of artifacts in Type B bathymetry. At the same time, grids based on satellite altimetry often depict seamounts not resolved by grids based solely on acoustic sounding data sources. The global depth distribution in Type B datasets is smoother than in Type A datasets, which have depth values biased towards the IBCAO contour values.

IBCAO v.2.23

SS v.13

SRTM30_Plus v.6

Projection North Polar Stereographic
Central Meridian Greenwich
Latitude of origin 90 N
True Scale at 75 N

Depth in meters:

-6000   -4000   -2000   0   2000
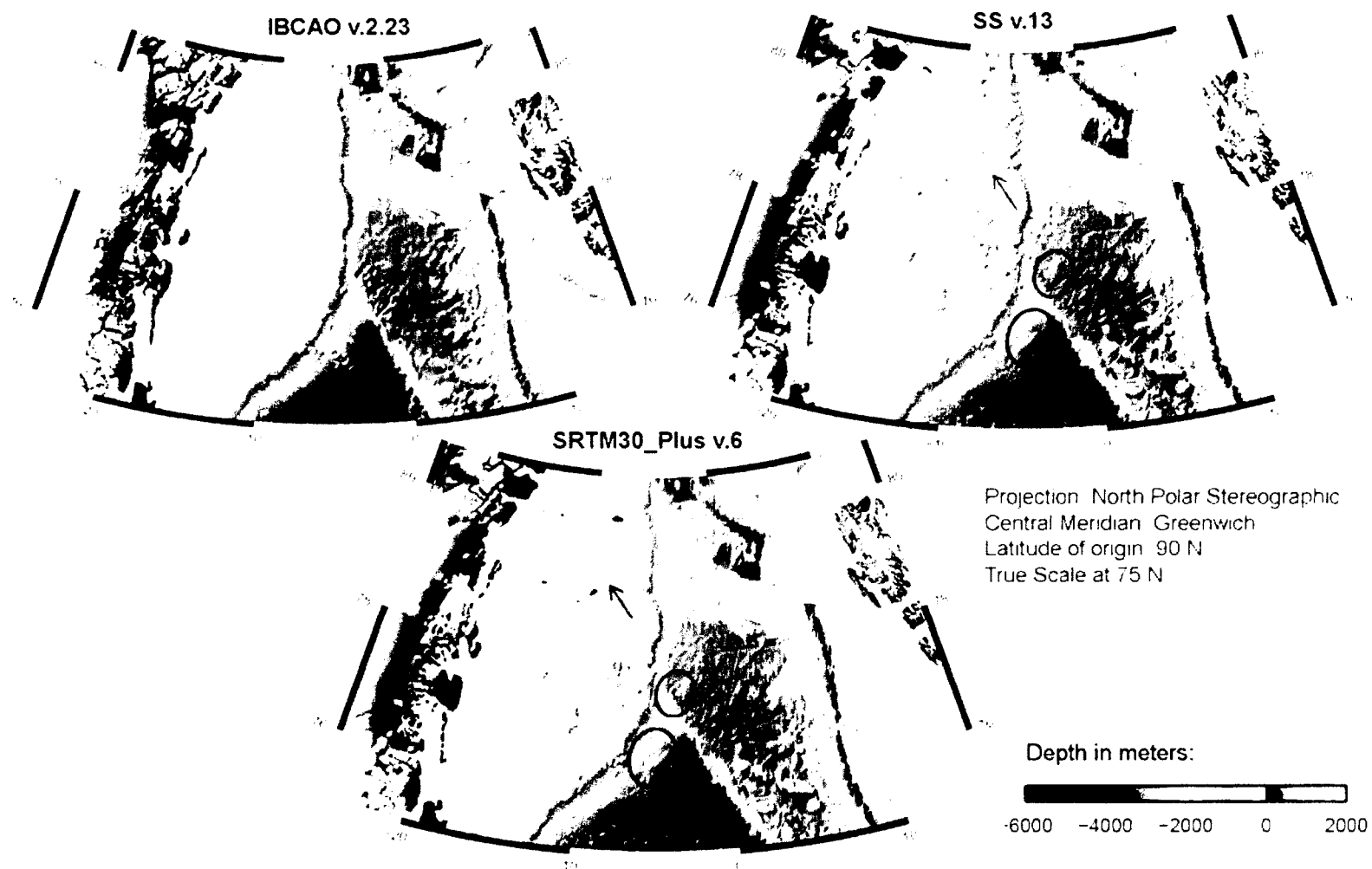
Figure 4-1: (a) Visual differences and similarities between analyzed datasets in the area of Norwegian-Greenland Sea: between IBCAO, S&S and SRTM30_Plus grids. Circles and arrows are explained in the text.
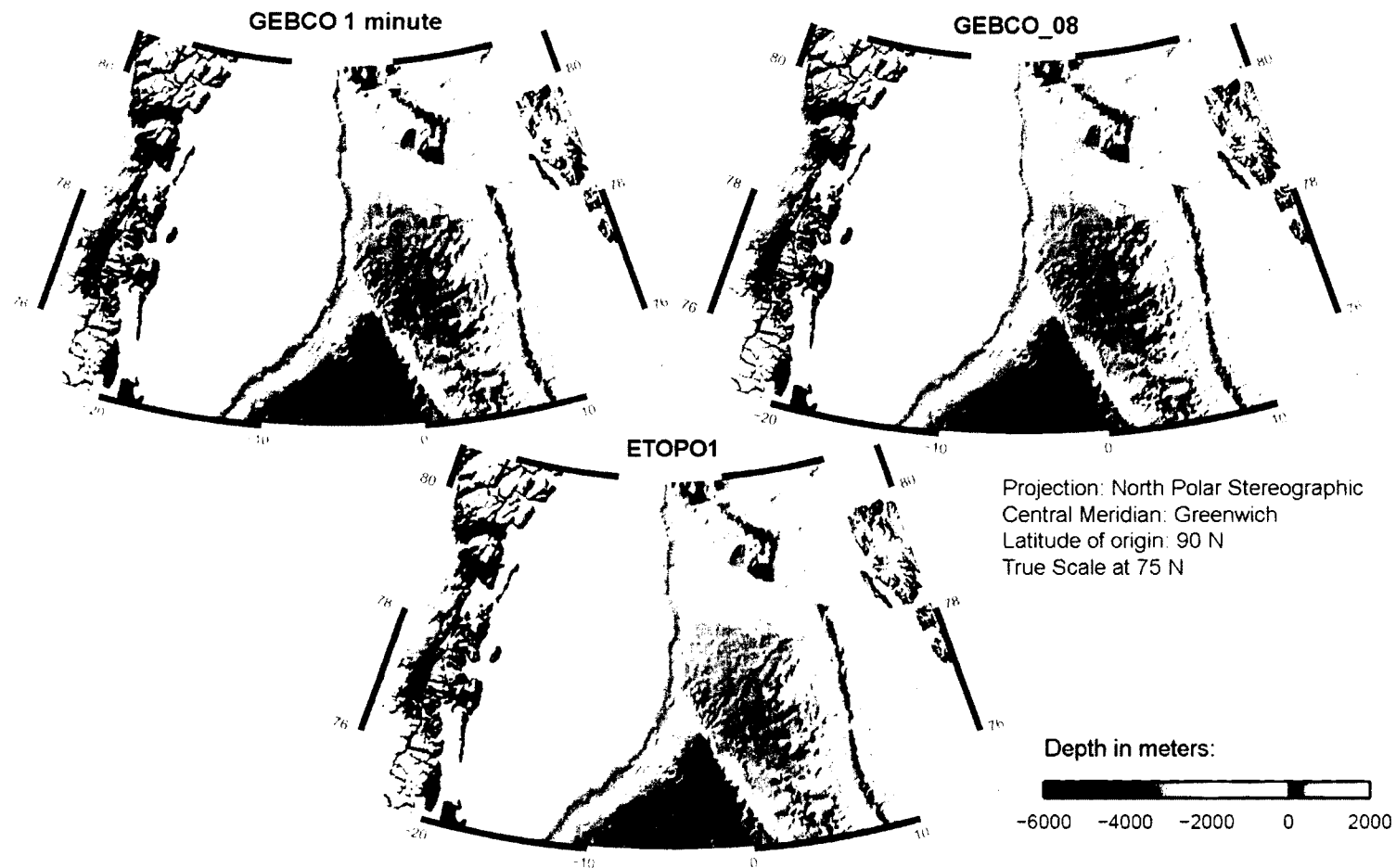
Figure 4-1 (continue): (b) Visual similarities between analyzed datasets in the area of the Norwegian-Greenland Sea: between GEBCO 1 minute, GEBCO_08 and ETOPO1 grids.
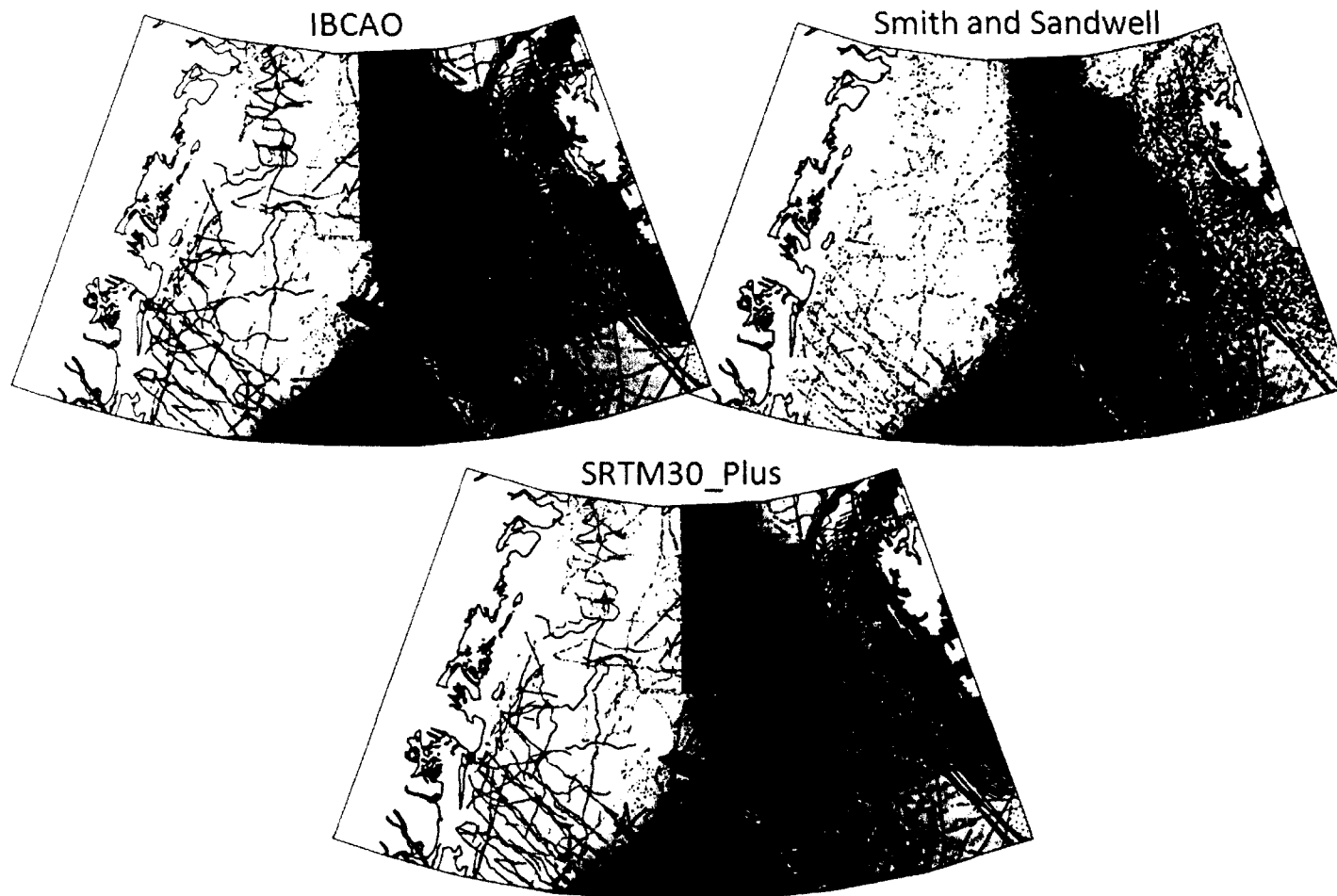
Figure 4-2: Source data coverage used in the construction of the grids in the area in Figure 4-1. Tracklines are overlaid on shaded relief bathymetry of the corresponding grid. Overall all grids have very similar source data and only few differences can be noticed in the source data coverage. Observed differences of source data density is mainly due to gridding the source data over different cell sizes: source data is already gridded over the corresponding grid resolution, e.g. IBCAO over 2 km in polar stereographic projection, S&S over 2 km in Mercator projection and SRTM30_Plus over 30 arc sec in geographic coordinate system.
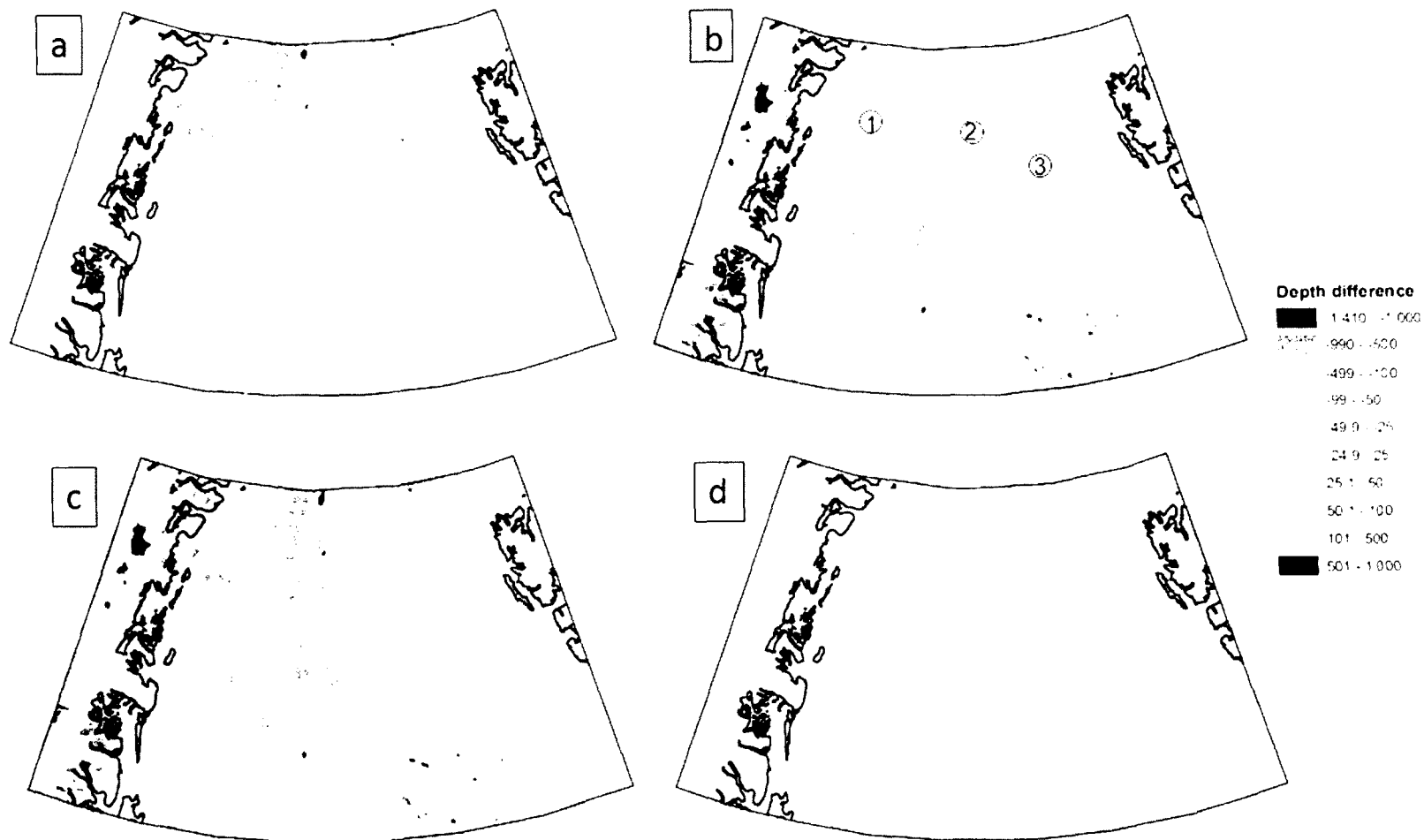
Figure 4-3: Results of surface difference (in meters) between the grids which are expected to be similar, such as (a) S&S minus SRTM30_Plus, (d) GEBCO 1 minute minus GEBCO_08, and the grids which are expected to be different such as (b) SRTM30_Plus minus GEBCO_08 and (c) S&S minus GEBCO_08. Areas 1, 2 and 3 on (b) are discussed in text.

a)

b)

■ GEBCO_08   GEBCO 1 min ■ IBCAO   ■ Smith & Sandwell   SRTM30_Plus
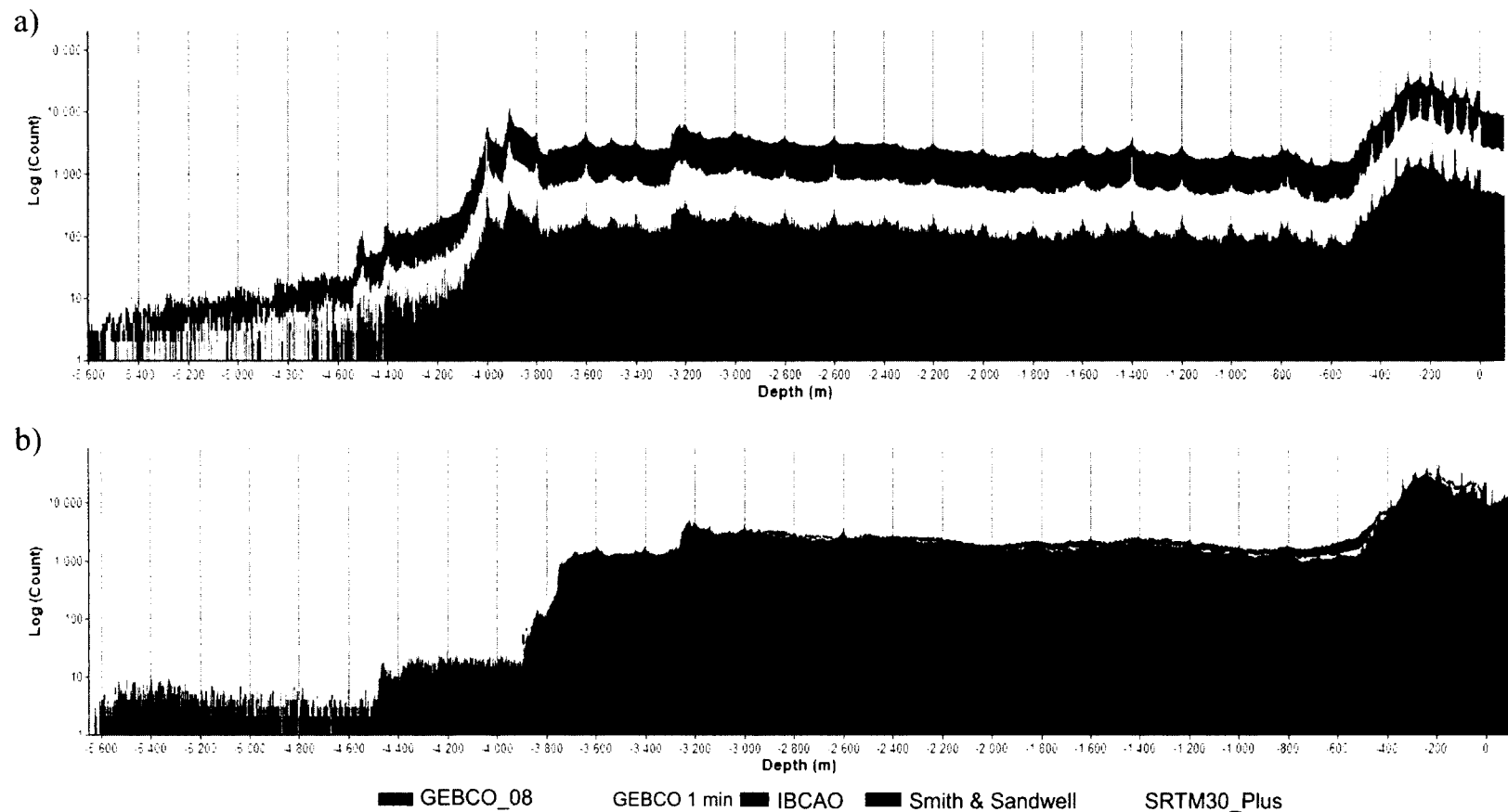
Figure 4-4: Comparison of depth distribution between analyzed datasets: (a) between IBCAO 2 km grid, GEBCO 1 minute and GEBCO_08 for the region 30°E-52°W 64°N-85°N, (b) between S&S, GEBCO_08 and SRTM30_Plus for the region 30°E-52°W 64°N-80°N. See Figure 4-5 for separate histograms of S&S, SRTM30_Plus and GEBCO_08.

Depth distribution of Smith & Sandwell grid in the study area

Depth distribution of SRTM30_Plus grid in the study area

Depth distribution of GEBCO_08 grid in the study area
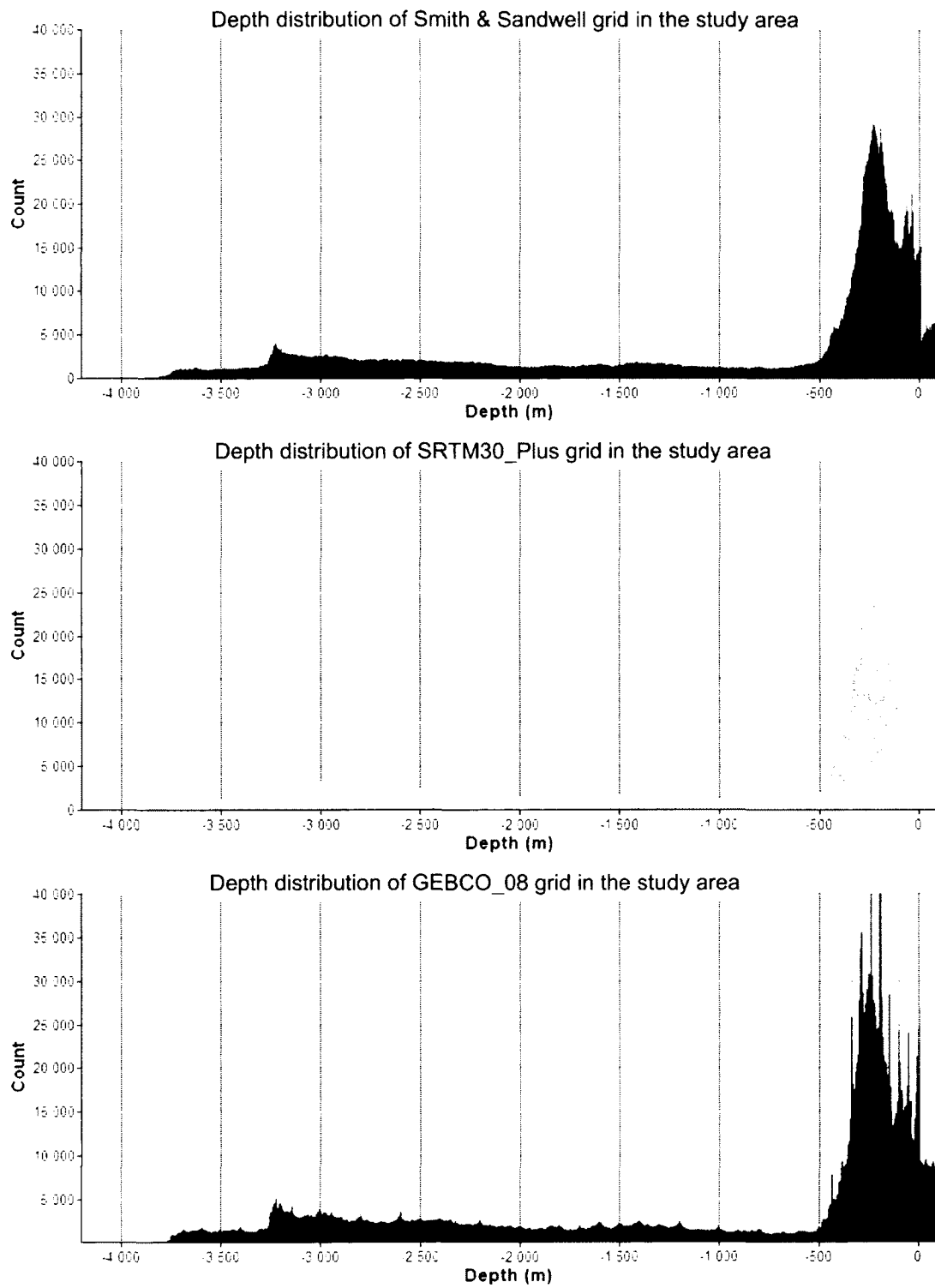
Figure 4-5: Separate histograms of depth distribution for S&S, SRTM30_Plus and GEBCO_08 grids (see group histogram for all three grids in Figure 4-4b).

49

4.2 Accuracy assessment (comparison with multibeam data)

4.2.1 GIN RAS multibeam data uncertainty and accuracy estimates

GIN RAS multibeam sonar bathymetry grids are used in this study as ground truth. The differences between GIN RAS multibeam grids and the analysed bathymetry grids is used as a measure of accuracy. Meanwhile, an estimate of uncertainty range for GIN RAS grids is necessary in order to determine which differences are considered significant. The uncertainty of GIN RAS multibeam sonar grids is not assessed in this study. The uncertainty of the gridded surface is affected by vertical and horizontal uncertainties of each sounding, together with the slope. The estimated worst case total propagated uncertainty of GIN RAS raw multibeam sonar data is used as a measure of confidence level for GIN RAS multibeam sonar grids.

In order to get rough estimates of GIN RAS multibeam soundings uncertainty, sample raw multibeam data and sound speed profiles were provided by the Geological Institute Russsian Academy of Sciences. The sample raw multibeam data was processed in CARIS HIPS & SIPS. Sixteen survey lines were selected in depths ranging from 380 m to 5100 m. The values for sensor offsets were taken from the *Strakhov* cruise reports. These values are provided in Appendix B.1. Depths were processed and horizontal and vertical total propagated uncertainty (TPU) values were computed for each sounding. In order to get estimates of uncertainty for the range of depths of interest, 16 subsets of 15 swaths (pings) were selected (Figure 4-6). Only beams ranging from 60 to 190 within a swath were used in the computation because the outer beams are usually filtered due to the poor quality. Each swath consisted of approximately 130 soundings.

The uncertainty budget for each sounding is mainly a function of vertical and horizontal uncertainties together with the local slope. The TPU for each GIN RAS multibeam sounding was calculated according to the formula:

$$TPU = \sqrt{(\text{vertical TPU}^2 + \text{horizontal TPU}^2 \times \tan^2 \text{slope})}$$

50
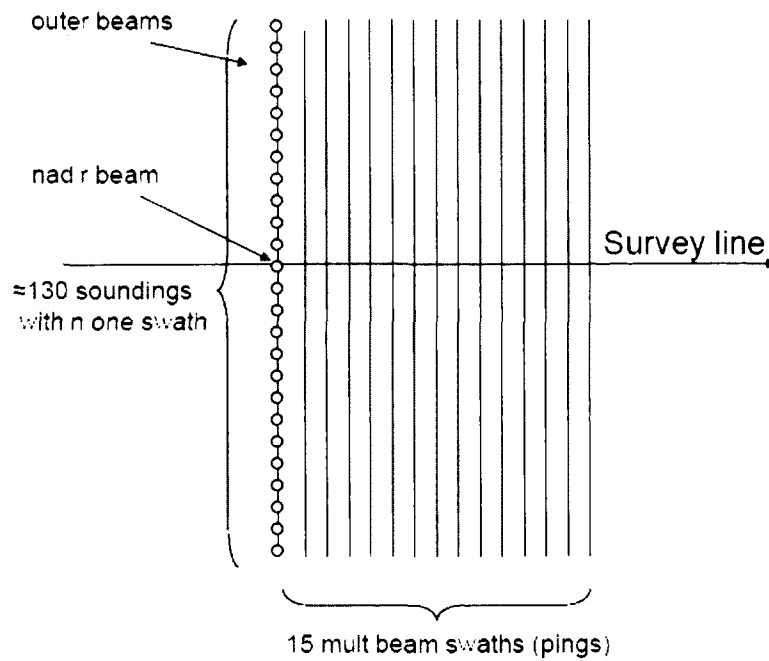
Figure 4-6: Illustrates schematically one subset of 15 multibeam swaths.
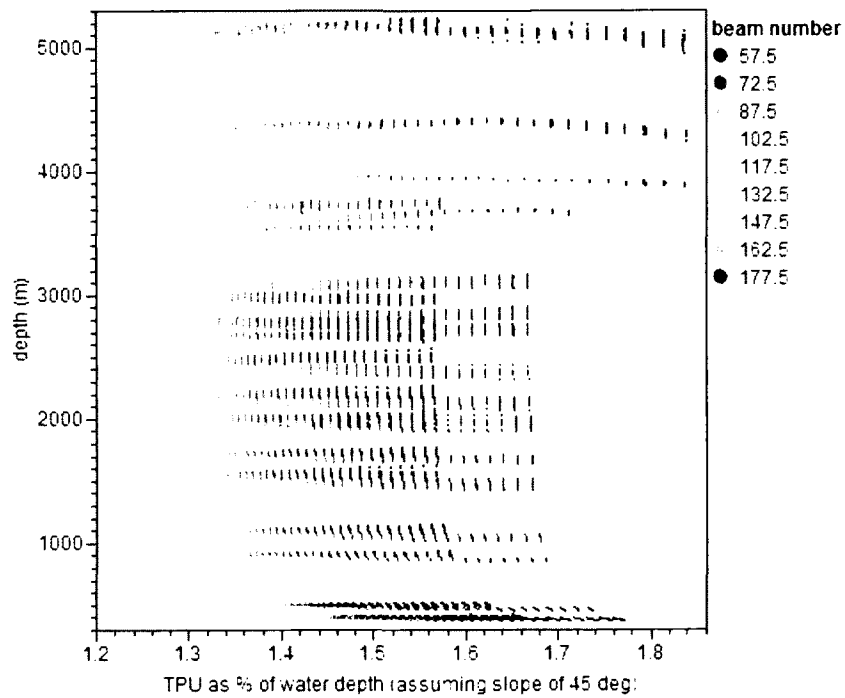
Figure 4-7: TPU values calculated for each GIN RAS multibeam sounding according to the formula in the text, slope of 45° is used. TPU values for sixteen subsets of multibeam swaths (Figure 4-6) colored by beam number are shown.

51

Each study polygon is characterized by different slope distribution, ranging from 0° to 45° in a few areas of very rough morphology (polygon 1 and 5). The mean slope for the polygons varies from 0.06° (polygon 4) to 5.2° (polygon 5).

The worst case TPU estimates of GIN RAS multibeam data were estimated according to the TPU values of the outer beams, which have the highest uncertainties, and assuming a slope of 45°. Figure 4-7 illustrates the TPU values computed for each sounding. As can be seen from Figure 4-7, the outer beams have maximum TPU of 1.85% of water depth (WD). For comparison, the TPU computed for GIN RAS soundings, assuming a slope of 5.2 degrees (mean slope in polygon 5) have a maximum value of 1.05% of WD.

In order to check the overall accuracy of the GIN RAS multibeam gridded data, it was compared to gridded multibeam data from independent surveys of USCGC *Healy* and RV/Icebreaker *Oden*. The USCGC *Healy* data from HLY0503 (August - September 2005) was obtained from US NGDC online delivery. The *Healy* data was available as raw SeaBeam files prefiltered of major outliers in MBsystem [HLY0503 Cruise report]. According to the cruise report [HLY0503 Cruise report], all the sensor offsets were applied during the acquisition, which made it possible to carry out editing using CARIS HIPS & SIPS. Several transit lines which had overlap with the GIN RAS multibeam surveys were cleaned of outliers. Sound speed corrections were applied using the SSP profiles available for the same area and season from the GIN RAS cruises. The cleaned soundings were gridded to 20 m resolution grid in UTM32N WGS84 coordinate system. The results of depth differences with the GIN RAS gridded multibeam data are presented in Table 4.1

The RV/Icebreaker *Oden* gridded multibeam data was obtained from the *Oden* Mapping Data Repository at Stockholm University. Small subsets of publicly available multibeam bathymetry grids from cruises LOMROG2007 [Jakobsson, Marcussen et al., 2008; Jakobsson et al., 2010] and SAT0809 2008 had overlapped the GIN RAS multibeam surveys. The grids were available in polar stereographic projection (true scale at 75°N) (SAT0809) and in geographic

coordinate system (LOMROG2007) and were regridded into UTM32N in order to compute surface differences. The results of depth difference with GIN RAS gridded multibeam data can be seen in Table 4.1.

Research vessel	cruise index	difference statistics, m		difference grid cell size, m	original grid coordinate system*	acquisition dates	aquistion system	depth range, meters
		mean	std					
Oden	SAT0809	6.14	18.07	29.4	geographic	Sept 2008	EM 122	-2500 to -5300
Oden	SAT0809	8.24	68.83	30.4	geographic	Sept 2008	EM 122	-1100 to -2600
Oden	LOMROG2007	-0.19	14.85	100	PS 75N	Sept 2007	EM 120	-300 to -900
Healy	HLY0503	-3.71	36.43	20	UTM32N	Sept 2005	SeaBeam 2112	-2000 to -3400
					*all are in WGS84			

Table 4.1: Statistics for the depth differences in meters between GIN RAS multibeam grid, *Oden* multibeam grid and *Healy* multibeam grid. Depth difference calculation was carried out in Fledermaus. *Healy* and *Oden* multibeam grids were subtracted from the GIN RAS multibeam grid.

Comparison between GIN RAS multibeam grids with USCGC *Healy* gridded multibeam data and RV *Oden* gridded multibeam in one of the study areas shows no systematic errors in the GIN RAS data. The means of the differences are negligible (Table 4.1) and are within the uncertainty of the GIN RAS multibeam data which implies that the GIN RAS multibeam does not appear to contain serious systematic errors and can be used as a ground truth in the study. The estimated worst case uncertainty for the GIN RAS multibeam data comprises around 1.85% of WD at 95% confidence level.

4.2.2 Source data accuracy for analyzed datasets

Difference values with GIN RAS gridded multibeam are used as the measure of accuracy as follows (Chapter III discusses the method). The analysis was performed for IBCAO and S&S source data. As discussed in Chapter II, Type A datasets are all based on IBCAO source data, and Type B datasets share the same source data but are gridded in different coordinate systems. Source data for IBCAO and S&S is available only as averaged source data values over the cell of the corresponding grid, here referred to as a gridded source data. Accuracy of the gridded source

data is assessed by taking the difference between the GIN RAS multibeam gridded values and the source values of the corresponding grid cell (the latter is subtracted from the former).

The source data coverage for the IBCAO grid was available from David Sandwell and is assumed to be the data on which the current version of IBCAO is based. The source data coverage for the S&S grid was derived from the S&S bathymetry grid as encoded in the S&S odd depth values. According to the construction procedure for the S&S dataset (Chapter II), the values in the grid were replaced by the original source values in the grid cells based on source sounding data.
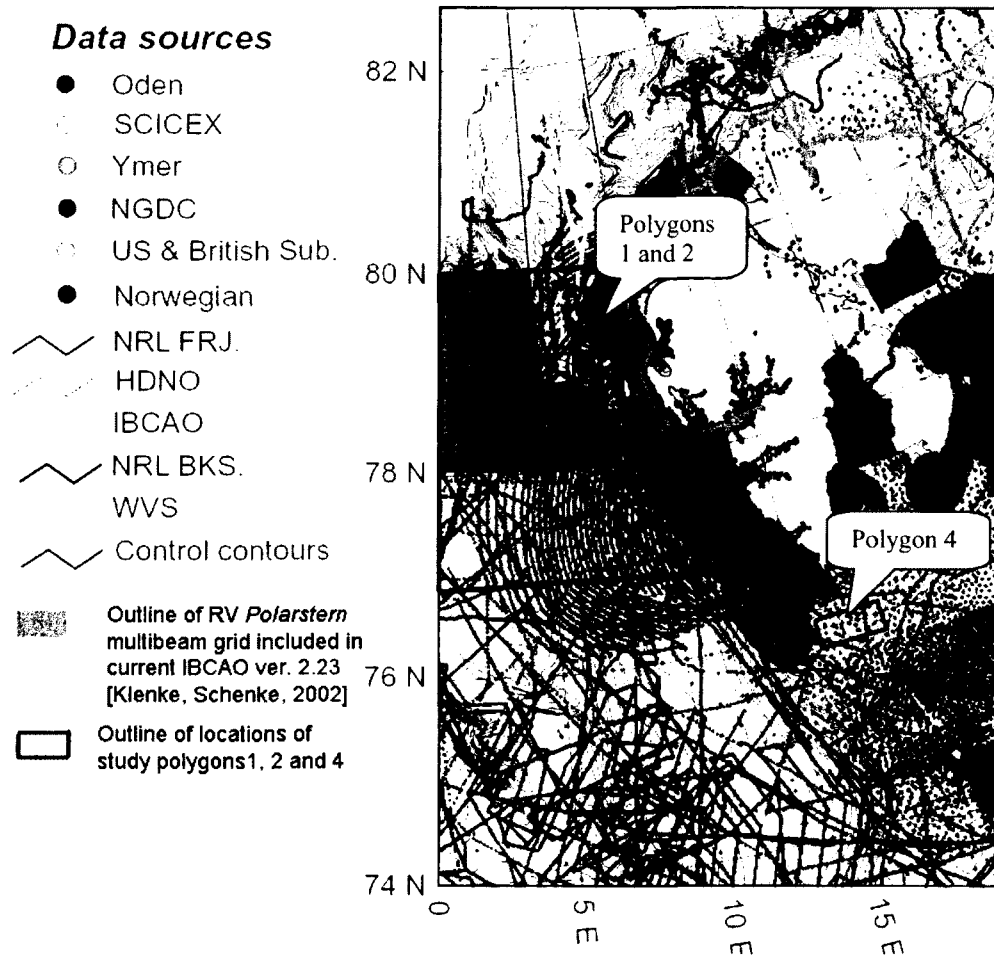
Figure 4-8: Source data coverage for the IBCAO ver.1.0 (2001) database available from [Jakobsson et al., 2002]. The grey polygon outlines RV *Polarstern* multibeam grid included into IBCAO ver.2.23. The red polygons outline location of study polygons 1, 2 and 4. The published map does not provide coverage for the polygons 3, 5 and 6.

A comparative analysis was performed for four of the six study polygons (Figure 2-4, Table 2.2). The polygons include 1, 2, 3 and 4. Polygons 5 and 6 are not used in the comparison because available source data was not complete for those regions (see Appendix C, Figures C.5, C.6, C.11, C.12; additionally the count of source data points was not high enough to calculate useful statistics).

Each study polygon is represented by one or several types of data sources (Table 2.2, Figure 4-8). The source data types were derived from Jakobsson et al. [2002, 2008], but are assumed to be very similar for both S&S and IBCAO datasets. For the construction of IBCAO and S&S grids the following data sources are used (Table 2.2): RV *Polarstern* multibeam grid [Klenke and Schenke, 2002] (polygon 1), Norwegian single soundings and NGDC singlebeam data (polygon 2) [Jakobsson et al., 2002], Norwegian Petroleum Directorate multibeam data [Jakobsson et al., 2008] (polygon 3), and Norwegian single soundings (polygon 4). Additionally, GEBCO_08 contour data from various data sources was used in construction of IBCAO (Figure 4-8) within polygon 2. These data sources have different accuracies, and ideally each data source should be assessed separately. This study is limited to assessment of source data accuracy on a polygon by polygon basis, for the lack of data separated by the source.

The results of differences between source data and GIN RAS multibeam data for each polygon are summarized in Table 4.2 for IBCAO source data and in Table 4.3 for S&S source data. The histogram of differences is shown in Figure 4-9.

A bias of 50 m in depth difference is observed in the S&S source data in polygon 1 (Figure 4-9). This polygon covers Area 3 (Figure 4-3), where a step in the bathymetry of S&S and SRTM30_Plus is observed. As noticed before, the source data for polygon 1 in both S&S and IBCAO datasets is a multibeam grid based on RV *Polarstern* multibeam surveys between 1984-1997 [Klenke and Schenke 2002, 2006]. Figure 4-10 and Figure 4-11 illustrate the distribution of source data points and difference values with GIN RAS multibeam for IBCAO and S&S respectively at polygons 1 and 2. Within polygon 1 IBCAO source values have near zero

55

differences, whereas S&S has a consistent bias of 50 m in the area (the grid is ~50 m deeper than

the GIN RAS multibeam). Personal correspondence with the authors of the grids revealed that in

the case of IBCAO, the proper sound speed for the area was applied to the *Polarstern* multibeam

grid before incorporating it into the final grid. In the case of S&S data, the *Polarstern* multibeam

grid was included in the final grid without any post processing. According to [Klenke and

Schenke, 2002], for the construction of the *Polarstern* multibeam grid the mean sound speed of

1500 m/s was assumed, although the authors note that the local sound speed profiles could be

applied to the dataset later.
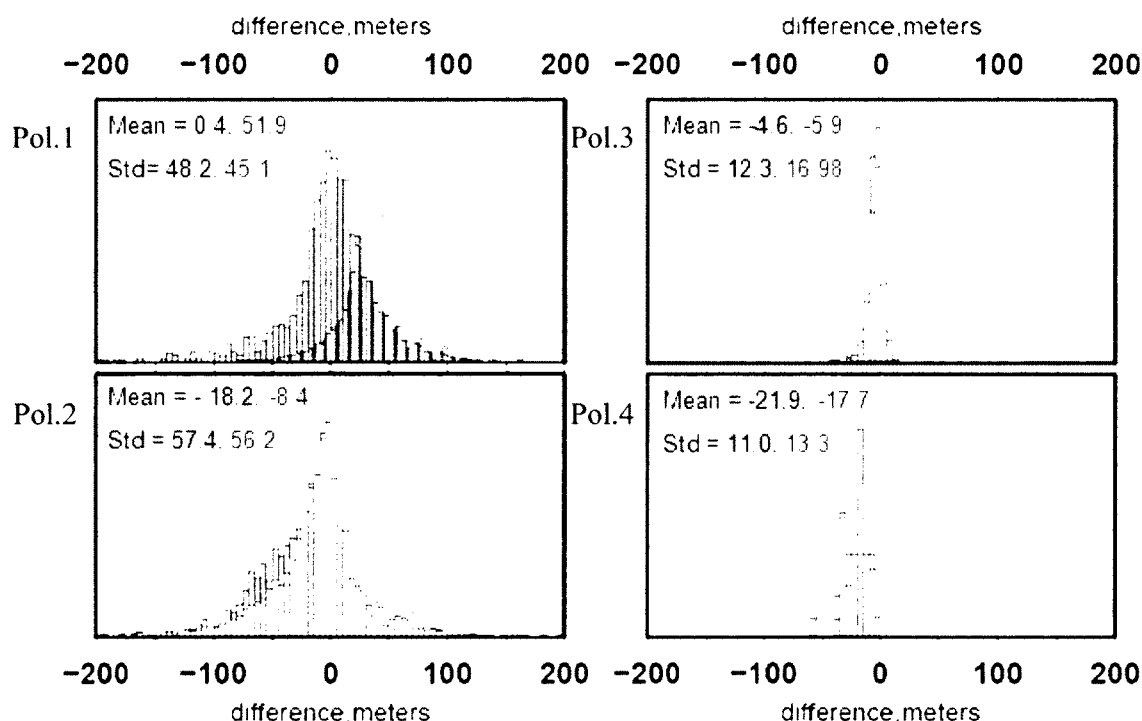
Figure 4-9: Histogram and main statistics in meters for the depth differences between
GIN RAS multibeam values and source data values of IBCAO (grey) and S&S (red) at
the polygons 1, 2, 3 and 4. Detailed statistics are given in Tables 4.2 and 4.3.

The comparison revealed negative bias in the depth difference of the S&S and IBCAO

source data with GIN RAS multibeam for polygons 2 and 4 (Figure 4-9). This implies that source

data values are shallower than the GIN RAS multibeam values, since the former is subtracted

from the latter. The bias is caused by the presence of Norwegian single soundings at these two

56

polygons. A comparison of the source data coverage (Figure 4-8) to the map of source data differences (Figure 4-10 and Figure 4-11) reveals that Norwegian single soundings, for the most part, have negative differences with the GIN RAS multibeam. This fact explains the negative bias in the polygon 4, where only Norwegian data sources are used. The bias in the means of differences of 20 m (Figure 4-9) could possibly be due to the sound speed applied.

Lastly, it can be noticed that source data coverage for the S&S and IBCAO grids is quite similar for polygons 1 and 2 (Figure 4-10 and Figure 4-11). Several common tracklines (mainly NGDC data, Figure 4-8) have noticeable bias in S&S, but are less biased in IBCAO. This could imply that sound speed corrections were applied to this data before including it in the IBCAO dataset, which was not done for S&S. This reflects differences in the approaches of postprocessing the data before including it into the final product.

Polygon No	Count	Min	Max	Mean	Standard Deviation	Mean depth
1	1638	-236.82	371.62	0.35	48.17	-2700
2	2641	-495.67	634.74	-18.19	57.41	-2300
3	1151	-110.68	206.03	-4.63	12.26	-2800
4	36	-59.89	-3.69	-21.95	11.00	-350

Table 4.2: Statistics in meters for the depth differences between GIN RAS multibeam grids and IBCAO source gridded values

Polygon No	Count	Min	Max	Mean	Standard Deviation
1	54866	-527.89	587.30	51.92	45.04
2	6172	-551.95	652.69	-8.39	56.23
3	2137	-355.24	174.61	-5.90	16.98
4	44	-57.87	25.87	-17.66	13.30

Table 4.3: Statistics in meters for the depth differences between GIN RAS multibeam grids and S&S source gridded values

57
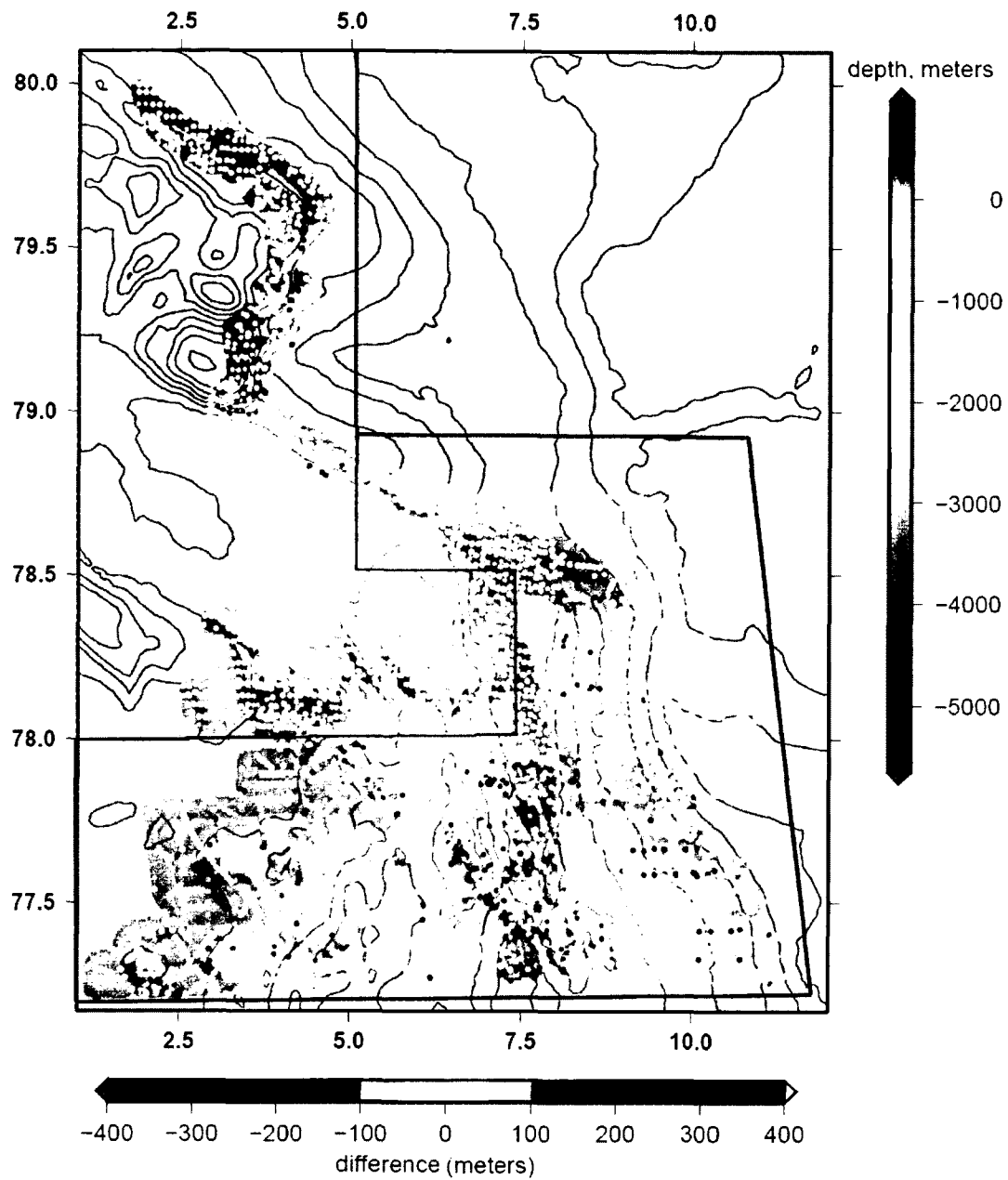
Figure 4-10: Map of differences between GIN RAS multibeam gridded values and IBCAO gridded source values overlain over GIN RAS multibeam bathymetry and IBCAO contours. Black and blue polygons outline Polygons 1 and 2 respectively.
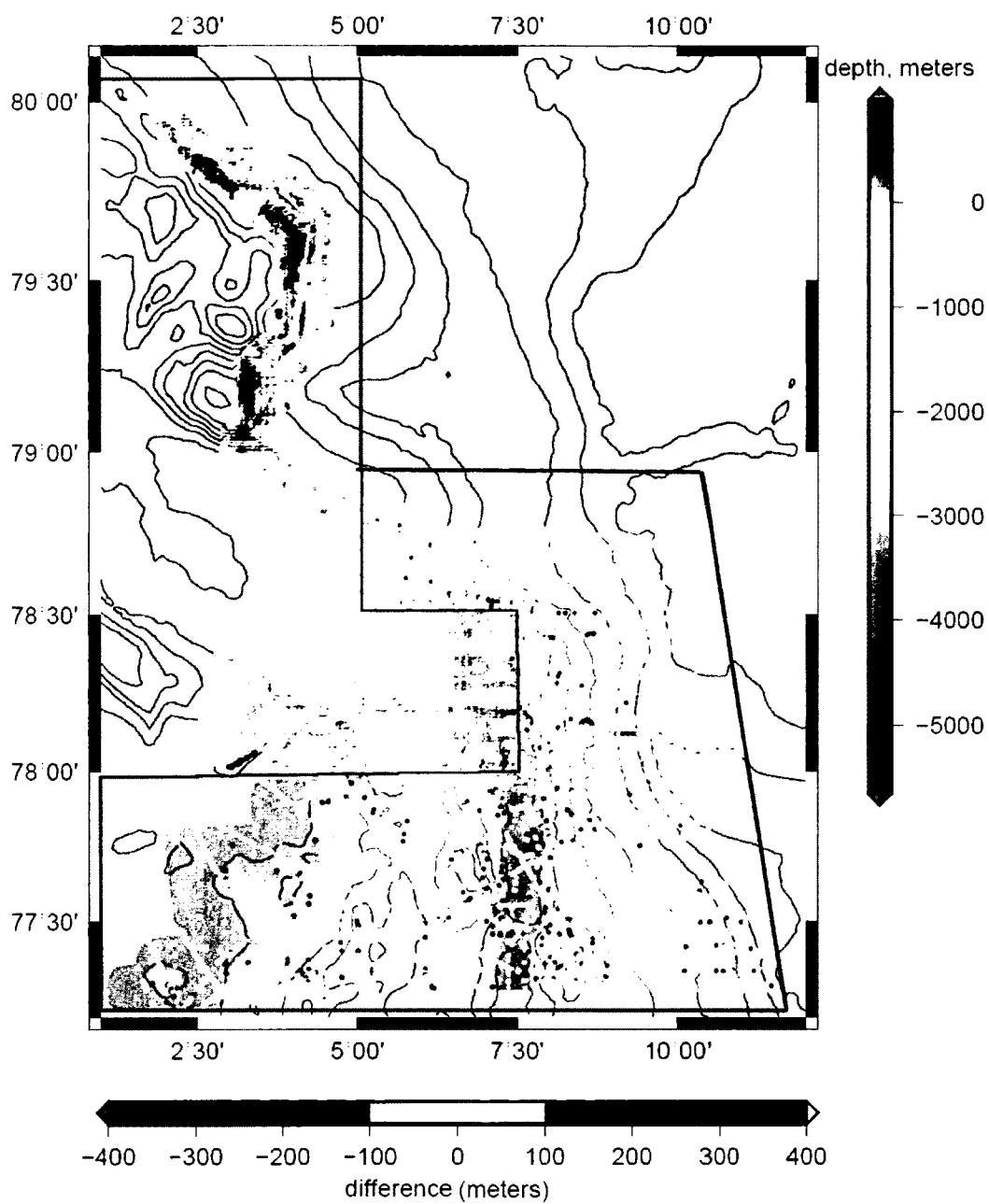
Figure 4-11: Map of differences between GIN RAS multibeam gridded values and S&S gridded source values overlain over GIN RAS multibeam bathymetry and IBCAO contours. Black and blue polygons outline Polygons 1 and 2 respectively. Positive bias in depth difference within polygon 1 is discussed in the text.

The accuracy of source data was tested by comparison of IBCAO and S&S source data with GIN RAS multibeam data in four polygons (polygons 1, 2, 3, and 4). Within the four analyzed polygons, Type A and Type B datasets have very similar data source coverage (figures in Appendix C): within polygons 1 and 3 the grids are based on multibeam data; within polygons 2 and 4 the grids are based primarily on Norwegian single soundings (polygon 4) or Norwegian data sources together with NGDC singlebeam data (polygon 2). The comparison revealed that Norwegian data sources (in polygons 2 and 4) are in general shallower than the GIN RAS multibeam data and NGDC data is possibly deeper than GIN RAS multibeam data. A considerable bias is observed in S&S source data at polygon 1. These results show the consequences of different postprocessing (possibly sound speed corrections) applied to the source data before incorporating it into the grids.

4.2.3 Depth accuracy of GEBCO_08, S&S and SRTM30_Plus

The accuracy of the bathymetry grids is assessed by taking the difference between the GIN RAS multibeam gridded values and the bathymetry grid values at the corresponding grid cells (the latter is subtracted from the former). The analysis was performed for GEBCO_08, S&S and SRTM30_Plus, since these are the three datasets where differences are expected (See chapter III). The comparison was performed for six study polygons (Figure 2-4) for GEBCO_08 and SRTM30_Plus. Only five polygons (1 through 5) were within the coverage of S&S dataset, which is limited to South of 80°N.

The six study polygons cover different morphological provinces (Table 2.2): mid oceanic ridge (polygons 1, 2), abyssal plain (polygon 3), shelf area (polygons 4, 5) and continental slope (polygon 6). Besides differences in morphology, these polygons cover areas with different types of source data, as discussed in the Section 4.2.2. These differences in source data accuracy, source data coverage, morphology, together with interpolation method will affect the final accuracy of the output bathymetry surface.

Statistics of the absolute surface difference are provided in Tables 4.4, 4.5 and 4.6. The

60

results of differences as a percentage of WD are provided in Tables 4.7, 4.8 and 4.9. The histogram of differences can be seen in Figure 4-12 and Figure 4-13. The resultant maps of differences for each polygon are given in Appendix D.

From the Figure 4-12 and Figure 4-13 can be seen that GEBCO_08 performs similar to S&S and SRTM30_Plus at the polygons 2 and 3, and differences are observed at the polygons 1, 4, 5 and 6. A bias is observed in S&S and SRTM30_Plus at polygon 1, where the error in source data (discussed in Section 4.2.2) caused bias of 1.95% of WD in these two grids. This bias can be considered significant according to the worst case TPU of GIN RAS multibeam data. Bias in the mean of differences is observed for all three grids at the polygons 2 (1% - 1.3% of WD depending on the grid) and 4 (6.7 - 8.2% of WD depending on the grid), which is also caused by the bias in the source data (Section 4.2.2). The bias in the polygon 2 is not significant compared to the estimated worst case TPU of GIN RAS multibeam data. GEBCO_08 has much narrower depth difference distribution compared to S&S and SRTM30_Plus at three polygons (4, 5 and 6). Better performance of GEBCO_08 in the shelf polygons (5) and on the slope (6) could be caused by presence of multibeam data sources in GEBCO_08 grid which are not present in S&S at these polygons.

The other factor affecting final surface accuracy is the interpolation method. As discussed in the previous section, S&S has less biased source data at polygons 2 and 4 compared to GEBCO_08 (same as IBCAO). Comparing the statistics of the source data accuracy (Figure 4-9) to the accuracy of the final surface (Figure 4-12), the means and standard deviations of differences for polygons 2 and 4 worsened considerably in S&S, especially at polygon 4 on the shelf. The fact that the source data was relatively accurate implies that the interpolation method added error into the surface [Wechsler and Kroll, 2006]. The differences at the shelf exceed 25% of WD for polygon 4 and exceed 40% for polygon 5 in S&S and SRTM30_Plus grids (Figure 4-13). Additionally, a slightly narrower histogram of differences is observed in S&S and SRTM30_Plus within polygons 1 and 2 (Figure 4-13). These two polygons cover the area of mid

oceanic ridge; this might imply slightly better precision of S&S and SRTM30_Plus in deep water.

As discussed before, S&S and SRTM30_Plus are based on the same source data, but gridded in different resolutions and projections. It was interesting to see whether there were differences between the output grids. As can be seen from Figure 4-12, S&S and SRTM30_Plus perform in a similar manner at all five polygons, although the distribution is slightly narrower for SRTM30_Plus at polygons 4 and 5. Overall, SRTM30_Plus performs slightly better on the shelf area, probably because of finer grid resolution.

Comparison with the high-resolution and accuracy, independent GIN RAS multibeam data revealed that GEBCO_08 is more accurate than S&S over three of the six polygons, which include mid oceanic ridge, shelf and continental slope areas (polygons 1, 5 and 6). The observed differences in the accuracy between GEBCO_08 and S&S are due to the source data accuracy for polygon 1, better source data coverage in GEBCO_08 for polygons 5 and 6, and poor performance of the interpolation in the shelf areas for S&S at polygons 4, 5 and 6. SRTM30_Plus has very similar accuracy to S&S in all the polygons except in the shelf polygons 4 and 5, where it performs slightly better. The observed bias for all three grids at the polygons 2 and 4 is caused by the bias in the Norwegian data sources. These results show that source data accuracy and coverage, together with interpolation affect the accuracy of the final output bathymetry surface.

Polygon No	Count	Min	Max	Mean	Standard Deviation
1	54548	-360.53	472.62	0.84	53.14
2	123063	-995.43	591.09	-27.59	69.74
3	26592	-255.84	282.80	-5.69	13.84
4	4915	-51.92	18.81	-23.46	7.59
5	2185	-218.61	132.79	-11.88	54.74
6	19917	-629.36	396.91	7.52	120.43

Table 4.4: Statistics in meters for the depth differences between GIN RAS multibeam grids and GEBCO_08 grid.

Polygon No	Count	Min	Max	Mean	Standard Deviation
1	69653	-527.89	678.57	50.87	47.41
2	148977	-945.69	666.70	-20.69	70.16
3	21415	-322.27	266.41	-7.03	14.98
4	5320	-96.99	64.89	-29.39	35.33
5	3866	-290.79	115.53	-66.35	83.83

Table 4.5: Statistics in meters for the depth differences between GIN RAS multibeam grids and S&S grid.

Polygon No	Count	Min	Max	Mean	Standard Deviation
1	54548	-288.20	578.58	50.50	52.25
2	123063	-995.43	672.82	-22.39	67.37
3	26592	-395.46	249.17	-7.65	15.89
4	4915	-90.92	45.73	-28.19	26.47
5	2185	-262.36	225.70	-30.31	82.18
6	19917	-530.69	907.32	-41.32	203.36

Table 4.6: Statistics in meters for the depth differences between GIN RAS multibeam grids and SRTM30_Plus[1] grid.

---

[1] SRTM30_Plus here is used from 33 original tiles rather than global grid, since a shift was identified in the global grid, see section 4.5

Polygon No	Count	Min	Max	Mean	Standard Deviation
1	54548	-19.02	12.09	-0.04	1.94
2	123063	-126.47	73.17	1.31	4.91
3	26592	-14.17	9.88	0.21	0.55
4	4915	-11.32	20.23	6.65	2.15
5	2185	-76.67	57.66	1.86	17.31
6	19917	-39.25	44.91	0.03	8.48

Table 4.7: Statistics for the depth differences between GIN RAS multibeam grids and GEBCO_08 grid, in % of WD.

Polygon No	Count	Min	Max	Mean	Standard Deviation
1	69653	-23.78	15.80	-1.95	1.64
2	148977	-50.78	69.76	1.04	3.69
3	21415	-14.58	12.90	0.25	0.59
4	5320	-19.72	35.72	8.21	10.03
5	3866	-125.08	74.09	15.97	24.43

Table 4.8: Statistics for the depth differences between GIN RAS multibeam grids and S&S grid, in % of WD.

Polygon No	Count	Min	Max	Mean	Standard Deviation
1	54548	-20.63	10.90	-1.95	1.85
2	123063	-51.52	73.17	1.11	3.48
3	26592	-12.06	14.96	0.28	0.63
4	4915	-13.76	30.12	7.90	7.43
5	2185	-108.36	72.60	6.99	25.02
6	19917	-328.50	56.84	-1.60	37.33

Table 4.9: Statistics for the depth differences between GIN RAS multibeam grids and SRTM30_Plus[2] grid, in % of WD.

---

[2] SRTM30_Plus here is used from 33 original tiles rather than global grid, since a shift was identified in the global grid, see section 4.5

difference,meters

-300 -200 -100 0 100 200 300

Pol.1 Mean = 0.84, 50.9, 50.5

Std= 53.14, 47.4, 52.25

Pol.2 Mean = -27.6, -20.7,-22.4

Std = 69.7, 70.16, 67.4

Pol.3 Mean = -5.7, -7.03, -7.7

Std = 13.8, 14.9, 15.9

difference,meters

-300 -200 -100 0 100 200 300

Pol.4 Mean = -23.5, -29.4, -28.2

Std = 7.6, 35.4, 26.5

Pol.5 Mean = -11.9, -66.4, -30.3

Std = 54.7, 83.8, 82.2

Pol.6 Mean = 7.52, -41.3

Std = 120.43, 203.4

300 -200 -100 0 100 200 300
difference,meters

300 -200 -100 0 100 200 300
difference,meters
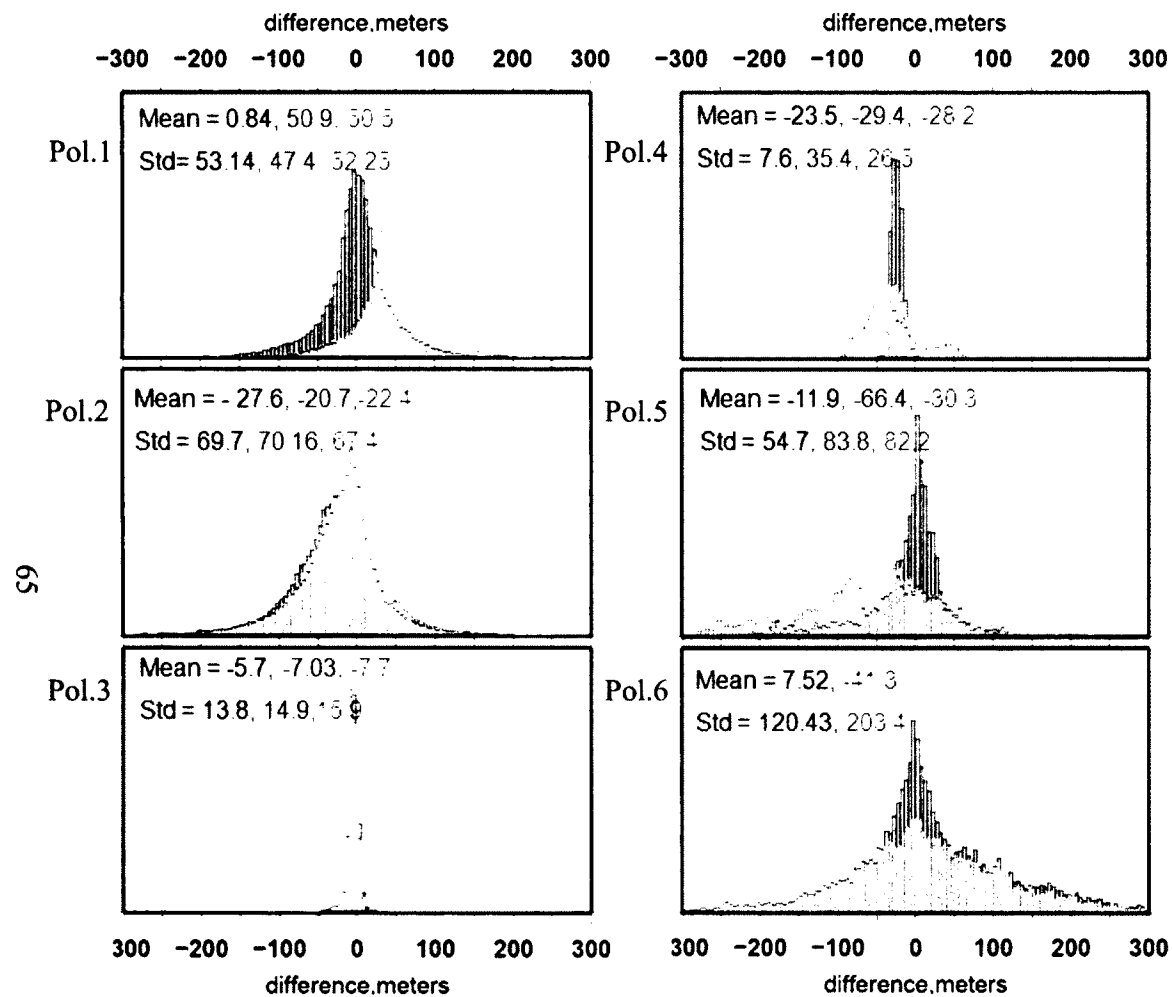
Figure 4-12: Histograms of depth differences in meters between the GIN RAS multibeam grids and GEBCO_08 (grey), S&S (red) and SRTM30_Plus (green) grids for the study polygons one through six.

difference,%W.D.

-40 -30 -20 -10 0 10 20 30 40

difference,%W.D.

-40 -30 -20 -10 0 10 20 30 40

Pol.1

Mean = -0.01, -1.9, -1.95

Std= 1.94, 1.7, 1.85

Pol.4

Mean = 6.7, 8.2, 7.9

Std = 2.2, 10, 7.4

Pol.2

Mean = 1.3, 1.0, 1.1

Std = 4.9, 3.7, 3.5

Pol.5

Mean = 1.86, 15.9, 6.99

Std = 17.3 24 4, 25

Pol.3

Mean = 0.2, 0.25, 0.3

Std = 0.5, 0.6, 0.6

Pol.6

Mean = 0.03, -1.6

Std = 8.5, 37.3

-40 -30 -20 -10 0 10 20 30 40

difference,%W.D.

-40 -30 -20 -10 0 10 20 30 40
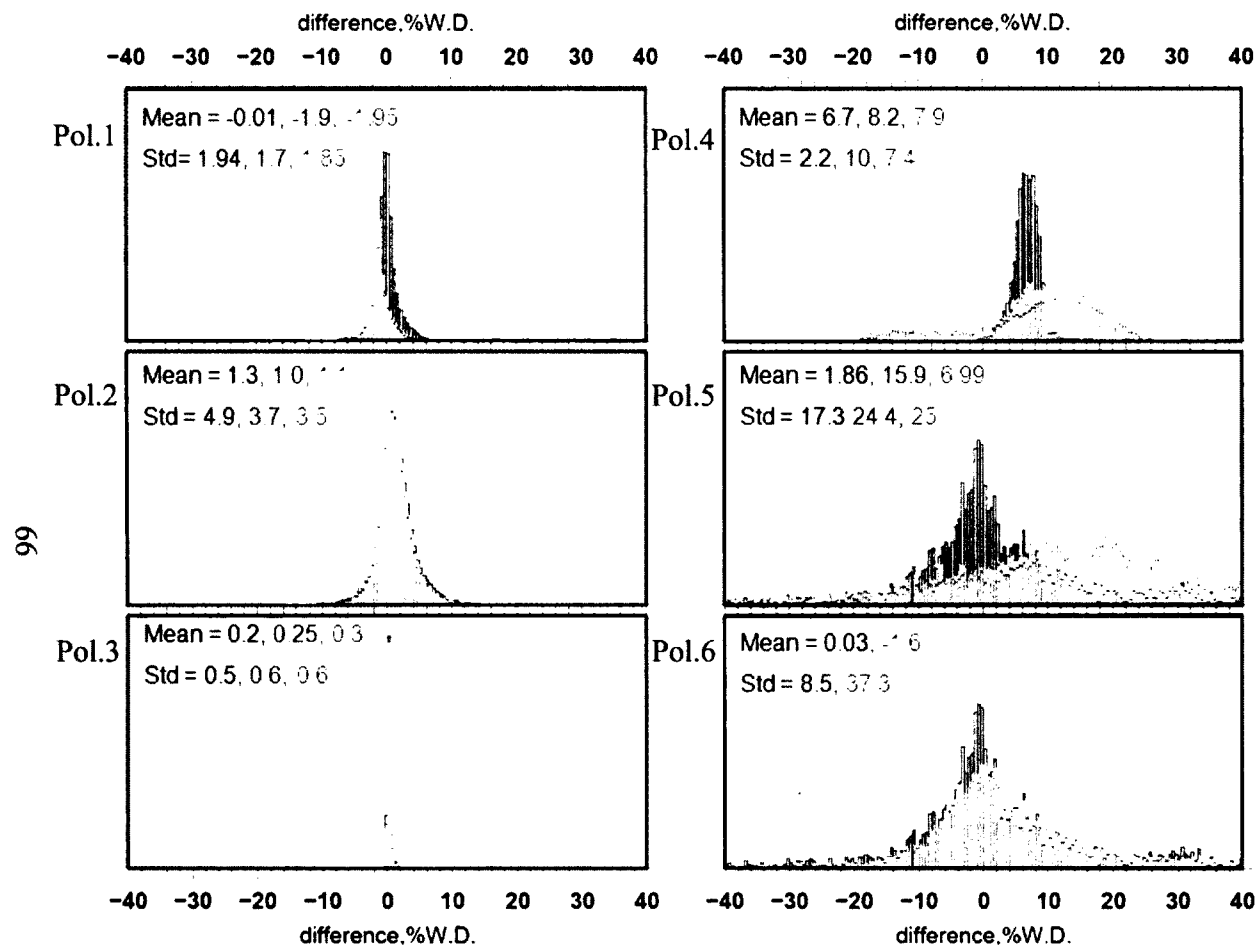
difference,%W.D.

Figure 4-13: Histograms of depth differences in % of WD between the GIN RAS multibeam grids and GEBCO_08 (grey), S&S (red) and SRTM30_Plus (green) grids for the study polygons one through six.

4.3 Internal consistency assessment

4.3.1 Artifacts in the bathymetry surface (qualitative assessment of internal consistency)

Artifacts in gridded bathymetry can be defined as any dubious features in the bathymetry surface. Dubious features are those whose existence is questionable according to geologic knowledge of the processes in the area.

Consistency of datasets was assessed qualitatively by visual inspection of bathymetry of GEBCO_08 and S&S grids for the presence of artifacts. Three regions inspected are shown in Figure 3-3. The types of artifacts encountered are classified according to the nature of the source data types which characterize them. The classification table and description of the artifacts' "morphology" is given in Table 4.10.

Source data type	"Morphology" of an artifact	Illustrations	Type of grid where encountered
a) multibeam	artificial high frequency peak-like features in the bathymetry	Figure 4-14, Profile 1	Type A, B
b) singlebeam	linear artifacts such as artificial "ridges" and "troughs" or point features like those caused by single soundings	Figure 4-14, "ridges" Profile 4, "troughs" Profile 2	Type A, B
c) single soundings	artificial peak-like ("bumps") or pit-like ("holes") features	Figure 4-15, Profiles 1, 3	Type A, B
d) contours	terracing on slopes, or artificial features where contours don't agree with surrounding soundings	Figure 4-18	Type A
e) no sounding data in the grid Type A	flat areas, artificial deeps	Figure 4-19	Type A
f) no sounding data in the grid Type B	artificial deeps and highs in the areas where there is no correlation between bathymetry and gravity	Figure 4-16, Profiles 2,3, Figure 4-17	Type B
g) patching several data sources	artificial steps	Figure 4-14, Profile 1	Type A, B

Table 4.10: Classification table of types of artifacts encountered in the analyzed grids, classification is given according to the source data types which characterize them.
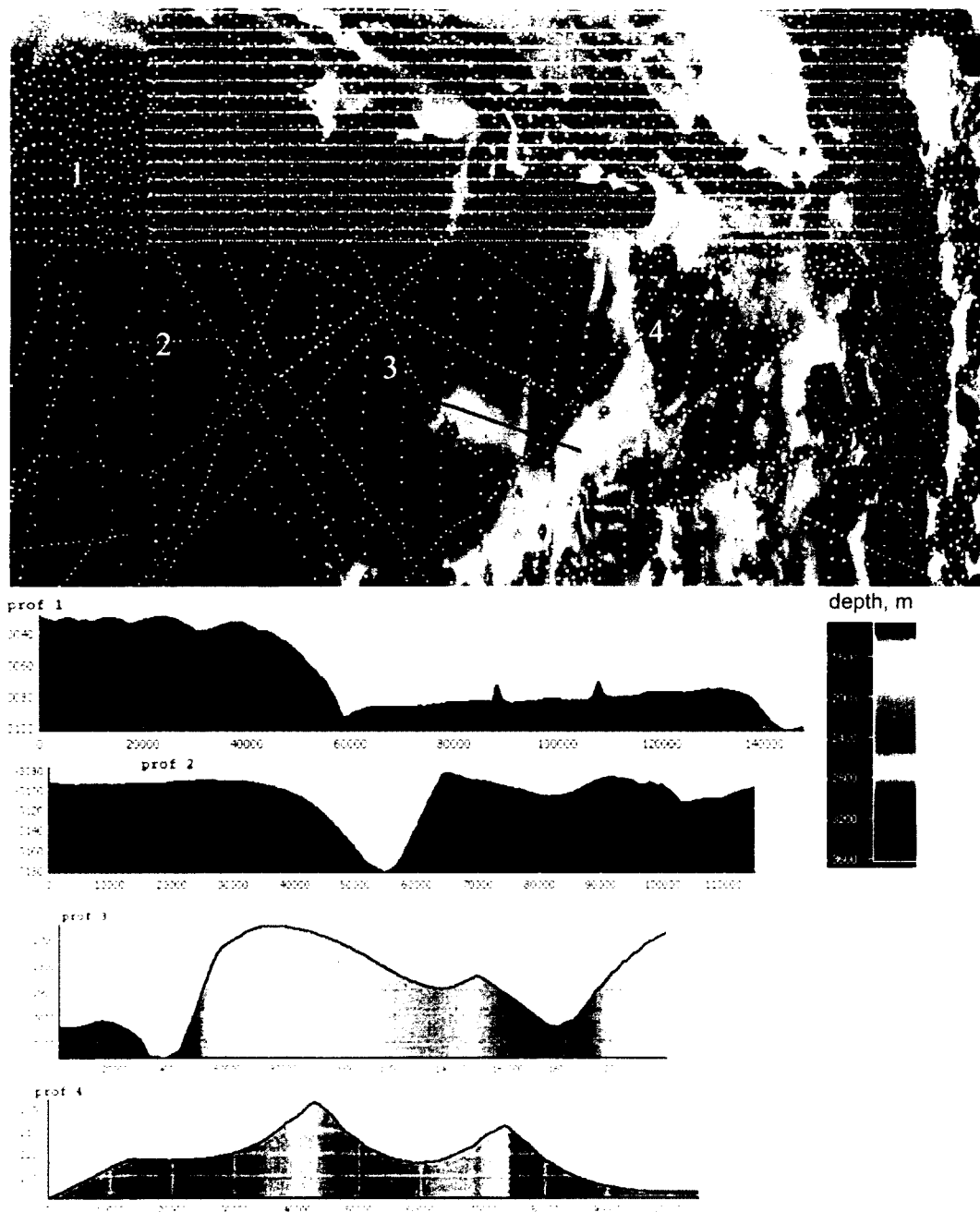
Figure 4-14: S&S bathymetry in region 3 (Figure 3-3) overlain by source tracklines (white dots). The figure illustrates artifacts caused by singlebeam, multibeam and interpolation with gravity (Table 4.10). Profiles show depth in meters.
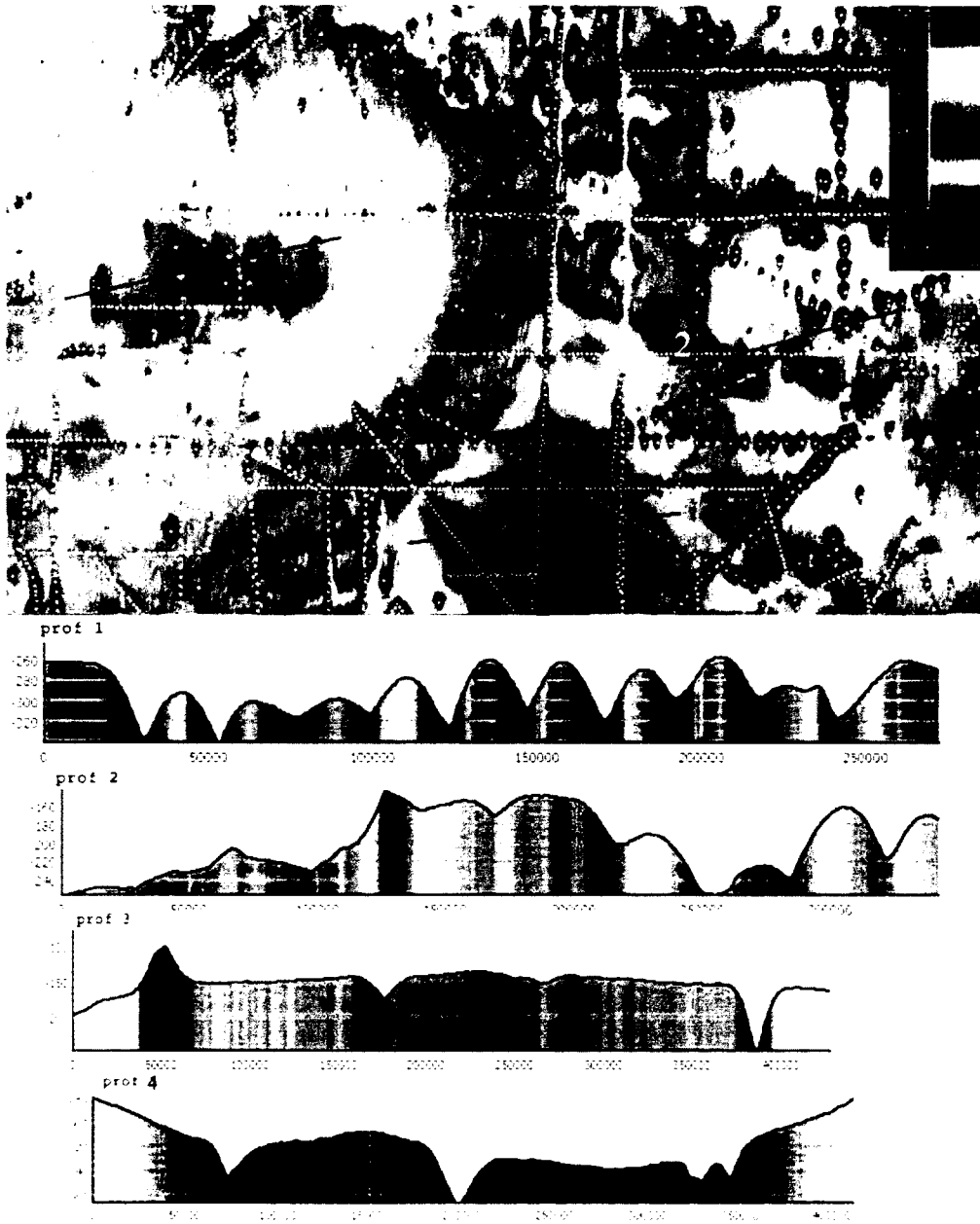
Figure 4-15: S&S bathymetry in region 1 (Figure 3-3) overlain by source tracklines (white dots). The figure illustrates artifacts caused by singlebeam, historical single soundings and interpolation with gravity data (Table 4.10). Profiles show depth in meters.

69
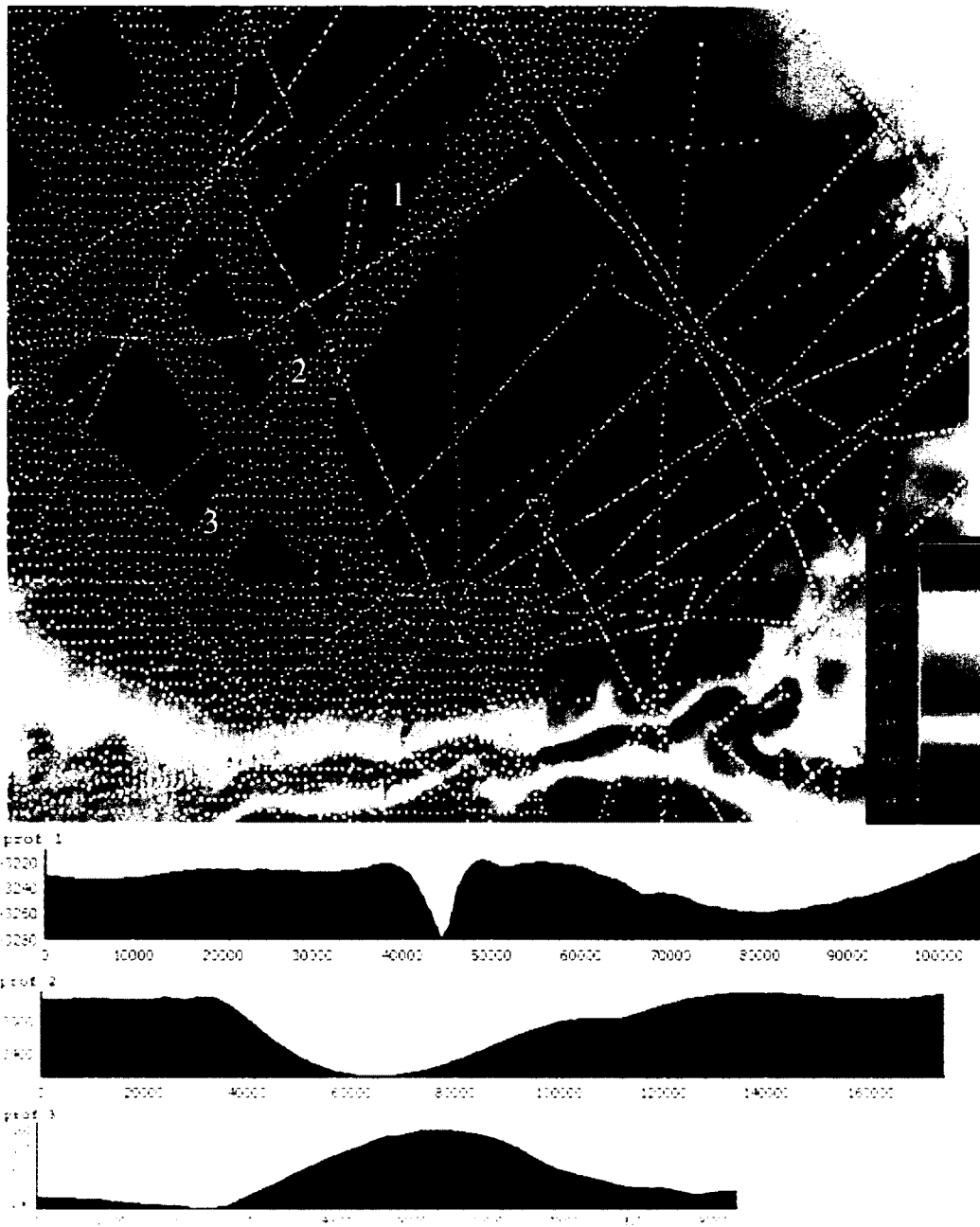
Figure 4-16 : S&S bathymetry in region 2 (Figure 3-3) overlain by source tracklines (white dots). The figure illustrates artifacts caused by erroneous singlebeam tracks (Profile 1) and interpolation with gravity in the area where there is no correlation between bathymetry and gravity (abyssal plain with high sediment thickness) (Profiles 2, 3). See Figure 4-17 for gravity and bathymetry profiles. Profiles show depth in meters.
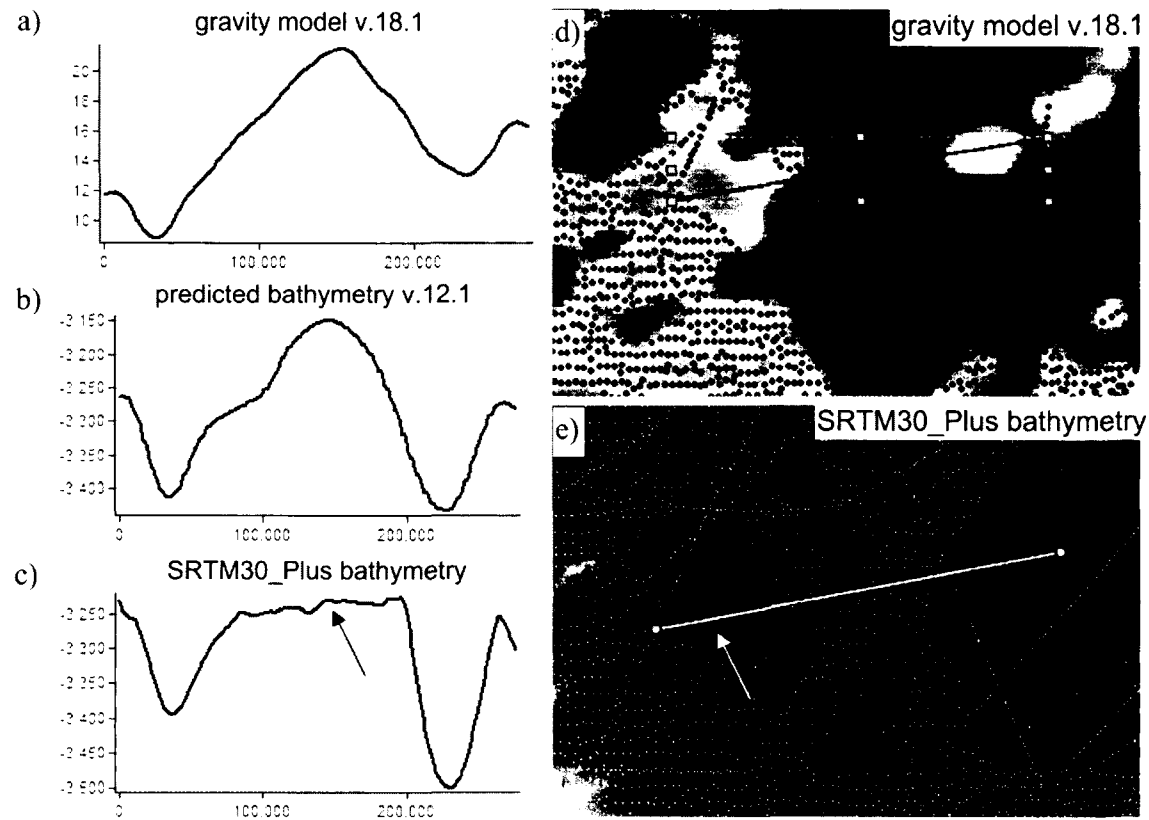
Figure 4-17: Illustrates area where artifacts from gravity interpolation are observed. Maps of gravity model v.18.1 (d) [Sandwell and Smith, 2009] and SRTM30_Plus bathymetry (e) are shown in the area of Region 2 (Figure 3-3). The dots on the maps (d, e) show the sounding source trackline coverage used for construction of S&S and SRTM30_Plus. As discussed in Chapter II, the gravity (a) is scaled by correlation coefficient to the predicted depths (b), and then the measured depths are "polished" to the predicted bathymetry grid to create the final bathymetry grid (c). As can be seen from the profiles, the bathymetry is taken from scaled gravity in the area with no sounding coverage (yellow arrow). Although when gravity and bathymetry profiles are compared in the area where the source sounding data is present (red arrow), there is no observed correlation between them. Predicted bathymetry v.12.1 grid [Smith and Sandwell, 1997] (b) was provided by M. Wolfson at UNH. Gravity model v.18.1 is publicly available for download through the internet.
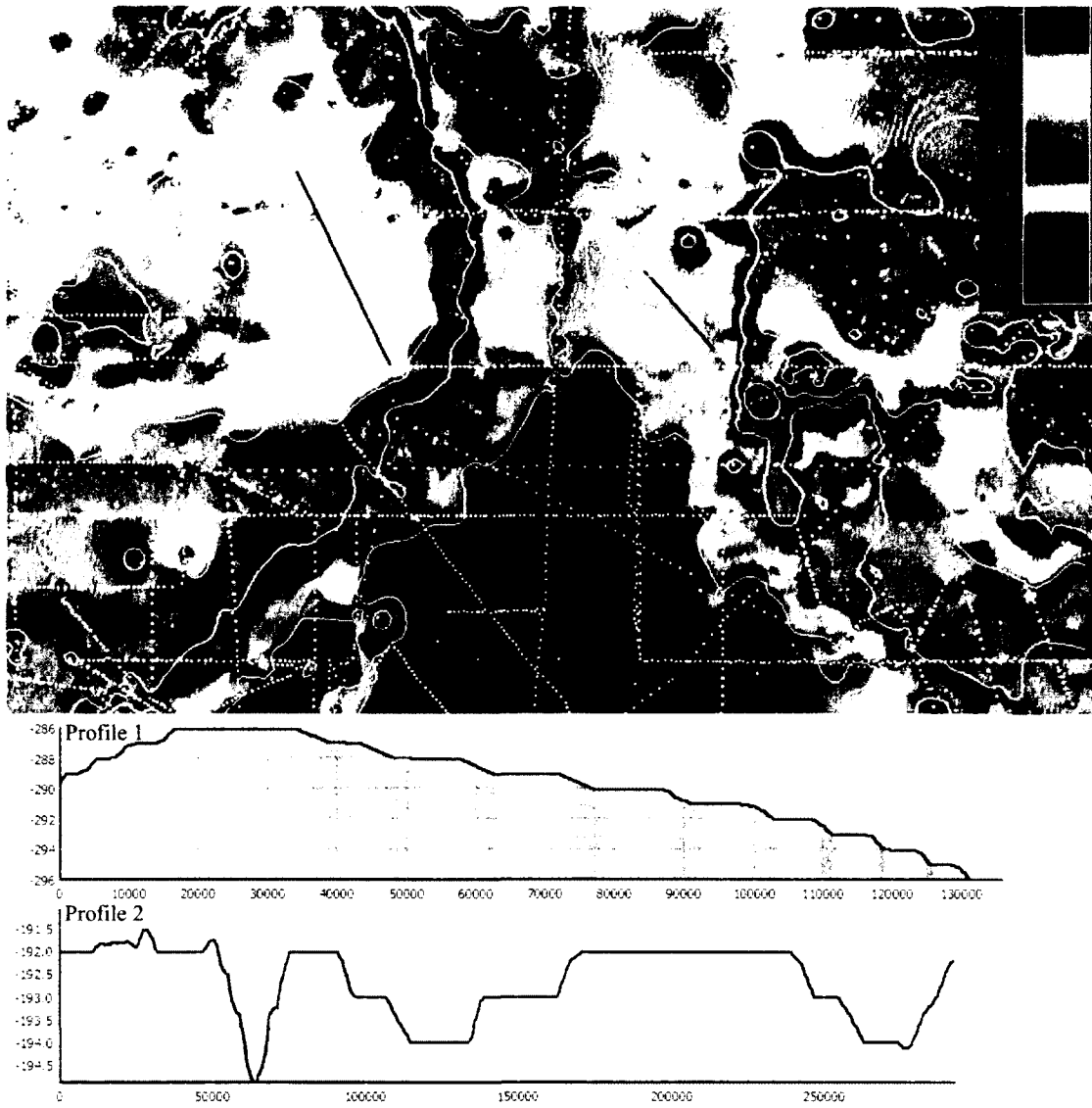
Figure 4-18: GEBCO_08 bathymetry in region 1 (Figure 3-3) overlain by source tracklines and contours (white dots). The figure illustrates a terracing effect due to using contours for interpolation (Table 4.10). Profiles show depth in meters.
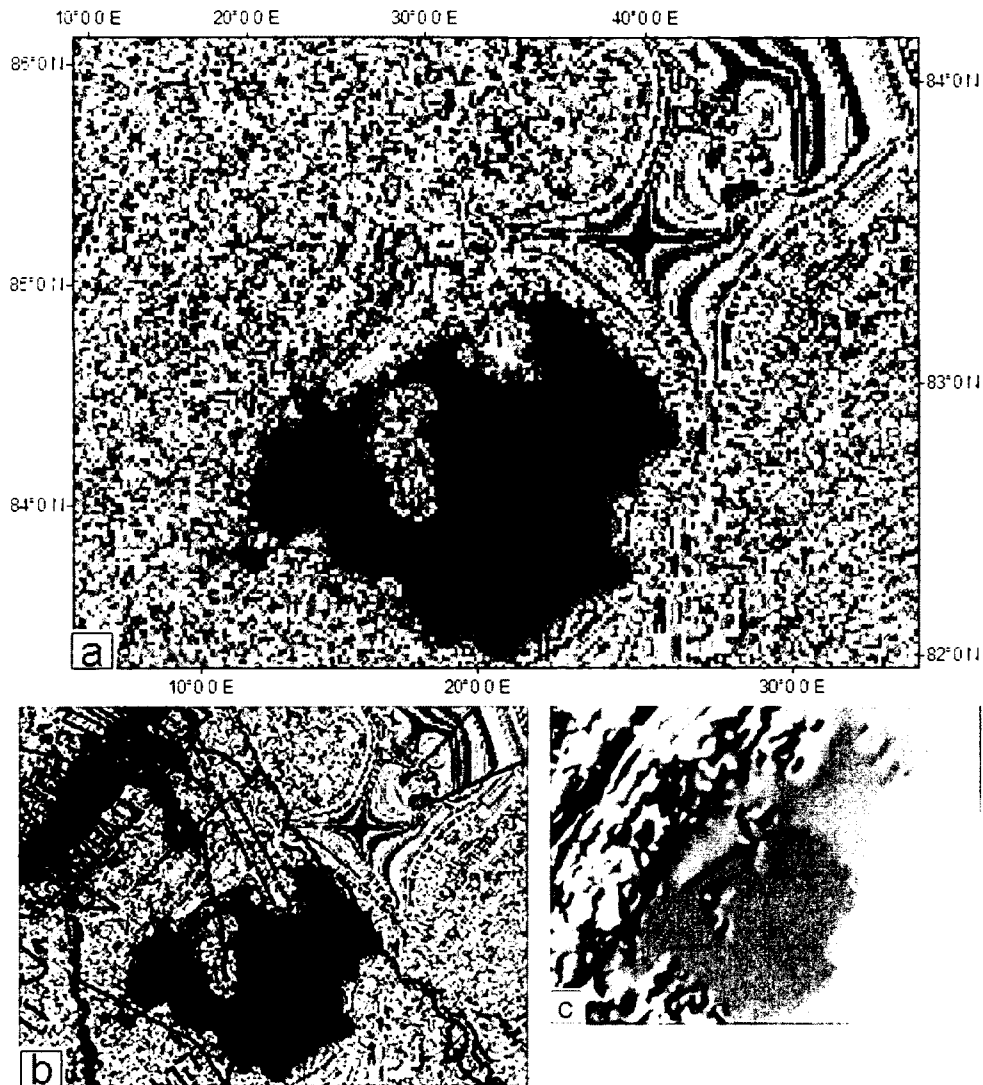
Figure 4-19: Example of artificial plain and artificial star like feature in the IBCAO bathymetry in the region of the Gakkel Ridge (blue polygon in Figure 3-3) caused by lack of data in the region: (a) unique values color scheme (individual color is assigned to each depth value) applied to the bathymetry highlights these two artifacts; (b) as (a) with trackline information; (c) shaded relief of the area.

Besides classification based on data sources, artifacts can also be classified according to their "morphology" into positive and negative features, e.g. peak-like, ridge-like (positive) versus pit-like, trough-like (negative) features. Also artifacts can be classified according to their scale into short and long wavelength features, where small-scale features are caused by the presence of source data, while long-scale features are caused by interpolation between data gaps.

Visual inspection of GEBCO_08 and S&S bathymetry, as representatives of Type A and Type B grids, showed that there are artifacts present in both Types of datasets. The artifacts encountered in the bathymetry of S&S and GEBCO_08 were classified according to the source data types, since that is the major factor that characterizes them. Artifacts encountered are in general more pronounced in Type B than in Type A grids (e.g. Figure 4-15 versus Figure 4-18). All types of artifacts can be encountered in both Type A and B datasets, except types (e) and (f) (Table 4.10), where acoustic sounding source data is not present and interpolation is used. In the following section the magnitude of those artifacts is assessed quantitatively.

4.3.2 Quantitative assessment of internal consistency

The internal consistency of Type A and Type B datasets was assessed by comparing depth values in the grid cells based on source data to the neighbor depth values. The analysis was performed for GEBCO_08 and S&S grids in the shelf area (Region 1, Figure 3-3). The differences between the values in the grid based on source data and median of the surrounding depth values within a specified window is defined as variability (Section 3.2.2 describes the method). The distribution of variability for GEBCO_08 and S&S was compared to the "true" variability to assess which dataset is more consistent and to estimate the magnitude of artifacts on shelf.

Figure 4-20 shows that GEBCO_08 has narrower variability distribution compared to S&S. GEBCO_08 compares well with distribution of "true" values. The variability distribution in
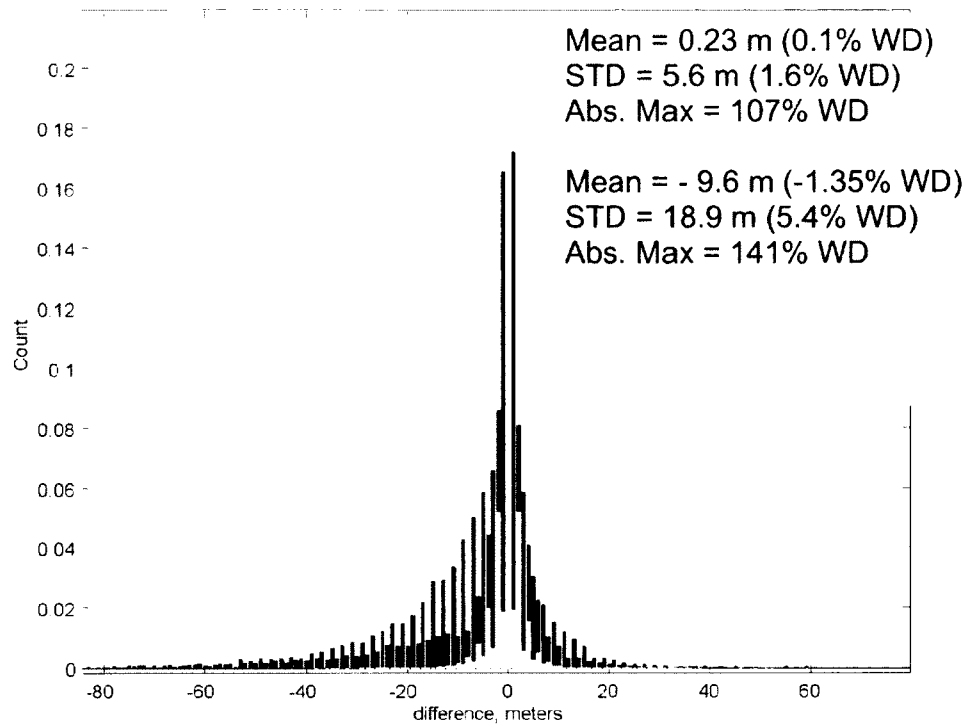
Figure 4-20: Histogram of normalized distribution and statistics of variability in meters within a specified window for GEBCO_08 (blue), S&S (red) and "truth" (yellow).

S&S is much wider than GEBCO_08 variability, and is biased towards negative values (with mean of 1.35% of WD), which means that grid cell values based on source data are more frequently deeper than surrounding depth values (Figure 3-4). Observed spikes at even values in the distribution of S&S variability is caused by the fact that S&S has even values at the grid cells defined by gravity prediction, and odd values at the locations of the source soundings. The variability at each grid cell in S&S grid is computed as a difference between the odd value (grid cell value based on source soundings) and a median over even number (24 grid cells, see Section 3.2.2) of even values (grid cell values defined by gravity prediction). From the histogram can be seen that the variability for S&S is an even value more frequently than the odd value due to the described above computation.

Quantitative assessment of consistency performed on one representative grid from each Type revealed that the GEBCO_08 dataset is more consistent than the S&S dataset in the shelf

75

area of the Barents Sea. The standard deviation (SD) of depth differences between source data points and the surrounding area within a specified window is smaller in GEBCO_08 (5.6 m and 1.6% of WD) than in S&S (18.9 m and 5.4% of WD). This gives a quantitative measure of the magnitude of the artifacts for these two grids. The artifacts in bathymetry can be as deep (shallow) as 141% of WD in S&S grid and 107% of WD in GEBCO_08 grid.

4.4 Interpolation accuracy

Interpolation accuracy is tested by plotting differences between GIN RAS multibeam grid values and analyzed grid values versus the distance to the closest source data point (method discussed in Section 3.3). The analysis was performed in order to test the performance of interpolation on sounding sources alone (GEBCO_08 grid) versus interpolation with additional gravity information (S&S grid). The analysis was performed on GEBCO_08 and S&S at four of the six polygons. Two polygons were not used in the analyses because the available source data for the grids within these two polygons was not complete (see Section 4.2.2).

The continuous curvature spline in tension algorithm [Smith and Wessel, 1990] is used for construction of both GEBCO_08 and S&S grids. At the same time, this algorithm is employed in a different manner. In the construction of the GEBCO_08 grid a continuous curvature spline in tension (tension = 0.35) is used to interpolate across the data gaps. In the construction of S&S the predicted bathymetry surface is used to interpolate across the data gaps. The spline algorithm is used at the "polishing" step of grid creation (Section 2.1.2), when the differences between predicted and measured depths are interpolated with a spline (tension = 0.75) and are blended smoothly back into the prediction grid. Therefore, the effect of using spline interpolation can be observed only close to the source data points.

Figure 4-21 and Figure 4-22 show the distribution of differences between the values in analyzed grids and the GIN RAS multibeam data as a function of distance to the nearest source data point for GEBCO_08 and S&S grids respectively. It can be seen that the distribution of

76

differences varies from polygon to polygon for the reason of differences in data density and number of data points within each polygon. One similarity can be noticed for both GEBCO_08 and S&S: the distribution of differences is wider near the source data points and decreases with the distance from source data at all the polygons except polygon 4 for S&S. The difference at the zero distance corresponds to the accuracy of the source data. As can be noticed from the figures, the differences do not get considerably higher than the differences at zero distance and rapidly decrease at some distance which varies from polygon to polygon. The observed distribution of differences is caused by the spline in tension interpolation algorithm. In spline in tension interpolation method, the interpolated surface fits the source data points exactly [Smith and Wessel, 1990]; therefore the method does not take into account uncertainty of the source data. The wide distribution of differences closer to the source data reflects the uncertainty of the source data. The distance at which the differences decrease is defined by the tension parameter, since the tension defines the distance at which source data values affect the interpolated values. Beyond the certain distance interpolated values are less affected by the uncertainty of the source data and, possibly, the uncertainties of the interpolated values converge to the mean uncertainty of surrounding source data values.

Besides the tension parameter in spline interpolation method, the number of data points within each polygon, as well as the data density affects the distribution of differences. Figure 4-23 shows two-dimensional histograms of the count of data points versus difference and distance for GEBCO_08 and S&S for all four polygons. As can be seen from the figure, very few data points are far from the source data points, with the counts being typically an order of magnitude lower than those closer to the source. Distance maps (provided in Appendix F) show that the areas in the grids with significant distance from source data are in general very small, which explains the small count of data points. Therefore the decrease in differences with the increase in distance from source data corresponds to the decrease in the number of data points.

Distance to the nearest source data point was converted from pixels to kilometers for the S&S grid (Figure 4-22) in order to assess predicted bathymetry performance as well as to estimate the data density within the study polygons. The conversion from pixels to kilometers was made according to approximate dimensions of the S&S grid cell in the real world depending on the polygon. The furthest distance to the source data points varies within the polygons from 2 km to 10 km, with the maximum distance of 17 km. The stated spatial resolution of predicted bathymetry is 20 - 160 km [Smith and Sandwell, 1997, 2001]. Therefore, in order to assess how well the gravity derived bathymetry interpolates across the data gaps, larger areas with no soundings are required, with maximum distance to the nearest source data point exceeding 20 km.

The analysis shows that both Types of datasets perform similarly: closer to the source data points differences with GIN RAS multibeam grid are higher than further away from the source data points. The distance at which the differences decrease is controlled by source data density, number of data points within the polygons as well as the tension parameter used in spline interpolation method. The data density within the polygons of study is relatively high to test performance of interpolation with gravity, with stated spatial resolution of 20 - 160 km.
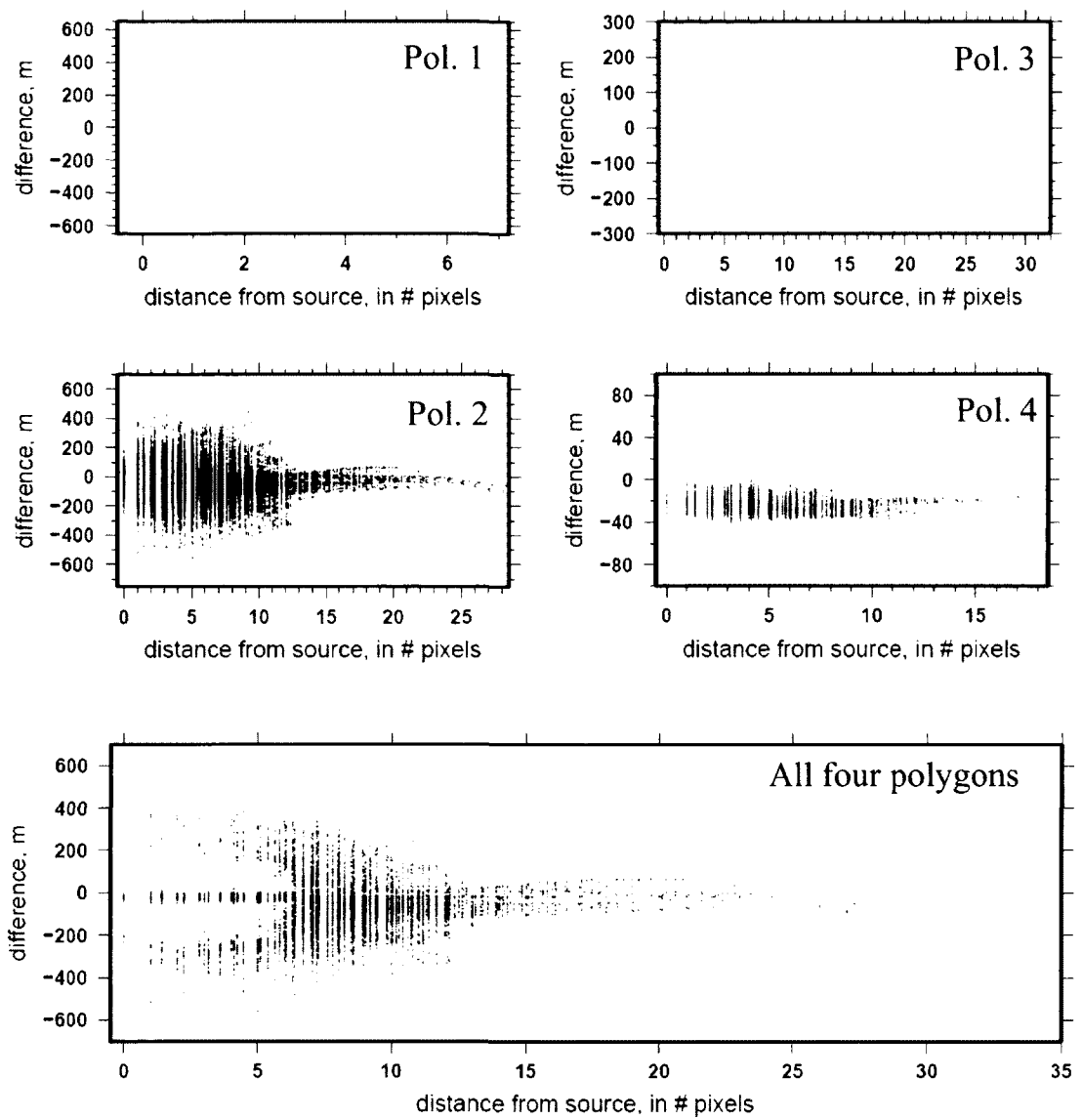
Figure 4-21: Plots of differences between GEBCO_08 and GIN RAS multibeam grid values versus distance to the nearest source data point at the polygons 1, 2, 3 and 4 and combined plot for all polygons colored by the polygon.
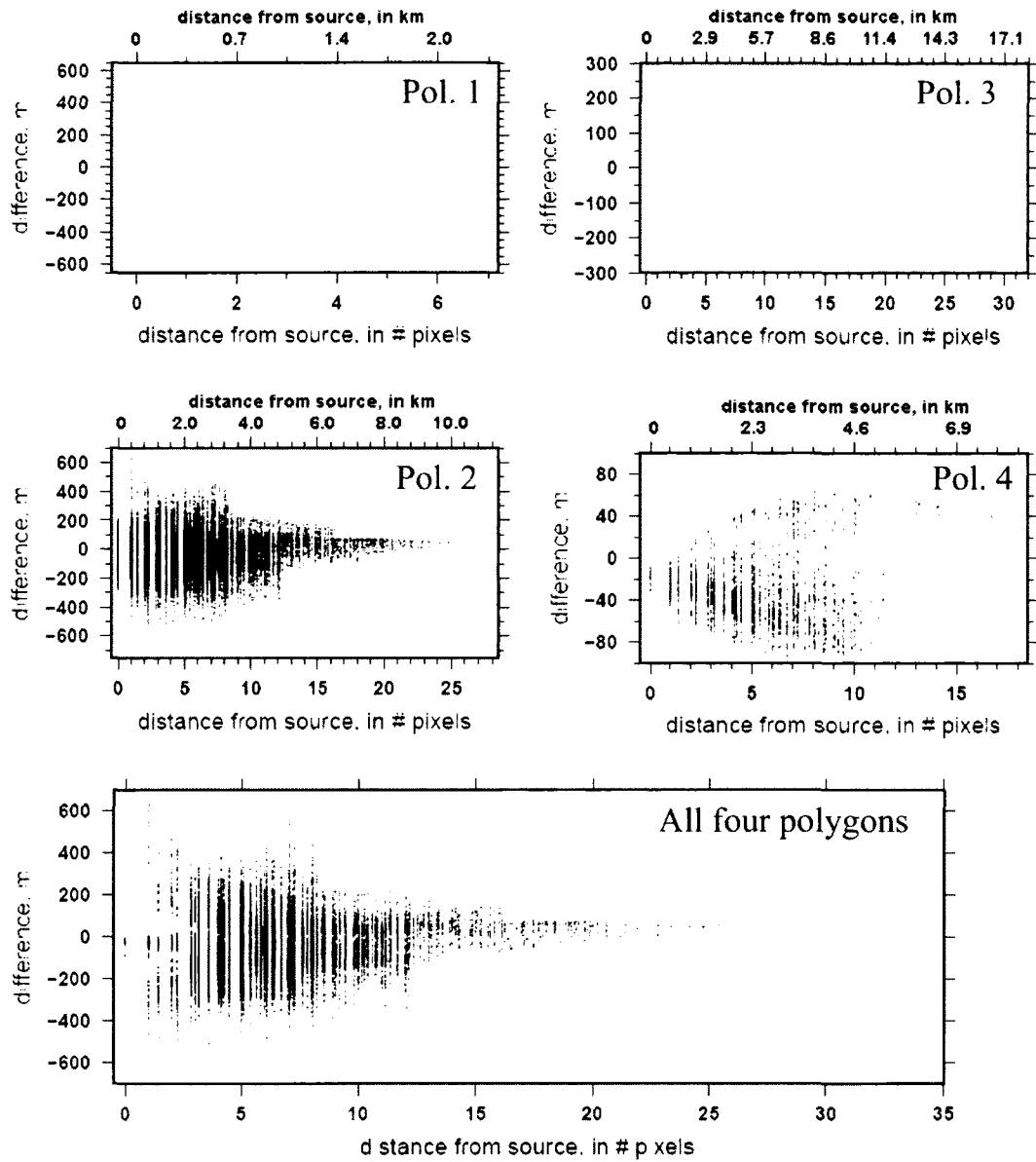
Figure 4-22: Plots of differences between S&S and GIN RAS multibeam grid values versus distance to the nearest source data point at the polygons 1, 2, 3 and 4 and combined plot for all polygons colored by the polygon. The distance in kilometers is an approximate distance in the real world and is calculated according to approximate dimensions of a grid cell at a particular polygon (see captions for figures in Appendix F.1).

ALL polygons GEBCO 08

count

a)

600

400

200

difference, m

0

-200

-400

-600

0   5   10   15   20   25   30   35

distance from source, in # pixels

1000
900
800
700
600
500
400
300
200
100
0

ALL polygons S&S

count

b)

600

400

200

difference, m

0

-200

-400

-600

0   5   10   15   20   25   30   35

distance from source, in # pixels

1000
900
800
700
600
500
400
300
200
100
0
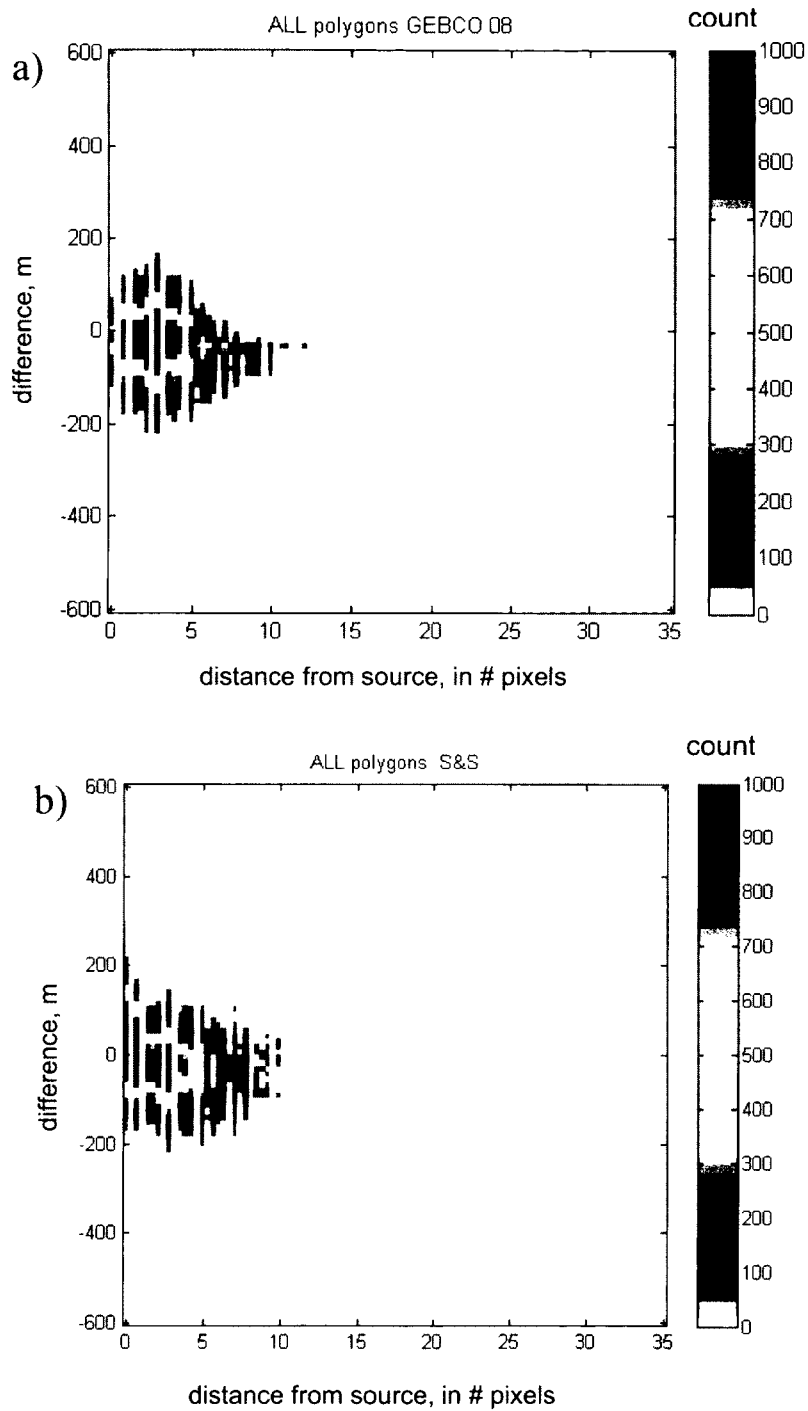
Figure 4-23: Two-dimensional histogram of count of events (per bin of 12 m by 0.35 pixels - each axis divided into 100 by100 equal bins) of difference values between S&S and GEBCO_08 and GIN RAS multibeam versus distance to nearest source data point for all four polygons (Figure 4-21 and Figure 4-22). See Appendix E, Figures E.1, E.2 for the 2-D histogram for each polygon.

4.5 Registration issues in the grids (comparison of derived contours)

Contours produced from the bathymetry of the analyzed datasets were compared in order to test whether depth values in the grids match and whether any misregistration was present.

Figure 4-24 shows that contours produced from GEBCO 1 minute, GEBCO _08 and S&S grids all agree (Figure 4-24 (a, d)). Overall, contours based on S&S are shallower than those based on GEBCO_08 (Figure 4-24d). The slight difference between the contours in GEBCO 1 minute and GEBCO_08 are likely due to the different cell size of the two grids. The slight difference between the contours from the GEBCO_08 grid and the S&S grid are likely due to interpolation of different data sources (contour interpolation versus interpolation with satellite altimetry).

As can be seen from Figure 4-24b, ETOPO1 and GEBCO 1 minute grid contours look almost identical, although a consistent northern offset of ETOPO1 relative to the GEBCO 1 minute grid contours is observed (Figure 4-24b). The figures were made in GMT, which recognizes both registration methods; therefore the shift is not caused by pixel-gridline registration differences.

A similar offset is observed in the registration of SRTM30_Plus data, where a systematic southern offset of contours with respect to the S&S contours occur (Figure 4-24c). Personal communication with the authors of SRTM30_Plus confirmed the offset in the global SRTM30_Plus grid. It was found that the offset is not present in the original 33 tiles of SRTM30_Plus grid, available for download. For this reason bathymetry from the tiles and not from the global grid was used in the analyses in Section 4.2.3.

a) GEBCO 1 minute vs. GEBCO 08
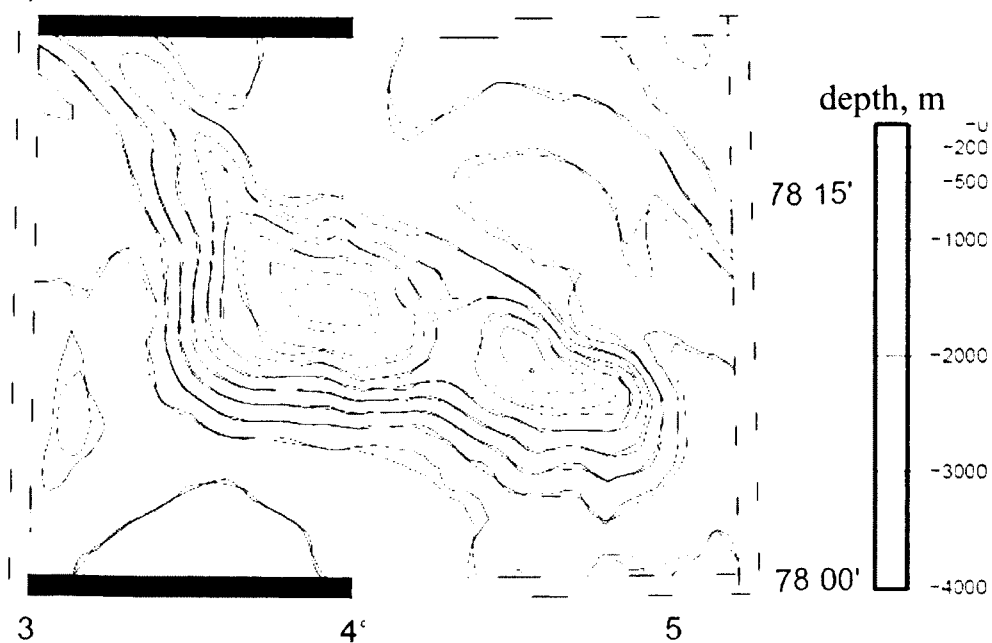
b) GEBCO 1 minute vs. ETOPO1
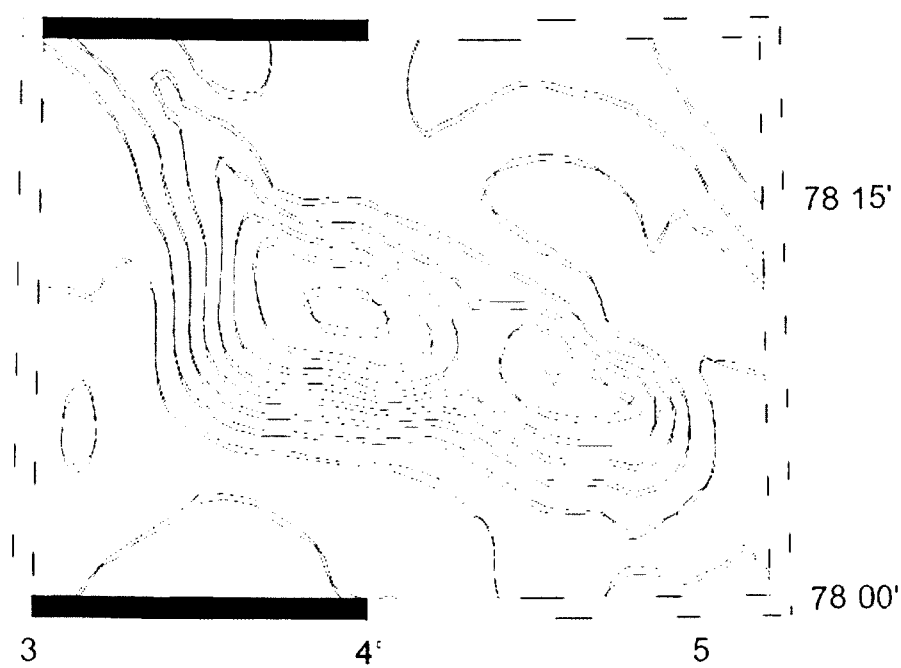
Figure 4-24: GEBCO 1 minute bathymetry overlain by contours (200 m interval): (a) GEBCO 1 minute (purple) and GEBCO_08 (blue) contours; (b) GEBCO 1 minute (purple) and ETOPO1 (green) contours.

c) S&S vs. SRTM30_Plus

78 15'

78 00'

3   4'   5

d) S&S vs. GEBCO_08

78 15'

78 00'

3   4'   5
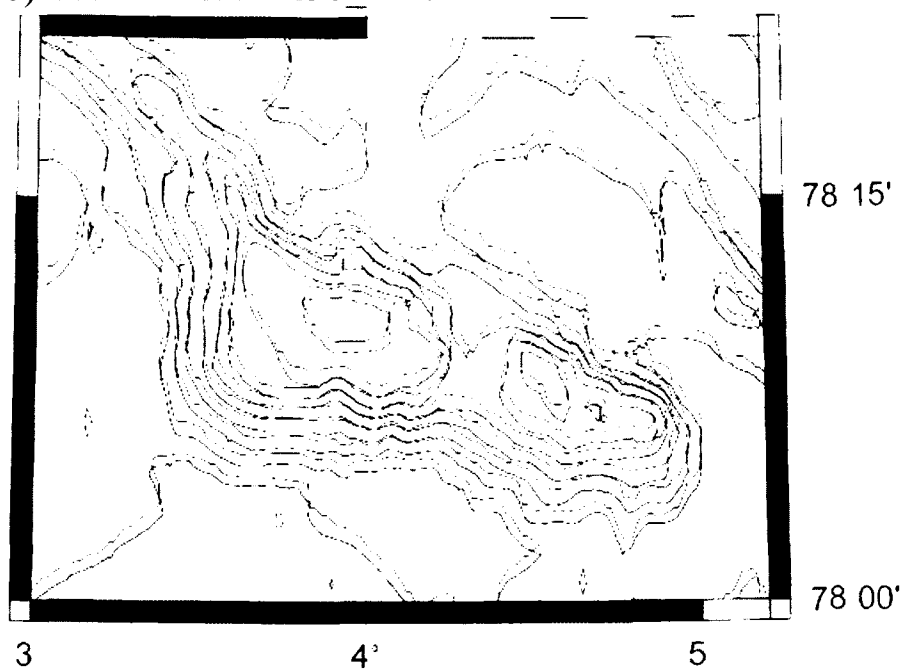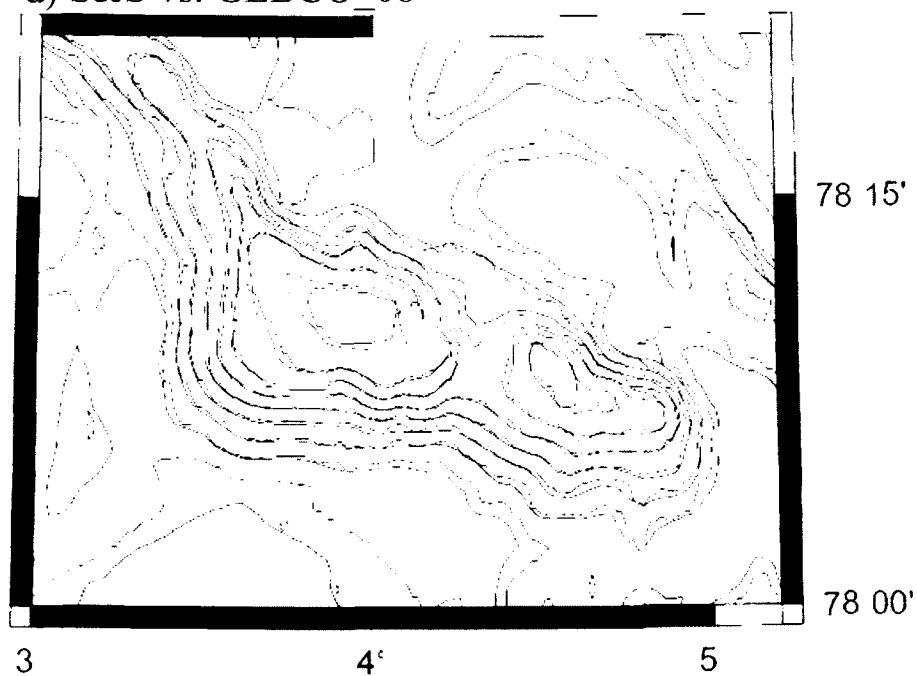
Figure 4-24 (continue): GEBCO 1 minute bathymetry overlain by contours (200 m interval): (c) S&S (red) and SRTM30_Plus (brown) contours; (d) S&S (red) and GEBCO_08 (blue) contours.

84

4.6 Resolution of the coastline

The GEBCO shoreline was used to visually assess how well the grids represent the shoreline. It is not the purpose of this section to discuss the accuracy of the shoreline on which the grids are based, but rather to illustrate how well gridding performs in the coastal zones. The GEBCO shoreline in the study area is based on the World Vector Shoreline [Soluri and Woodson, 1990], updated in Greenland and northern Ellesmere Island with the Danish National Survey (KMS) shoreline and in Kvitoya with GTOPO30 DEM [Jakobsson and Macnab, 2008]. The GEBCO coastline is considered to be the most accurate in the study region. The comparison was carried out in two coastal areas of Greenland and Svalbard (Figure 4-25).
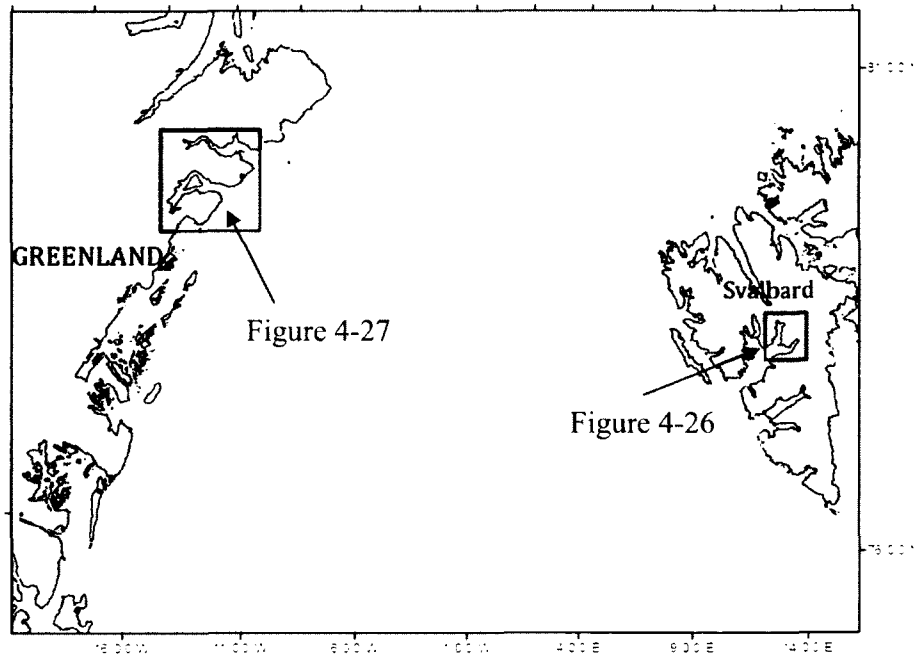
Figure 4-25: Location map for the Figure 4-26 and Figure 4-27.

Figure 4-26 shows that in Svalbard area GEBCO 1 minute, IBCAO and ETOPO1 do not resolve the shoreline mainly due to the resolution of the grids. There is an apparent northern shift between the shoreline and gridded values in S&S and ETOPO1 grids (Figure 4-26(e, b)), a north-western shift in GEBCO_08 (Figure 4-26c), and a southern shift in SRTM30_Plus grid (Figure 4-26d). Shift magnitudes are approximately one grid cell, i.e., one minute shift in the first two

85

grids and 30 arc seconds shift in the last two grids. SRTM30_Plus shows the best resolution of the shoreline in the region. The shift of the data in the coastal region of SRTM30_Plus and ETOPO1 is consistent with the previously discussed shift in contours. The reason for the shift in S&S is unknown.

In the Greenland area (Figure 4-27), the IBCAO, ETOPO1 and GEBCO 1 minute grids are limited by the resolution of the grid and do not resolve narrow fiords and small bays, whereas the GEBCO_08 grid resolves smaller features. All grids based originally on the GEBCO coastline, such as IBCAO, ETOPO1 and the two GEBCO grids nicely resolve between positive and negative values and do not have negative elevation values within land. Shifts between the coastline and bathymetry can be observed for SRTM30_Plus and S&S. Other problems for these two grids include negative values on the land which can be noticed in Figure 4-27(e, f) (red arrows).

Comparison between grids and the GEBCO shoreline shows that in the Svalbard area GEBCO_08 and SRTM30_Plus resolve shorelines better. In the Greenland area, all Type A datasets resolve shorelines better than Type B datasets. Type B datasets have non-uniform shifts in bathymetry relative to coastlines with depths below zero observed within land.
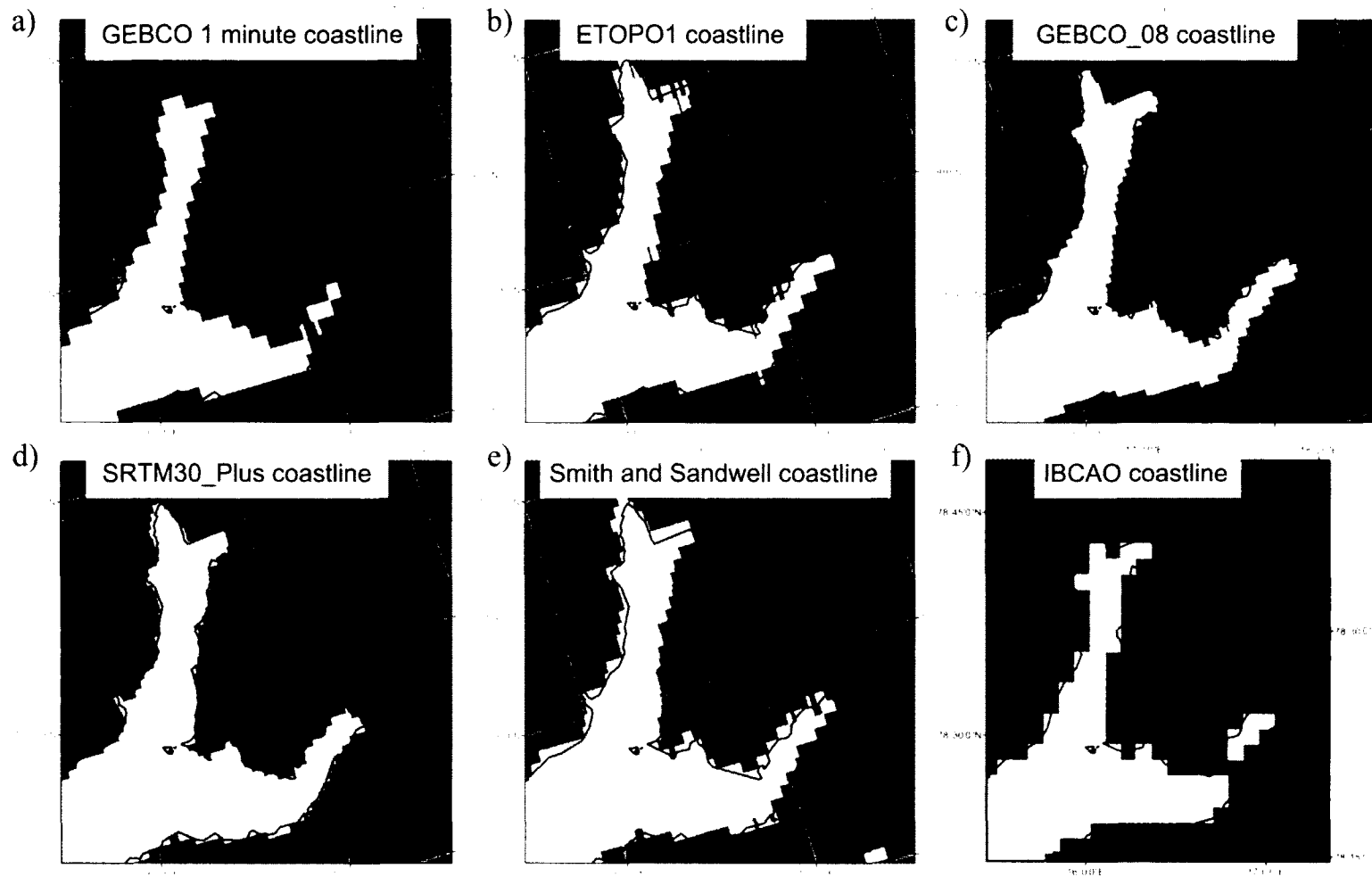
Figure 4-26: Comparison of how well grids resolve coastline in the Svalbard region. The gridded bathymetry is overlain by the GEBCO shoreline.
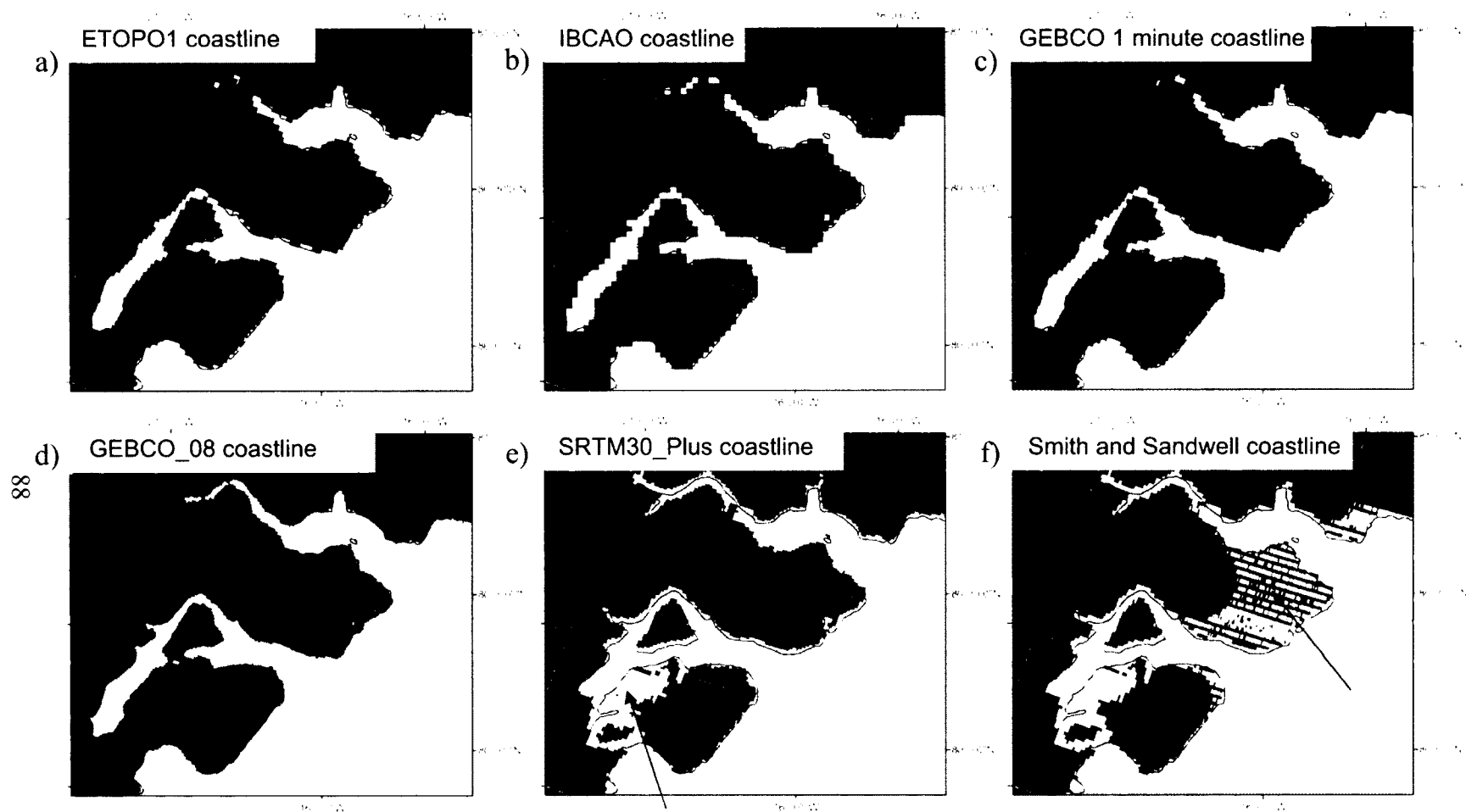
Figure 4-27: Comparison of how well grids resolve coastline in the Greenland region on a relatively large scale. The gridded bathymetry is overlain by the GEBCO shoreline.

CHAPTER V

DISCUSSION

The main objective of this thesis was to evaluate the differences between current versions of publicly available bathymetry datasets in the Arctic, with the goal of providing guidance on the choice of the most appropriate grid to the users. The differences were evaluated in terms of source data accuracy, depth accuracy, internal consistency, presence of artifacts, interpolation accuracy, registration issues and resolution of the coastline. These parameters were chosen as quality metrics important for the choice of the grid for any given purpose. During the analyses several problems were identified in the datasets. These problems were reported to the grid compilers and will be corrected in the next versions of the datasets. The results of the thesis fall into short and long-term objectives of the thesis. In the short term, new upcoming versions of the bathymetry grids will be improved. In the long term, methods provided for difference assessment can be applied to evaluate any other bathymetry datasets.

5.1.1 Differences between the grids

It was essential to separate all analyzed grids into two Types: Type A grids, based solely on acoustic sounding data sources interpolated using contours in the areas that lack data; and Type B grids, based on acoustic sounding data sources combined with satellite-derived gravity data. These Types have very distinct differences and, at the same time, grids falling into the same Type are very similar. The fact that grids within each Type are very similar reduced most of the analyses to the comparison between Type A and Type B grids with one representative dataset of each Type, namely GEBCO_08 and S&S.

The most distinct difference lies in the visual appearance of the datasets and their internal consistencies (Figure 4-1). Type A datasets visually have a smoother appearance compared to

89

Type B datasets, which have obvious artifacts. These artifacts are not only undesirable for visualization purposes, but can be mistakenly taken as real features by unaware users (Figure 4-14, Figure 4-15, Figure 4-16).

The main reason for the distinct artifacts in Type B datasets is the construction procedure taken to create the grid. The original acoustic depth values are assigned back to the grid after the bathymetric prediction is carried out [Smith and Sandwell, 2001]. This is done in order to retain the resolution in areas with multibeam coverage. At the same time, large areas are based on singlebeam and single soundings. When these depth values do not match gravity-predicted bathymetry, these artifacts become pronounced. These artifacts create wavelengths in the bathymetry (in the areas of no multibeam data sources) that are not represented by satellite-derived gravity with the stated spatial resolution of 20 - 160 km [Smith and Sandwell, 2001]. Based on the internal consistency assessment, there are frequencies present in S&S with less than 12.5 km spatial wavelength. The magnitudes of artifacts in S&S in the shelf areas reach 141% of WD (abs. max) (Figure 4-20). According to Marks et al. [2010], "errors" in S&S bathymetric prediction are not dependent on WD and amount to 50 m 50% of the time and 220 m 90% of the time. These "errors" are negligible in deep water but are crucial in shallow areas.

On the other hand, these artifacts can show how well the gravity-predicted bathymetry surface fits the measured depth values. There are several limitations of predicted bathymetry in the Arctic. Satellite-derived gravity at high latitudes can be unreliable due to the ice conditions which add noise to the altimetry data [Smith and Sandwell, 2001; McAdoo et al., 2008]. High sediment thickness in the Arctic, in general, and in the shelf areas, in particular, causes poor correlation between gravity and bathymetry. In addition, according to McAdoo et al., [2008], the maximum spatial resolution of the gravity in the Arctic (south of 80°N) is 35 km, as compared to 20 km used in Smith and Sandwell prediction. These limitations should be kept in mind while using Type B datasets in the Arctic. The magnitude of the artifacts reflects the fitness of predicted bathymetry surface to the measured soundings and visually represents how reliable predicted

bathymetry is.

In terms of interpolation accuracy, the similarity of the interpolation performance was observed for both dataset Types (Figure 4-21 and Figure 4-22). The reasons for similar performance can be explained by the spline interpolation algorithm used for construction of both grids, together with the similar and relatively dense source data coverage for both grids. On average, the furthest distance to the source data points is 6 - 10 km, depending on the polygon, with a maximum distance of 17 km in polygon 3. According to Smith and Sandwell [2001], gravity-predicted bathymetry resolves spatial wavelengths of 20 - 160 km. In order to assess how well the gravity derived bathymetry interpolates across the data gaps, larger areas with no soundings are required, with maximum distance to the nearest source data point exceeding 20 km [Marks et al., 2010]. According to the results, interpolation of acoustic data with relatively dense source data coverage performs as well as interpolation of satellite altimetry. Type A datasets might be preferred over Type B datasets in areas of relatively good source density, considering the artifacts present in Type B datasets.

5.1.2 Implications of results

Factors affecting accuracy of the grids

Based on the results of accuracy assessment of the bathymetry grids, several parameters can be defined which affect the accuracy of the grids. These parameters, identified by Li [1990] and Li and Gold [2005], are shown in Figure 5-1. The parameters include accuracy, distribution and resolution of the source data, the interpolation method used, resolution of the grid chosen and roughness of the morphology being modeled. It is a combination of all these parameters, which affect the final accuracy of the modeled surface. Since these factors vary in space, some have more weight than others depending on the area. In this study, only accuracy of the source data and accuracy of the final grid were assessed (Figure 4-9, Figure 4-12 and Figure 4-13). Discussion of the accuracy of the grids based on the results of analyses from polygon to polygon

is given below. Source data distribution and roughness of morphology are discussed qualitatively and are summarized in Table 2.2.
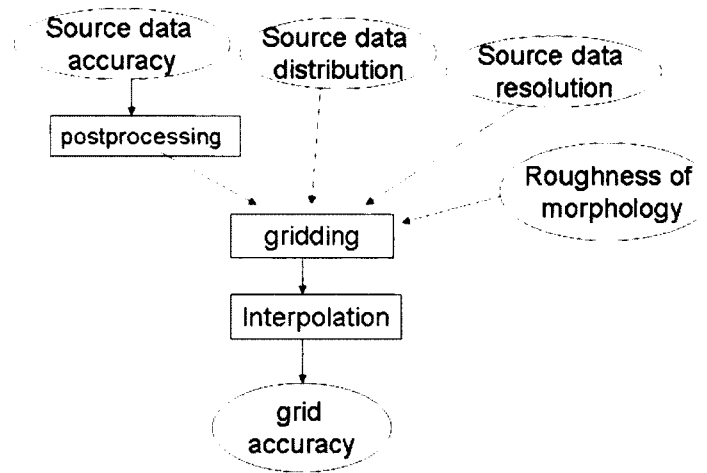
Figure 5-1: Parameters that affect the accuracy of analyzed datasets [modified after Li and Chen, 1999; Li and Gold, 2005].

Polygon 1 covers the area of the Molloy mid-oceanic ridge with depths ranging from 1200 m to 5400 m (Figures C.1, C.7, Table 2.2). The major factors affecting the accuracy of GEBCO_08, S&S and SRTM30_Plus within this polygon are the rough morphology of the mid-oceanic ridge together with the accuracy and dense distribution of source data. The primary source data for this polygon is the RV *Polarstern* multibeam grid (Figure 4-8). Bias in the RV *Polarstern* multibeam grid (Figure 4-9) creates bias in the S&S and SRTM30_Plus grids in this area (Figure 4-13). The bias is not observed in GEBCO_08, since the proper sound speed corrections were applied to the data before including it into the grid. The means of differences between the GIN RAS multibeam data and the grids as a percentage of WD are 1.9% and 1.95% for S&S and SRTM30_Plus respectively, which is significant compared to the GIN RAS multibeam data worst case uncertainty estimates of 1.85%. Additionally, the effect of rough morphology can be observed in the wide distribution of differences between the GIN RAS multibeam data and the grids, with SD around 50 m.

Polygon 2 covers the area of the Knipovich mid-oceanic ridge with abyssal hills and

continental slope, with depths ranging from 100 m to 3600 m (Figures C.1, C.7, Table 2.2). The major factors affecting the accuracy of the grids within this polygon include rough morphology and the slight bias in the source data. The primary source data for this polygon includes Norwegian single soundings and NGDC data sources (Figure 4-8). As discussed before, Norwegian data sources are shallow biased (Figure 4-9). Since Norwegian data was the primary data source for the grids within this polygon, a slight shallow bias (mean of 1% - 1.3% of WD) is observed in GEBCO_08 and Type B grids (Figure 4-13). Meanwhile the bias in the grids is below the GIN RAS multibeam data worst case uncertainty estimates and therefore cannot be considered significant. The wide distribution (with SD around 3.5% - 4.9% of WD) of differences can be explained by the rough morphology of the mid-oceanic ridge. The SD values are higher than in polygon 1 possibly due to the lower source data density compared to multibeam coverage in polygon 1.

Polygon 3 covers the area of abyssal plain within the Norwegian Basin and the foot of the continental slope with depths ranging from 1700 m to 3000 m (Figures C.3, C.9, Table 2.2). Within polygon 3 all grids perform well, since in this area all grids are based on high accuracy multibeam source data and the local morphology is smooth. Observed differences with the GIN RAS grid have small means of 0.2 - 0.3% and SD of 0.6% of WD.

Polygon 4 covers the area within a shelf of the Norwegian and Barents Seas with depths ranging from 150 m to 400 m (Figures C.4, C.10, Table 2.2). The major factors affecting the accuracy of the grids within this polygon include source data accuracy, smooth morphology and interpolation performance in Type B grids on the shelf. Norwegian data sources are the only data sources present within this polygon (Figure 4-8). The shallow bias in the source data (Figure 4-9) causes the bias in the GEBCO_08 and Type B grids (Figure 4-12, Figure 4-13). Considerable bias is observed in the distribution of differences with the GIN RAS multibeam data between GEBCO_08 and Type B grids (Figure 4-12), with a mean of around 25 m (7% of WD). Type B grids have a wide distribution of differences, with a SD around 35 m (10% of WD). Comparing

the accuracy of the source data for S&S (Figure 4-9) to the grid accuracy (Figure 4-12), the statistics worsened with the mean going from -17 m to -29 m, and the SD increasing from 13 m to 35 m. This implies that the interpolation method added considerable error to the Type B grids, with differences exceeding 20% of WD (Figure 4-13).

For polygons 5 and 6, source data accuracy was not assessed. The best available description of source data is given here. Polygon 5 covers the trough within the Barents Sea shelf with depths ranging from 50 m to 500 m (Figures C.5, C.11, Table 2.2). The major factors affecting the accuracy of the grids within this polygon include source data density and distribution, the rough morphology of the trough, and the interpolation performance of Type B grids on the shelf. The primary source data within this polygon for GEBCO_08 include Norwegian data sources, digitized contours and multibeam source data (Table 2.2, discussed in Figure C.5). The primary source data within this polygon for S&S include Norwegian data sources and NGA single soundings (Table 2.2, discussed in Figure C.11). The GEBCO_08 data has overall better performance than Type B grids (Figure 4-13) due to the presence of multibeam source data within this polygon. The primary reason for high means (around 7% - 15% of WD) and SD (around 25% of WD) in Type B grids within this polygon is the lack of sounding data which would resolve the trough (Figure C.11). Additionally, the poor performance of gravity-derived bathymetry on the shelf adds to the error in Type B grids.

Polygon 6 covers the area of the Barents Sea continental slope facing the Eurasian Basin with depths ranging from 60 m to 2900 m (Figures C.6, C.12, Table 2.2). The S&S grid does not provide coverage for this polygon, and only GEBCO_08 and SRTM30_Plus are used in the accuracy assessment (Figure 4-13). SRTM30_Plus is based solely on IBCAO data sources within this polygon (Becker et al., 2009), since S&S does not provide predicted bathymetry north of 80°N. IBCAO has additional multibeam data not present in SRTM30_Plus (discussed in Figure C.6). The major factors affecting the accuracy of the grids within the polygon include the source data distribution and sloped morphology. Additionally, the construction procedure used in

94

SRTM30_Plus (assignment of original depth values and "polishing" them into the grid) could have an effect on the final accuracy of SRTM30_Plus. Within this polygon the GEBCO_08 grid has overall better performance than SRTM30_Plus (Figure 4-13) due to the presence of multibeam source data.

The six study polygons cover different morphological provinces, such as: mid oceanic ridge (polygons 1, 2), abyssal plain (polygon 3), shelf area (polygons 4, 5) and continental slope (polygon 6). Besides differences in morphology, these polygons cover areas with different types of source data, such as multibeam (polygon 1, 3), Norwegian and NGDC data sources (polygon 2), Norwegian data sources (polygon 4). Within polygons 5 and 6, Type A and Type B grids have differences in source data coverage: GEBCO_08 has multibeam data present (but not documented), which is not present in Type B grids. Additionally contour data was used in GEBCO_08 in the polygons where multibeam surveys are not present. To summarize, the differences in source data accuracy and distribution, together with the local roughness of the morphology and the interpolation method used affect the final accuracy of the output bathymetry surface.

Metrics defined as important for the choice of the grid

Choice of the most appropriate bathymetry grid is always application dependent. The datasets analyzed here were evaluated in terms of metrics that might be important for a specific application. The quality metrics that were defined as important for the choice of the grid are given in Table 5.1. The table below provides a summary of the main findings within the metrics defined. The colored cells show if the dataset is not recommended if the particular metric is important.

Datasets / Metrics	Type A grids				Type B grids	
	IBCAO	GEBCO_08	ETOPO1	GEBCO 1 minute	Smith and Sandwell	SRTM30_Plus
projection issues	none	none	one grid cell northern shift	none	not common projection	one grid cell northern shift in the global grid within the tile 20E-20W, 40N-90N
source data information	publicly available as an image	based on IBCAO	based on IBCAO	based on IBCAO	present - encoded in the grid as odd values	SID provided, with unique ID for each cruise
shoreline resolution	poor due to resolution	good	poor due to resolution	poor due to resolution	shift/ negative values on land (Greenland)	shift/ negative values on land (Svalbard and Greenland)
global coverage	regional product	yes	yes	yes	no, South of 80°N	yes
internal consistency	good				bad	
artifacts	present. in general smooth				pronounced for visualization, esp. on shelf	
source data accuracy	Norwegian sounding sources in general shallower then GIN RAS MBES regional sound speed applied	based on IBCAO	based on IBCAO	based on IBCAO	Regional sound speed is not applied. Source data accuracy is tested by fitness to the predicted bathymetry surface	not evaluated
depth accuracy	not evaluated	Shows relatively good performance in 5 polygons out of 6	not evaluated	not evaluated	Performs slightly better then GEBCO_08 in deep water (except bias pol.1), poor on shelf	very similar to S&S. slightly better accuracy on shelf
interpolation accuracy	good - assessment limited due to relatively dense source data distribution				good - assessment limited due to relatively dense source data distribution	

Table 5.1: Quality metrics defined as important for choice of the grid and summarized information on grids for each metrics based on results of the study. Color indicates whether the grid is not recommended if the particular metric is important.
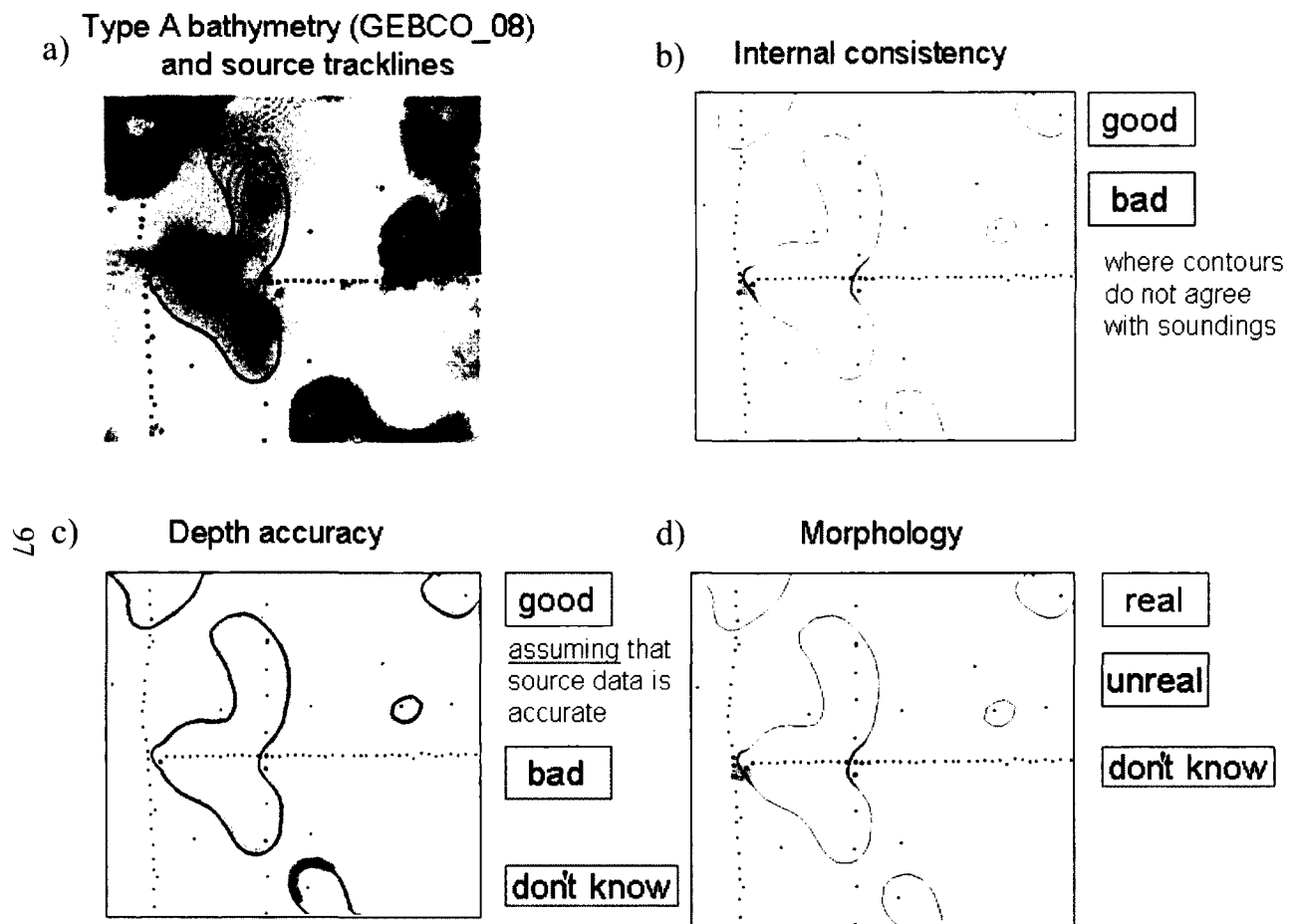
Figure 5-2: Qualitative assessment of GEBCO_08 grid performance expressed in quality terms: (a) GEBCO_08 bathymetry and source data coverage (black dots and contours); (b) internal consistency term; (c) depth accuracy term; (d) morphologic truthfulness term.

a) **Type B bathymetry (S&S) and source tracklines**

b) **Internal consistency**

good

bad

c) **Depth accuracy**

good

assuming that
source data
is accurate

bad
or **biased**

d) **Morphology**

real

assuming that
gravity correlates
with bathymetry

unreal
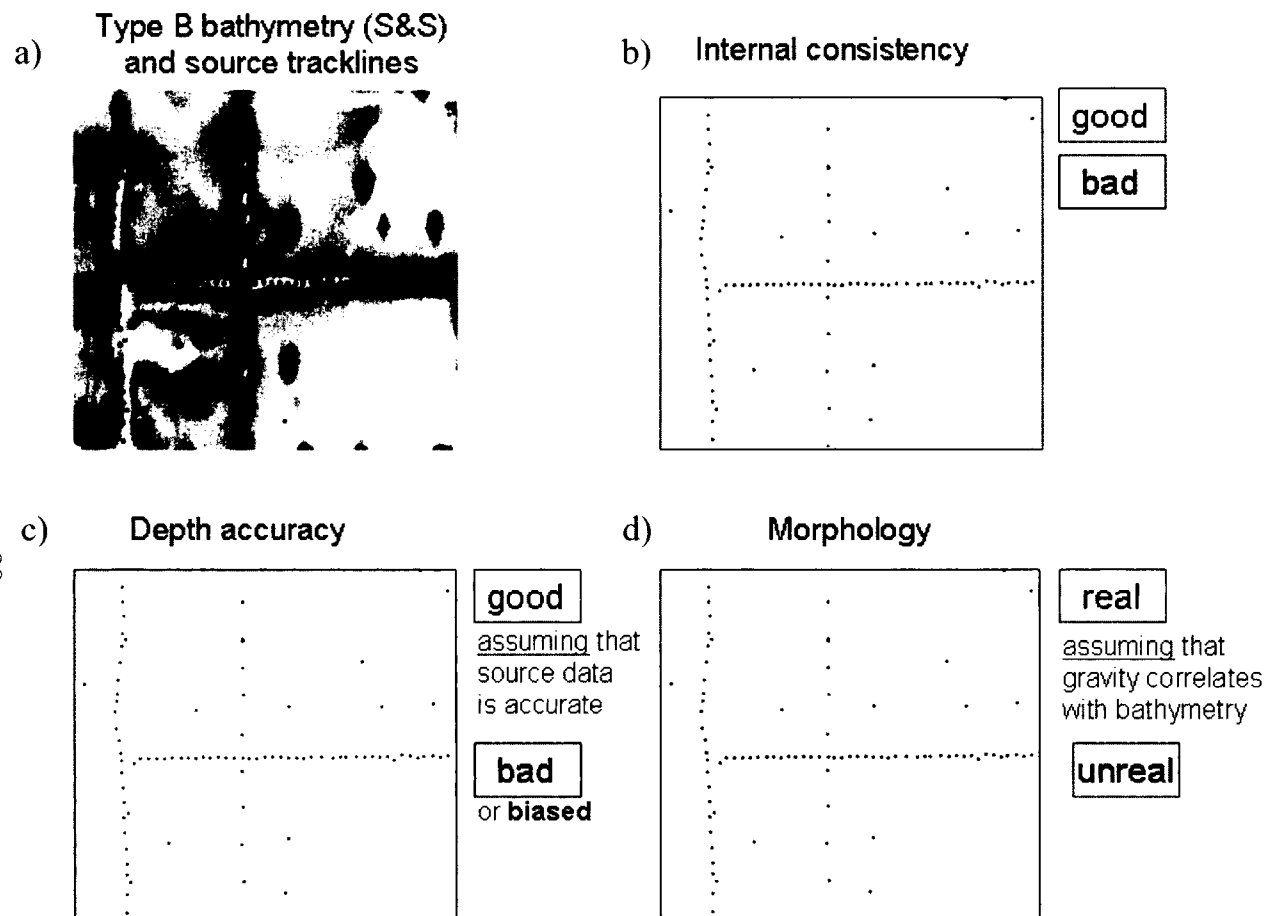
Figure 5-3: Qualitative assessment of S&S grid performance expressed in quality terms: (a) S&S bathymetry and source data coverage (black dots); (b) internal consistency term; (c) depth accuracy term; (d) morphologic truthfulness term.

Quality model important for different applications

Based on the analyses of differences between Type A and Type B datasets, a simple quality model is proposed to guide on choice of the grids. The quality of any grid is defined as follows: quality of the grid = internal consistency + external accuracy + morphologic truthfulness. Depending on the most important term for any given application, one Type of grid may be preferred over the other. These terms are assessed subjectively and are visualized in Figure 5-2 and Figure 5-3 for GEBCO_08 and S&S datasets. In general, the greater the area covered by color in Figure 5-2 and Figure 5-3, the less recommended it is to use a particular type of grid if a particular quality term is important for the application chosen.

Type A datasets (Figure 5-2) based primarily on sounding data sources and interpolated using contours in the areas with sparse sounding data have good performance in terms of internal consistency, with possible artifacts in areas where contours do not agree with acoustic sounding values (Figure 5-2b). In terms of accuracy (Figure 5-2c) the only areas in the grid that can be accurate are the ones based on acoustically surveyed depths, and only under the assumption that those depths are accurate. In terms of depiction of morphology (Figure 5-2d), interpolation based solely on contours cannot provide reliable depiction of morphology, although contours usually are drawn based on the local morphology expected in the area. Therefore, they can be trusted only to a limited extend.

Type B datasets (Figure 5-3) based on a combination of sounding data sources with gravity-derived bathymetry are more complicated. In terms of internal consistency (Figure 5-3b) they do not perform well in areas of sparse sounding measurements. Artifacts are observed in the bathymetry in areas where satellite-derived bathymetry does not match the measured depths. In terms of depth accuracy (Figure 5-3c), under the assumption that measured depths are accurate and gravity correlates with bathymetry, Type B grids should have good accuracy at the locations of the acoustic source data, and are biased in the areas based on gravity-prediction. In terms of depiction of morphology (Figure 5-3d), the construction procedure for S&S creates artificial

features at the location of soundings. At the same time, under the assumption of existing correlation between bathymetry and gravity, the morphology depicted outside of the source data area of influence is reliable.

5.1.3 Future work

Future work could include the following directions:

1) Perform spectral analyses and cross-correlation between bathymetry grids and gridded GIN RAS multibeam data to examine the spatial wavelengths that are resolved by the grids. Spectral analyses can also be used to identify the spatial wavelengths of the artifacts in the S&S bathymetry.

2) Quantitatively (rather than qualitatively) assess the accuracy of the grids as the function of source data density and distribution, as source data density appears to be one of the major contributing factors. Source data density maps could be created and data density values could be plotted against the grids' accuracy.

3) Studies show that interpolation performance is dependent on the roughness of the modeled morphology [Amante et al., 2011]. It would be interesting to perform the analyses on the distribution of "errors" (differences with GIN RAS multibeam and bathymetry grids) as a function of the regional slope.

4) The uncertainty of the GIN RAS multibeam grids could be a whole new thesis topic. In order to get comprehensive estimates of the accuracy of analyzed grids, the uncertainty of GIN RAS multibeam grids should be reevaluated.

5) The recommendation to the dataset compilers is to provide reliability grids supporting the bathymetry grids in order to facilitate more cautious interpretation by end-users.

CHAPTER VI

CONCLUSIONS

Six publicly available bathymetry grids were evaluated in the Arctic. The analyzed grids include the following: GEBCO 1 min, GEBCO_08, SRTM30_Plus, Smith and Sandwell, ETOPO1 and the regional grid IBCAO. The analyzed grids were separated into two Types: Type A grids (GEBCO 1 minute, GEBCO_08, IBCAO and ETOPO1), all based on the IBCAO dataset and therefore based solely on acoustic sounding data sources interpolated using contours in areas that lack data; and Type B grids (S&S and SRTM30_Plus) based on acoustic sounding data sources and combined with satellite-derived gravity data. These two Types have very distinct differences due to their respective construction methods. At the same time, the grids within each Type are very similar, therefore the major part of analyses was performed on a representative dataset from each Type, such as GEBCO_08 and S&S grids.

Differences between the grids were evaluated in terms of quality metrics which were defined as important when choosing a bathymetry grid. These metrics include source data accuracy, depth accuracy, internal consistency (presence of the artifacts), interpolation accuracy, registration issues and resolution of the coastline. The main findings within each metric are summarized in a table form in order to guide the choice of the most appropriate grid to the users.

High-resolution and accuracy, independent GIN RAS multibeam sonar grids were available as ground truth for comparison with the analyzed grids. Comparison between GIN RAS multibeam grids with USCGC *Healy* and RV *Oden* gridded multibeam data revealed no systematic errors in the GIN RAS data. The GIN RAS multibeam sonar grids were used for assessment of source data accuracy, depth accuracy and interpolation accuracy of analyzed grids at six separate study polygons of GIN RAS multibeam sonar grids coverage. The polygons of

study have distinct differences in morphology and water depth, and cover areas with different accuracy and distribution of source data used for the construction of analyzed bathymetry grids. The variety of conditions from polygon to polygon of study allowed addressing regional accuracy of the grids depending on the main accuracy-defining parameters.

Based on the accuracy assessment it was revealed that GEBCO_08 performs better than S&S over the three out of six polygons, namely polygons 1, 5 and 6. Within the polygon 1 both datasets are based on same source data (RV *Polarstern* multibeam grid), but the proper sound speed corrections was applied to the source data before incorporating it in GEBCO_08 grid, which was not done for the S&S grid. Within the polygons 5 and 6 GEBCO_08 has better source data coverage. Smith and Sandwell and SRTM30_Plus grids perform similar or slightly better than GEBCO_08 in deep areas. Poor performance of S&S and SRTM30_Plus was observed within shelf polygons (4, 5 and 6), with SD of differences exceeding 25% of WD. The main reasons for low accuracy and precision of S&S and SRTM30_Plus grids on shelf include scarcity of source data and poor performance of predicted bathymetry on shelf. The bias was revealed in the bathymetry of GEBCO_08, S&S and SRTM30_Plus grids within polygons 2 and 4; the bias is caused by the bias in the Norwegian source data on which grids are based within these two polygons. Based on the results of the accuracy assessment it was defined that source data accuracy, post processing of the source data (sound speed corrections), source data distribution, interpolation method and roughness of morphology are the main parameters which define the accuracy of analyzed bathymetry grids.

Based on the internal consistency assessment it was shown qualitatively and quantitatively that GEBCO_08 is more internally consistent than the S&S grid. It was revealed that both grid Types have artifacts present in the bathymetry, but artifacts in Type B grids are more pronounced for visualization purposes. The artifacts encountered in the bathymetry of GEBCO_08 and S&S grids were classified according to source data type which characterizes them. The classification of artifact types is provided in a table form with the morphological

description of each artifact type.

The quantitative assessment of internal consistency was performed on the shelf area. It was revealed that the artifacts in S&S grid can be as deep (or shallow) as 140% of WD. These artifacts create wavelengths in the bathymetry shorter than 12.5 km (in the areas of no multibeam data sources) that are not represented by satellite-derived gravity with the stated spatial resolution of 20 - 160 km [Smith and Sandwell, 2001]. The main reason for the obvious artifacts in Type B grids is the construction procedure taken to create Type B grids: the measured depth values are "polished" into the gravity-derived predicted bathymetry grid. The magnitude of the artifacts in S&S bathymetry can be used as a measure of how well the gravity-predicted bathymetry surface fits the measured depth values.

Based on the interpolation accuracy assessment it was shown that interpolation in Type A grids with solely acoustic data performs similar to interpolation with satellite-derived gravity data used in Type B grids. The similar performance of interpolation within both Types of grids is controlled by source data density as well as the same interpolation algorithm namely spline in tension interpolation method. Type A grids should be preferred over Type B grids in the area of relatively good source data density, considering the artifacts present in Type B grids. It was not possible to assess how well the gravity derived bathymetry interpolates across the data gaps, for the reason of relatively dense source data coverage within the study polygons. The stated spatial resolution of gravity is 20 - 160 km, while the furthest distance to the source data points varies within the polygons from 2 km to 10 km, with the maximum distance of 17 km. In order to assess accuracy of interpolation with gravity data, larger areas with no soundings are required, with maximum distance to the nearest source data point exceeding 20 km.

Comparison between grids within Type A revealed very few differences between the datasets, since they are all resampled versions of the IBCAO grid. A slight shift was found in ETOPO1 relative to the others, which could be due to misregistration while reprojecting to geographic coordinate system. GEBCO_08 should be preferred over the others in terms of higher

resolution, and fitness to the vector shoreline.

Comparison between grids within Type B showed that SRTM30_Plus is very similar to the S&S dataset. Regional differences directly correlate with differences in source trackline coverage and the finer resolution of SRTM30_Plus. SRTM30_Plus has very similar accuracy and precision to S&S in all the polygons except in the shelf polygons 4 and 5, where it has slightly better performance. Overall SRTM30_Plus has higher resolution, and due to that resolves shoreline better. It is represented in the more convenient geographic coordinate system (in terms of software applications which can handle it), while S&S is in GMT spherical Mercator. Also SRTM30_Plus has global coverage, while S&S provides coverage until 80°N. Meanwhile it should be noted that SRTM30_Plus has an observed shift relative to S&S in the area 20°E-20°W, 40°N-90°N.

Overall, it was shown that Type A grids perform better than Type B grids. In particular, the GEBCO_08 dataset performs well in terms of accuracy, internal consistency, and smoothness of the bathymetry and resolution of the coastline. Based on the analyses of interpolation accuracy, given the data density within the polygons of study, GEBCO_08 performs as well as the gravity-predicted bathymetry of S&S. GEBCO_08 is based on IBCAO source data and, considering its higher resolution and global coverage, should be preferred over other datasets. S&S and SRTM30_Plus, on the other hand, have pronounced artifacts caused by the "polishing" procedure and relatively poor accuracy on the shelf due mainly to the scarcity of source data and in general poor gravity prediction performance in these high latitudes and over shallow areas with great sediment thickness.

Based on the results of this study, several issues were reported to the grid compilers, in particular, observed misregistration in ETOPO1 and SRTM30_Plus, as well as step in bathymetry of S&S and SRTM30_Plus grids in the area of RV *Polarstern* multibeam sonar grid. In the upcoming versions of the bathymetry grids these issues will be addressed.

LIST OF REFERENCES

Amante, C. and Eakins, B.W., 2009, ETOPO1 1 arc-minute global relief model: procedures, data sources and analysis, NOAA Technical Memorandum NESDIS NGDC-24, 19 pp.

Amante, C., Love, M., Eakins, B., 2011, A method for quantifying digital elevation model (DEM) uncertainty introduced by interpolative gridding, 6th GEBCO Science day, poster, La Jolla, 4 October 2011

Becker, J.J., Sandwell, D.T., Smith, W.H., Braud, J., Binder, B., Depner, J., Fabre, D., Factor, J., et al., 2009, Global bathymetry and elevation data at 30 arc seconds resolution: SRTM30_Plus, Marine Geodesy, 32 (4), pp. 355-371

Bernhardsen, T., ed., 2002, Geographic information systems: an introduction, John Wiley & Sons, New York

Briggs, I.C., 1974, Machine contouring using minimum curvature, Geophysics, Vol. 39 (1), pp. 39-48

British Oceanographic Data Centre (BODC), 2003, The GEBCO 1 minute grid, Centenary edition of the GEBCO digital atlas [CD-ROM], Liverpool, UK, http://www.bodc.ac.uk/data/online_delivery/gebco/

British Oceanographic Data Centre (BODC), 2008, Documentation for the GEBCO_08 Grid, http://www.bodc.ac.uk/data/online_delivery/gebco/

British Oceanographic Data Centre (BODC), 2008, The GEBCO_08 grid, version 20091120, http://www.bodc.ac.uk/data/online_delivery/gebco/

Caress, D.W., and Chayes, D.N., 2002, Processing, archiving, and disseminating large swath mapping datasets using MB-System, EOS Trans., AGU, 83 (47)

Carpine-Lancre et al., 2003, The history of GEBCO 1903-2003, GITC bv., Lemmer, Netherlands, 140 pp.

Elmore, P.A., Fabre, D.H., Sawyer, R.T., Ladner, R.W., 2009, Uncertainty estimation of historical bathymetry data from Bayesian networks, MTS/IEEE Biloxi - Marine Technology for Our Future: Global and Local Challenges, OCEANS 2009 , art. no. 5422417, 26-29 Oct., pp. 1-8

Gallant, J.C., Wilson, J.P., 2000, Primary topographic attributes, in Terrain analyses: principles and application, eds. Wilson, J.P., Gallant, J.C., John Wiley & Sons, Inc., pp. 1-28

Geological Survey, ed., 1997, GTOPO30 Digital Elevation Model: U.S Geological Survey, EROS Data Center, Sioux Falls, South Dakota

Gonzalesz, R.C. and Woods, R.E., 1993, Image enhancement, in Digital image processing, Addison-Wesley Publishing Co., pp. 161-249

Goodwillie, A., 2003, User guide to the GEBCO one minute grid, Centenary Edition of the GEBCO Digital Atlas [CD-ROM], http://www.bodc.ac.uk/data/online_delivery/gebco/

Hall, J.K, 2006, GEBCO centennial special issue – charting the secret world of the ocean floor: The GEBCO project 1903-2003, Mar. Geophys. Res., 27, pp. 1-5

Hare, R., Godin, A., Mayer, L., 1995, Accuracy estimation of Canadian swath (Multibeam) and sweep (Multi Transducer) sounding systems, technical report, Canadian Hydrographic Serv., Ottawa

Hell, B. and Jakobsson, M., 2011, Gridding heterogeneous bathymetric data sets with stacked continuous curvature splines in tension, Mar. Geophys. Res. manuscript (preprint)

Hell, B., 2011, Mapping bathymetry: From measurements to applications, doctoral thesis, comprehensive summary, Department of Geological Sciences, Stockholm University, 41 pp.

HLY 0503 cruise report, http://www.icefloe.net/hly0503/HLY-05-03-MGG_Final_Report.pdf

Hutchinson, M.F. and Gallant J.C., 1999, Representation of terrain, in Geographical Information Systems: Volume 1 Principles and Technical issues, eds. Longley, P. A., Goodchild, M. F., Maguire, D. J., Rhind, D. W., Ch. 9, pp. 105-124

Hutchinson, M.F. and Gallant J.C., 2000, Digital elevation models and representation of terrain shape, in Terrain analyses: principles and application, eds. Wilson, J.P., Gallant, J.C, John Wiley & Sons, Inc., pp. 1-28

International Hydrographic Organization Committee, 2008, IHO standard for hydrographic surveys, Spec. Publ. 44, 5th ed., Int. Hydro. Org., Monaco

International Hydrographic Organization, 1994, Hydrographic dictionary, Spec. Publ. 32, 5th ed., Int. Hydro. Org., Monaco

Jakobsson, M. and Macnab R., 2008, Technical reference and user's guide to the International Bathymetric Chart of the Arctic Ocean (IBCAO), beta version, http://www.ngdc.noaa.gov

Jakobsson, M., Armstrong A., Calder B., Huff L., Mayer L., and Ward L., 2005, On the use of historical bathymetric data to determine changes in bathymetry, International Hydrographic Review, 6 (3), pp. 25–41

Jakobsson, M., Calder, B., Mayer, L., 2002, On the effect of random errors in gridded bathymetric compilations, Journal of Geophysical Research-Solid Earth, 107 (B12), pp. 1-14

Jakobsson, M., Cherkis, N.Z., Woodward, J., Coakley, B., Macnab, R., 2000, A new grid of Arctic bathymetry aids scientists and mapmakers, EOS Trans., AGU, 81 (9), pp. 89, 93, 96

Jakobsson, M., Macnab, R., Mayer, L., Anderson, R., Edwards, M., Hatzkt, J, Schenke, H-W., Johnson, P., 2008, An improved bathymetric portrayal of the Arctic Ocean: Implications

for ocean modeling and geological, geophysical and oceanographic analyses, Geophysical Research Letters, 35, pp. 1-5

Jakobsson, M., Marcussen, C., and LOMROG Scientific Party, 2008, Lomonosov Ridge Off Greenland 2007 (LOMROG) - Cruise Report, Special Publication Geological Survey of Denmark and Greenland, Geological Survey of Denmark and Greenland, Copenhagen, p. 122

Jakobsson, M., Nilsson, J., O'Regan, M., Backman, J., Löwemark, L., Dowdeswell, J.A., Mayer, L., Polyak, L., Colleoni, F., Anderson, L., Björk, G., Darby, D., Eriksson, B., Hanslik, D., Hell, B., Marcussen, C., Sellén, E., Wallin, A., 2010, An Arctic Ocean ice shelf during MIS 6 constrained by new geophysical and geological data in Quaternary Science Reviews 29, pp. 3505-3517

Jones, M.T., 1994, The GEBCO Digital Atlas, NERC News (29), pp. 17-20

Jones, M.T., ed., 2003, User guide to the Centenary Edition of the GEBCO Digital Atlas and its data sets, Centenary Edition of the GEBCO Digital Atlas [CD-ROM], http://www.bodc.ac.uk/data/online_delivery/gebco/

Karel W., Pfeifer, N., Briese, C., 2006, DTM quality assessment, in ISPRS Technical Commission II Symposium, Vienna 12-14 July, pp. 7-12

Kennett, J.P., 1982, Marine Geology, Prentice-Hall, Inc., New Jersey, 813 pp.

Klenke, M. and Schenke, H.W., 2006, Digital terrain model (DTM) of the central Fram Strait. supplement to [Klenke, & Schenke, 2002]

Klenke, M. and Schenke, H.W., 2002, A new bathymetric model for the central Fram Strait, in Mar. Gephys. Res., Vol. 23 (4), pp. 367-378

Lamont Doherty Earth Observatory (LDEO), Columbia University, http://www.ldeo.columbia.edu/

Laughton, A.S., 2001, Shape as a key to understanding the geology of the oceans, in Understanding the oceans: A century of ocean exploration, eds. Deacon, M., Rice, T., Summerhayes, C., Part 2, Ch. 5, UCL Press, London, UK and New York, NY, US, pp. 92-108

Laxon, S.W. and McAdoo, D.C., 1994, Arctic Ocean gravity field derived from ERS-1 satellite altimetry, Science, Vol. 265, pp. 621-624

Le Provost C., 2001, Inaccuracies in our knowledge of the ocean bathymetry: A limiting factor for tide modeling, in Improved global bathymetry: Final report of SCOR working group 107, Technical Series 63 of Intergovernmental Oceanographic Commission, UNESCO, pp. 23-28,

Lemments, M., 1999, Quality description problems of blindly sampled DEMs, in Proceedings of the international symposium on spatial data quality: 18 - 20 July 1999, Hong Kong, The Hong Kong Polytechnic University, Hong Kong, pp. 210-218

Li, Z., 1990, Sampling strategy and accuracy assessment for digital terrain modelling, Ph.D. Dissertation, University of Glasgow, 299 pp.

Li, Z. and Chen, J., 1999, Assessment of the accuracy of digital terrain models (DTM): Theory and practice, Proceedings of the international symposium on spatial data quality: 18 - 20 July 1999, Hong Kong, The Hong Kong Polytechnic University, Hong Kong, pp. 202-209

Li, Z., 1992, Variations of the accuracy of digital terrain models with sampling interval, in Photogrammetric Record, 14 (79), pp. 113-128

Li, Z., Zhu, Q., Gold, C., 2005, Digital terrain modeling: principles and methodology, CRC Press, 323 pp.

Lin, P., Yu, Q., Li., J, 1999, Accuracy of digital elevation models generated by ANUDEM at a macro-scale level, in Proceedings of the international symposium on spatial data quality: 18 - 20 July 1999, Hong Kong, The Hong Kong Polytechnic University, Hong Kong, pp. 191-201

Lindquist, K.G., Engle, K., Stahlke, D., Price, E., 2004, Global topography and bathymetry grid improves research efforts, EOS Trans., AGU, Vol. 85 (19), p. 186

Macnab, R. and Jakobsson, M., 2000, Something old, something new: Compiling historic and contemporary data to construct regional bathymetric maps, with the Arctic Ocean as a case study, Int. Hydrog. Rev., 1(1), pp. 2-16

Macnab, R., Jakobsson, M. et al., 2001, GSC Open File 4185, IASC/IOC/IHO Editorial Board for the International Bathymetric Chart of the Arctic Ocean, Third meeting of the Editorial Board: New Hampshire, May 27-28, 2001

Marks, K.M. and Smith, W.H.F., 2011, Assessing Errors in altimetric and other bathymetry grids, NOAA Technical Report NESDIS 132, http://ibis.grdl.noaa.gov/SAT/AltBathy/TechRep/Tech.Rep.132.pdf

Marks, K.M. and Smith W.H.F., 2009, An uncertainty model for deep ocean single beam and multibeam echo sounder data, Mar. Geophys. Res., Vol. 29 (4), pp. 239-250

Marks, K.M. and Smith, W.H.F, 2005, The 2500 meter isobath from satellite bathymetry, accuracy assessment in light of IHO S-44 standards, Internat. Hydrograph. Rev., Vol. 6 (2), pp. 19-29

Marks, K.M. and Smith, W.H.F, 2006, An evaluation of publicly available global bathymetry grids, Mar. Geophys. Res., Vol. 27 (1), pp. 19-34

Marks, K.M., Smith, W.H.F., 2010, Sandwell, D.T., Evolution of errors in the altimetric bathymetry models used by Google Earth and GEBCO, Mar. Geophys. Res., Vol. 31 (3), pp. 223-238

Maune, D.F., ed., 2007, Digital elevation model technologies and applications: the DEM user's manual, 2nd edition, American Society for Photogrammetry and Remote Sensing, 655 pp.

McAdoo, D.C., Farrell, S.L., Laxon, S.W., Zwally, H.J., Yi, D., Ridout, A.L., 2008, Arctic Ocean gravity field derived from ICESat and ERS-2 altimetry: Tectonic implications, Journal of Geophysical Research, 113 (B05408), pp. 1-12

Monahan, D., Clarke, J.H., Cartwright, D., Buzeta, M.-I., 2003, Hydrography and ocean science in marine protected areas: Lessons from Musquash, Canadian Technical Report of Fisheries and Aquatic Sciences, 2463, pp. 79-86

National Geophysical Data Center (NGDC), 1988, ETOPO-5 Bathymetry/Topography Data (Data Announcement 88-MGG-02), National Oceanic and Atmospheric Administration, U.S. Department of Commerce, Boulder, Colorado

National Geophysical Data Center (NGDC), 2001, 2-minute Gridded Global Relief Data (ETOPO2), National Oceanic and Atmospheric Administration, U.S. Department of Commerce, Boulder, Colorado, http://www.ngdc.noaa.gov/mgg/fliers/01mgg04.html

National Geophysical Data Center (NGDC), 2002, GEODAS CD-ROM worldwide marine geophysical trackline data (version 4.1) (Data Announcement 2002-MGG-01), National Oceanic and Atmospheric Administration, U.S. Department of Commerce, Boulder, Colorado

National Geophysical Data Center (NGDC), 2009, Marine Trackline Geophysics, GEODAS (version 5.0.10) On-line: http://map.ngdc.noaa.gov/website/mgg/trackline/viewer.htm

National Oceanic and Atmospheric Administration (NOAA), On-line Photo Library http://www.photolib.noaa.gov/

Oksanen, J. and Sarjakoski, T., 2005, Error propagation of DEM-based surface derivatives, Computers & Geosciences, 31(8), pp. 1015-1027.

Peyve et al., 2009, The structure of the Knipovich-Mohns Junction (North Atlantic), in Doklady Earth Sciences, Vol. 426, No 4, pp. 551-555, original Russian text in Doklady Akademii Nauk, Vol. 426, No 3, pp. 355-360

Rutledge, A.K., and Leonard, D. S., 2001, Role of multibeam sonar in oil and gas exploration and development, Offshore Technology Conference, 30 April - 3 May 2001, Houston, Texas

Ryan, W.B.F. et al., 2009, Global multi-resolution topography synthesis, Geochem. Geophys Geosyst., 10 (3), pp. 1-9

Sandwell, D.T. and Smith, W.H.F., 2009, Global marine gravity from retracked Geosat and ERS-a altimetry: ridge segmentation versus spreading rate, Journal of Geophys. Res., 114 (B01411), pp. 1-18

Schenke, H.W., 2003, Interpolation and contouring of sparse sounding data, GEBCO Centenary meeting, [CD-ROM]

Schenke, H.W., Arndt, J.E., Black, J., Jakobsson, M., Nitsche, F.O., Tate, A.J., 2011, The International Bathymetric Chart of the Southern Ocean IBCSO, AGU meeting, poster, San Francisco, 5 December 2011

Smith, W.H.F., 1993, On the accuracy of digital bathymetric data, Journal of Geophys. Res., 98 (B6), pp. 9591-9603

Smith, W.H.F. and Sandwell, D.T., 1994, Bathymetric prediction from dense satellite altimetry and sparse shipboard bathymetry, Journal of Geophys. Res., 99 (B11), pp. 21803-21824

Smith, W.H.F. and Sandwell, D.T., 1997, Global sea floor topography from satellite altimetry and ship depth soundings, Science, 277 (5334), pp. 1956-1962

Smith, W.H.F. and Sandwell, D.T., 2001, Bathymetric estimation, in Satellite Altimetry and Earth Sciences, Ch. 12, International Geophysics, 69, pp. 441-457

Smith, W.H.F. and Sandwell, D.T., 2004, Conventional bathymetry, bathymetry from space, and geodetic altimetry, Oceanography, 17 (1), pp. 8-23

Smith, W.H.F. and Wessel, P., 1990, Gridding with continuous curvature splines in tension, Geophysics , Vol. 55 (3), pp. 293-305

Soluri, E.A. and Woodson, V.A., 1990, World Vector Shoreline, International Hydrographic Review, LXVII (1)

Veregin, H., 1999, Data quality parameters, in Geographical Information Systems: Volume 1 Principles and Technical issues, eds. Longley, P. A., Goodchild, M. F., Maguire, D. J., Rhind, D. W., Ch. 12, pp. 177-189

Vogt, P.R., Carron, M.J., Jung, W.-Y., Macnab, R., 2001, The Global Ocean Mapping Project (GOMaP) and UNCLOS: Optimizing Article 76 surveys for re-use as components in the construction of a global bathymetric model, 2001 ABLOS (Advisory Board on the Law Of the Sea) Conference, http://www.gmat.unsw.edu.au/ablos/#ABLOS01

Wechsler, S. and Kroll, C., 2006, Quantifying DEM Uncertainty and its effects on topographic parameters, Photogrammetric Engineering & Remote Sensing, Vol. 72 (9), pp. 1080-1090.

Wessel, P. and Smith, W.H.F., 1991, Free software helps map and display data, EOS Trans., AGU, 72 (41), p. 441

Wessel, P. and Smith, W.H.F., 1996, A global, self-consistent, hierarchical, high-resolution shoreline database, Journal of Geophys. Res., Vol. 101 (B4), pp. 8741-8743

Wessel, P. and Smith, W.H.F., 1998, New, improved version of generic mapping tools released, EOS Trans., AGU, 79 (47), p. 578

Wessel, P. and Watts, A.B., 1988, On the accuracy of marine gravity measurements, Journal of Geophys. Res., 93 (B1), pp. 393-413

Wilson, J.P., Gallant, J.C., 2000, Digital terrain analysis, in Terrain analyses: principles and application, eds. Wilson, J.P., Gallant, J.C., John Wiley & Sons, Inc., pp. 1-28

Wise, S. M., 1998, The effect of GIS interpolation errors on the use of Digital Elevation Models in geomorphology, in Landform monitoring, modelling and analysis, eds. Lane, S., Richards, K., Chandler, J., Ch.2, John Wiley & Sons, Inc., pp. 21-37

Wood, J., 1996, The Geomorphological Characterization of Digital Elevation Models, Ph.D. Dissertation, Department of Geography, University of Leicester, Leicester, UK

Wood, J.D., and Fisher, P., 1993, Assessing interpolation accuracy in elevation models, IEEE Comp. Graphics and Applications, Vol. 13 (2), pp. 48-56

Zayonchek et al., 2009, Geological-Geophysical Studies in the Northern Barents Sea and on the Continental Shelf of the Arctic Ocean during Cruise 25 of the RV *Akademik Nikolai Strakhov*, in Doklady Earth Sciences, Vol. 427, No 5, pp. 740-745, original Russian text in Dollady Akademii Nauk, 2009, Vol. 427, No 1, pp. 67-72

Zayonchek et al., 2010, Structure of the Transition zone continent-ocean of the North Western enclosure of Barents Sea (The results of 24-26 cruises of RV *Akademik Nikolai Strakhov*, 2006-2009), original Russian text, in Results of expeditions in the framework of the International Polar Year, Vol. 4

APPENDICES

APPENDIX A

DEFINITIONS

Some definitions taken from IHO Special Publication S-32 (Hydrographic Dictionary) [IHO, 1994] and DEM Manual [Maune, 2007], and comments on how they are used in the thesis:

Accuracy: "The closeness of its estimated elevation (surveyed or computed) to a standard or accepted (true) correct value" [Maune, 2007]. In this study accuracy refers to as vertical accuracy with respect to the values in a high resolution and accuracy GIN RAS multibeam sonar grids. The measures of accuracy used here include standard deviation of the differences and the mean of differences.

Artifacts: "Detectable artificial anomalies that are introduced to surface model via system-specific collection or processing techniques" [Maune, 2007]. Artifacts can be caused by systematic or interpolation errors.

DEM Quality assessment: "Steps taken to test and report the *accuracy* of digital elevation dataset and *evaluate its usability*. This includes quantitative assessment of data accuracy as well as qualitative assessment of data usability. It is common for DEMs to pass vertical accuracy testing requirements and still fail other quality factors that impact the usability of the elevation data" [Maune, 2007].

Error: "The difference between an observed or computed value of a quantity and the ideal or true value of that quantity" [IHO, 1994]. Any model is a subject to errors introduced through data sources errors and through the modeling process. Three types of errors come from the source data: outliers, systematic errors and random errors [Maune, 2007; Li et al., 2005]. Interpolation errors are added to this group trough the interpolation process, which involves propagation of errors from measured data points to interpolated points and also introduces errors due to the surface modeling process [Li and Chen, 1999].

Precision: "Measure of tendency of a set of values to cluster about a number determined by set. Usual measure is standard deviation...Precision is distinguished from accuracy by the fact that accuracy is a measure of tendency to cluster about a number not determined by the data set but specified in some other manner. Precision may also be considered as a measure of consistency among repeat measurements. Measurements may be consistent but may be consistently inaccurate" [Maune, 2007].

Uncertainty: "The interval (about a given value) that will contain the true value of the measurement at a specific confidence level" [IHO, 1994].

APPENDIX B

GIN RAS MULTIBEAM DATA UNCERTAINTY VALUES

1. RV *Strakhov* instruments and their offsets according to PDS2000 conventions:

Vessel - Strakhov[Multibeam Survey]

Geometry | Equipment | Computations | Data Sources | Guidance | Logging | Simulation | Aliases | Alarms

Vessel contour

Strakhov ▼

New | Edit

Vessel wireframe

(None) ▼

Vessel draught

0

Sea level (positive above reference point)

0

Vessel turn radius

25

Offsets

Name	X	Y	Z
Zero Offset	0.00	0.00	0.00
Octans	0.00	0.00	0.00
Trimble GPS	0.97	5.40	19.58
SeaBat 7150	1.60	2.36	-5.78
Edgetech SBP	1.60	-0.87	-5.73

Add

Overview

OK | Отмена | Справка

Figure B.1: RV *Strakhov* vessel sensors offsets, print screen from PDS2000 software. PDS2000 convention: X axis positive to starboard, Y axis positive to bow, Z axis positive up. Sensors are entered from the Common Reference Point (CRP) to the sensors.

114

2. Instruments on *Strakhov* [cruise reports]: Seabat 8150, upgraded to Seabat 7150 (Oct 2006),

Seabat 8111, SVP-70, Trimble DSM132, IXSEA Octans III

3. TPU values (*Strakhov* vessel file) used to estimate uncertainty of *Strakhov* multibeam data. All

sensor offsets were recomputed according to CARIS convention (Z axis positive into the water,

MRU assumed 0,0,0 point):

MRU to Trans ...	MRU to Trans2...	MRU to Trans ...	MRU to Trans2...	MRU to Trans ...	MRU to Trans2...	Nav to Trans X...
1.600	0.000	2.360	0.000	5.780	0.000	0.630
Nav to Trans2 ...	Nav to Trans Y...	Nav to Trans2 ...	Nav to Trans Z...	Nav to Trans2 ...	Trans Roll (deg)	Trans Roll 2 (d...
0.000	-3.040	0.000	25.360	0.000	0.010	0.000

4. TPU standard deviation values (*Strakhov* vessel file) used for TPU estimates. Values are taken

from cruise reports and manufacturer accuracy values published by CARIS:

Motion Gyro (d...	Heave % Amp	Heave (m)	Roll (deg)	Pitch (deg)	Position Nav (m)	Timing Trans (s)
0.158	5.000	0.100	0.100	0.100	1.000	0.000

Nav Timing (s)	Gyro Timing (s)	Heave Timing (s)	Pitch Timing (s)	Roll Timing (s)	Offset X (m)	Offset Y (m)
0.000	0.000	0.000	0.000	0.000	0.20	0.200
					0.00	

Offset Z (m)	Vessel Speed (...	Loading (m)	Draft (m)	Delta Draft (m)	MRU Align Std...	MRU Align Std...	Comments
0.200	0.000	0.000	0.100	0.200	0.200	0.200	(null)

APPENDIX C

BATHYMETRY MAPS AND SOURCE TRACKLINE COVERAGE

C.1 Bathymetry maps of GEBCO_08 and trackline coverage for each study polygon
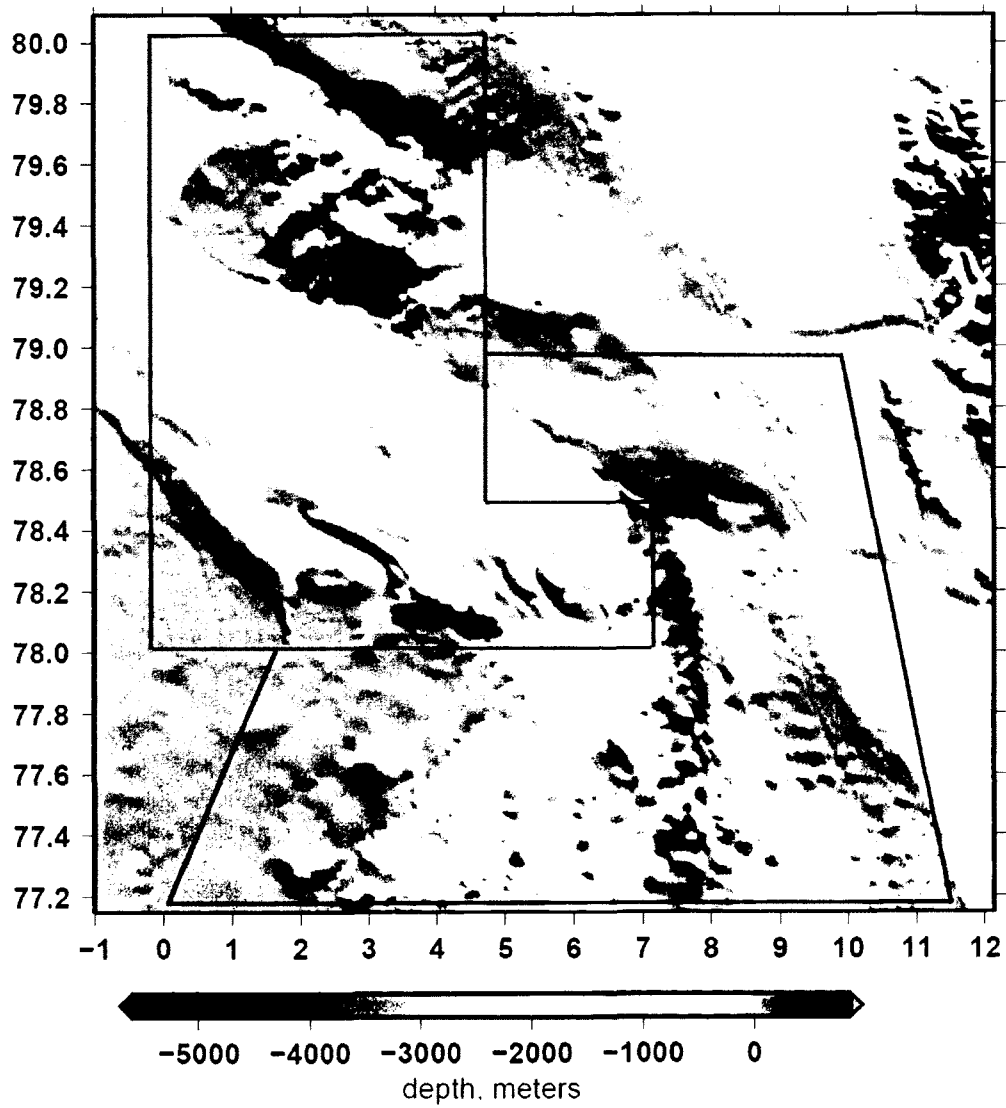
Figure C.1: Bathymetry of GEBCO_08 in polygons 1 (red) and 2 (blue).
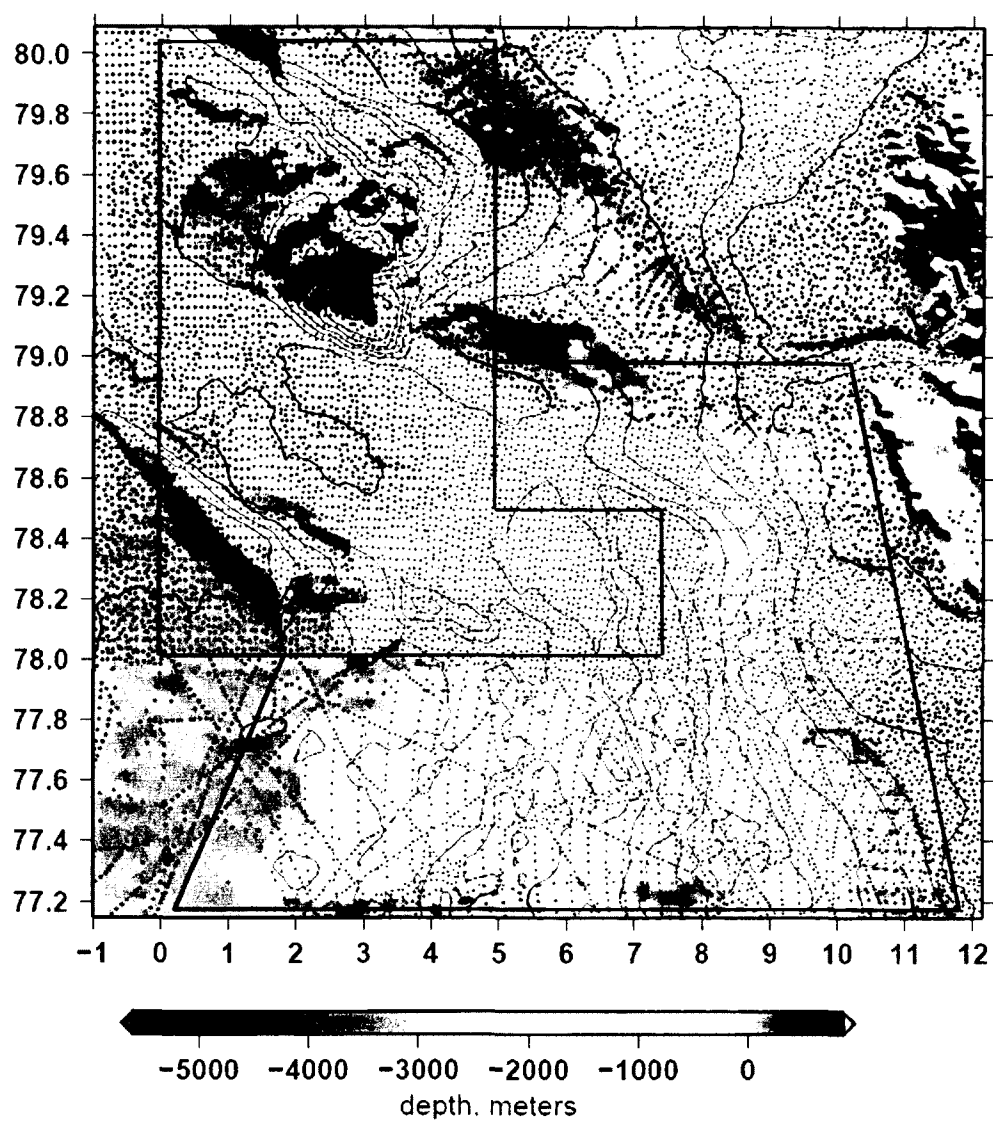
Figure C.2: Bathymetry of GEBCO_08 overlain by source tracklines (black points) and location of GIN RAS multibeam grid (bluescale layer) in polygons 1 (red) and 2 (blue).
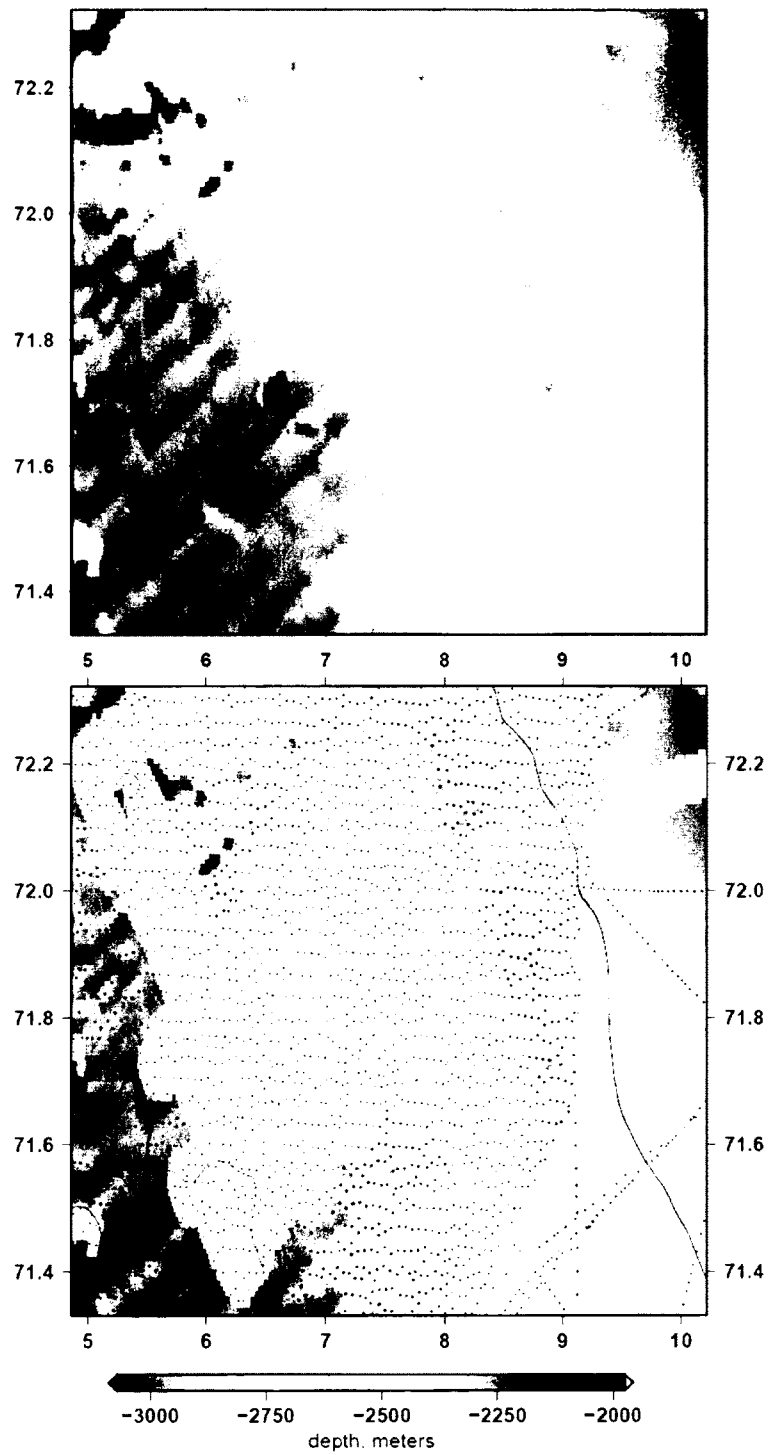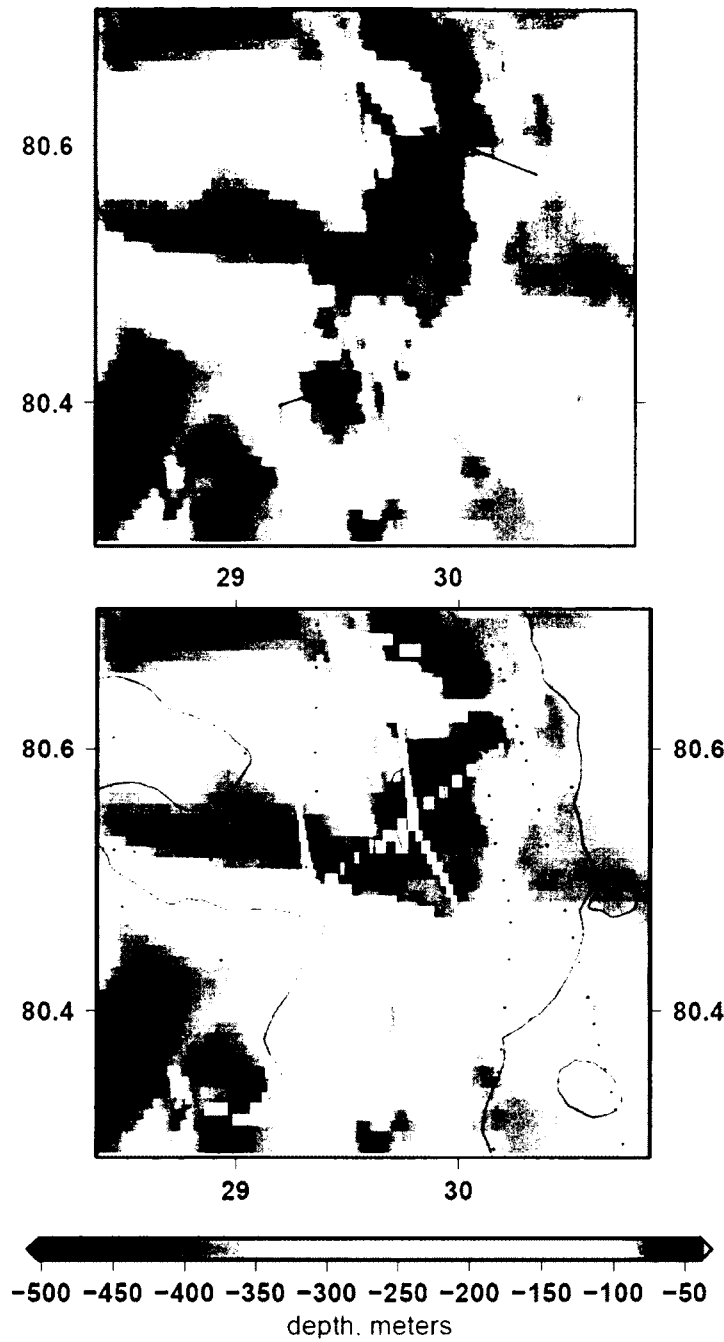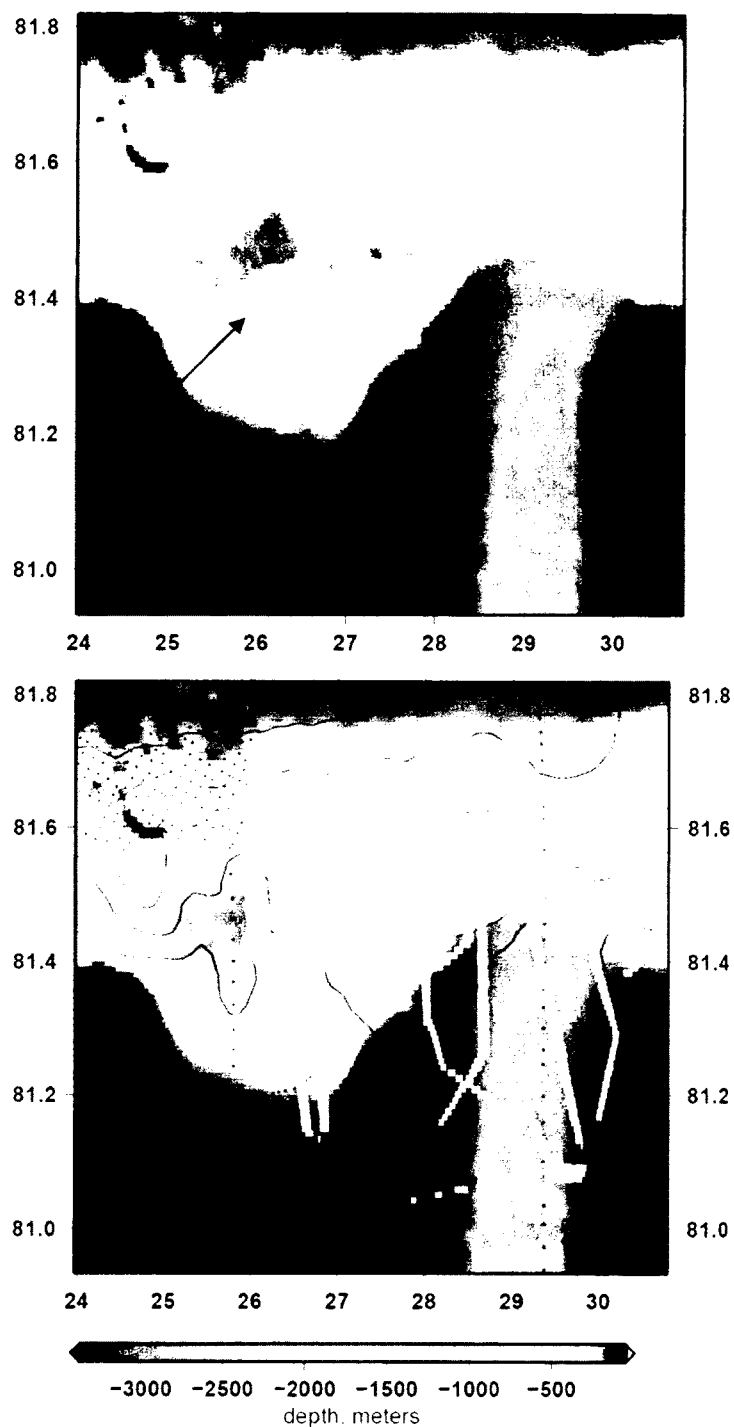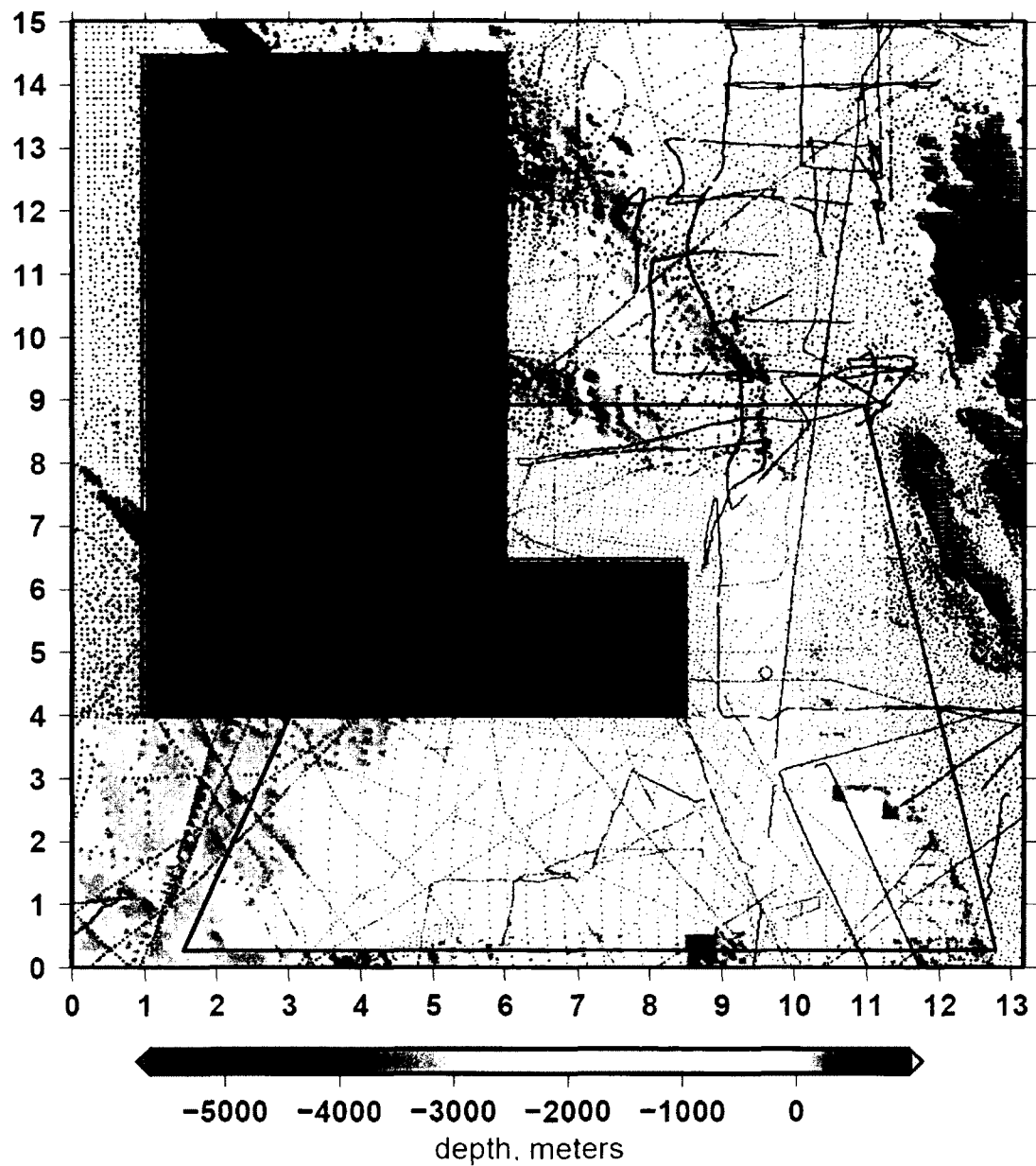
Figure C.3: Bathymetry of GEBCO_08 overlain by source tracklines (black points) and location of GIN RAS multibeam grid (bluescale layer) in polygon 3.
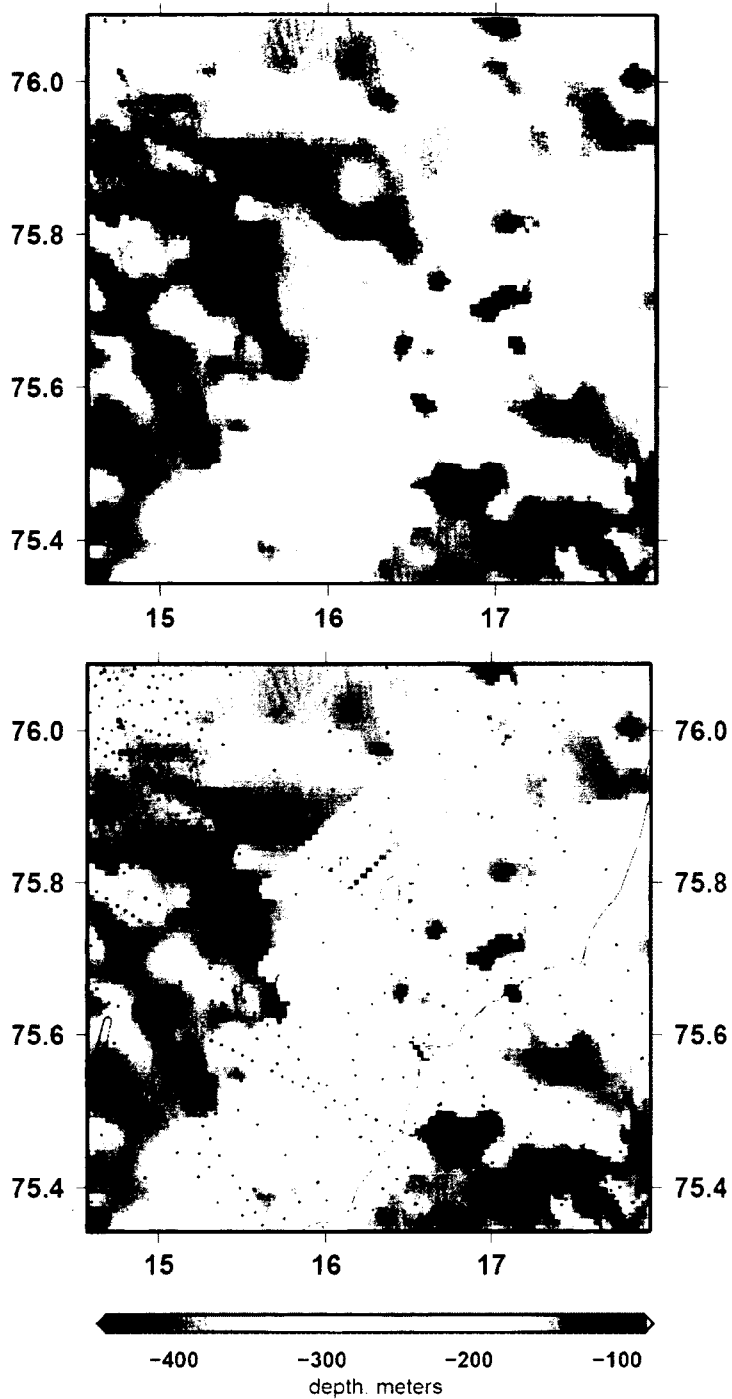
Figure C.4: Bathymetry of GEBCO_08 and bathymetry overlain by source tracklines (black points) and location of GIN RAS multibeam grid (bluescale layer) in polygon 4.
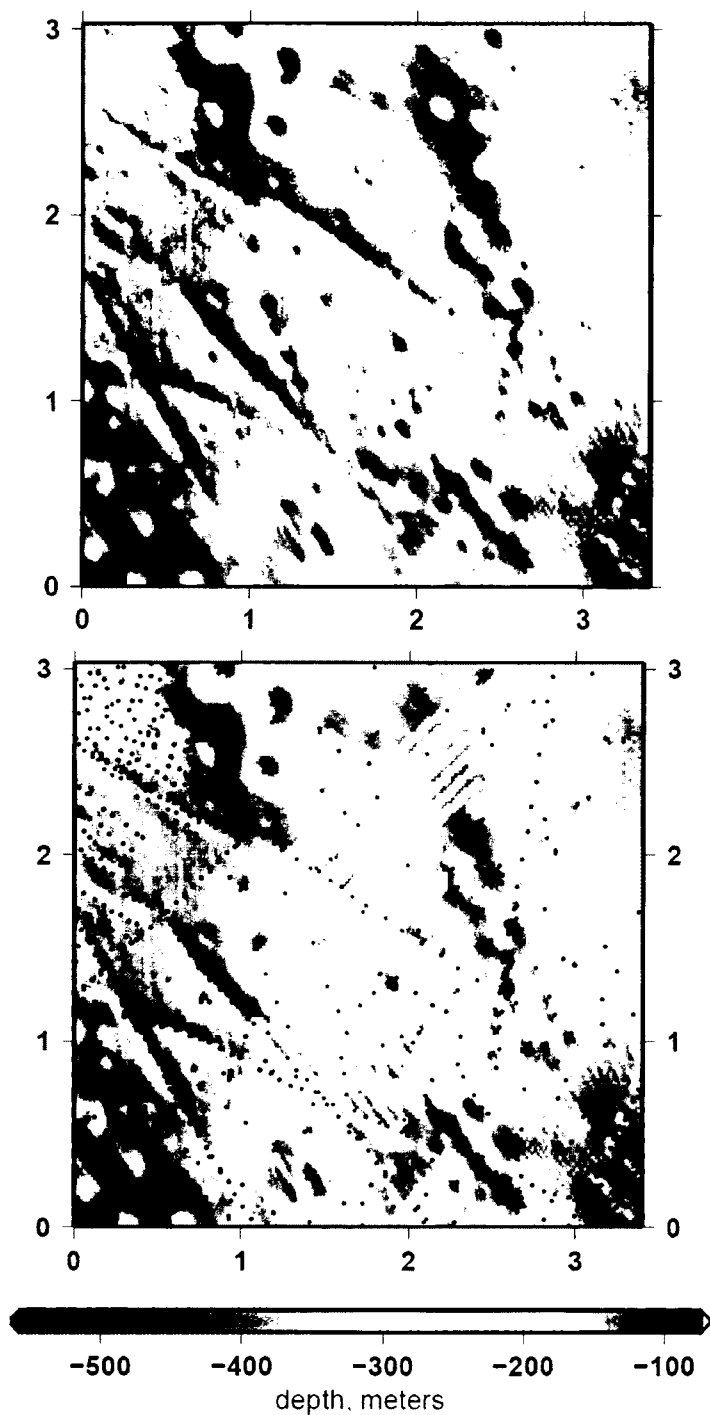
Figure C.5: Bathymetry of GEBCO_08 overlain by source tracklines and location of GIN RAS multibeam grid (bluescale layer) in polygon 5. The available source trackline information is not complete, because the details resolved in the bathymetry of the trough (arrows) could not be resolved by the trackline coverage provided. See Figure D.4: depth difference map with GIN RAS multibeam grid. The areas with small depth difference could be used to outline the location of possibly multibeam coverage not reflected by available source tracklines. The fact that source data coverage is not complete prevented the use of this polygon in analyses carried in sections 4.2.2 and 4.4.

120

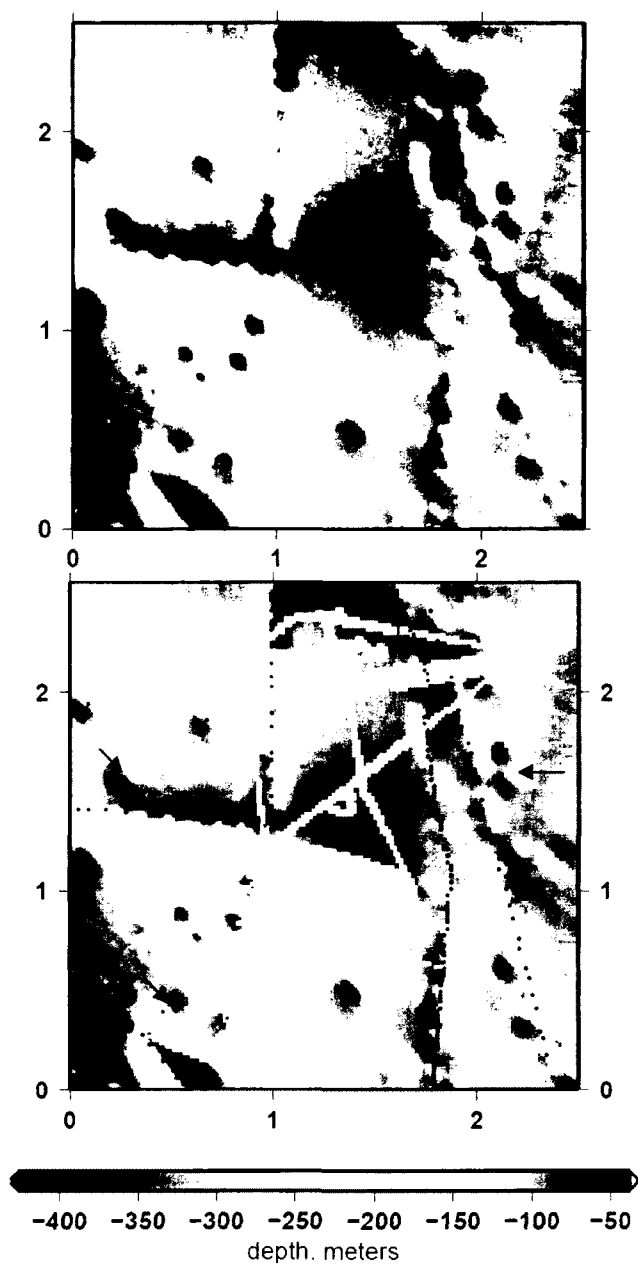Figure C.6: Bathymetry of GEBCO_08 overlain by source tracklines and location of GIN RAS multibeam grid (bluescale layer) in polygon 6. The available source trackline information is not complete, as the details in the bathymetry (arrows) could not be resolved by the trackline coverage provided. The fact that source data coverage is not complete prevented the use of this polygon in analyses carried out in sections 4.2.2 and 4.4.

C.2 Bathymetry maps of S&S and SRTM30_Plus (polygon 6) and trackline coverage for each study polygon
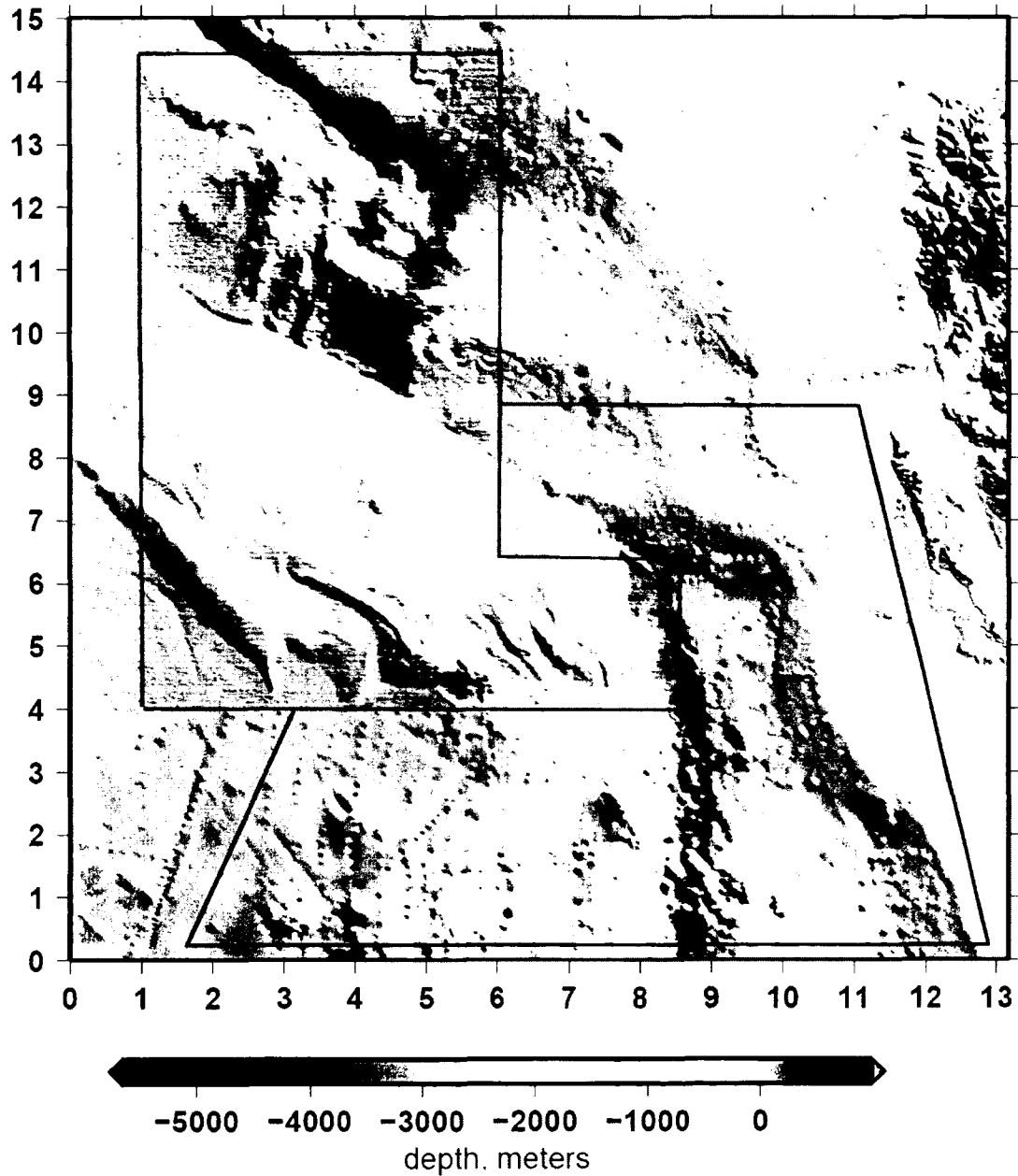
Figure C.7: Bathymetry of S&S in polygons 1 (red) and 2 (blue). Coordinates are in Mercator, see real coordinates on GEBCO_08 maps for the corresponding polygon.
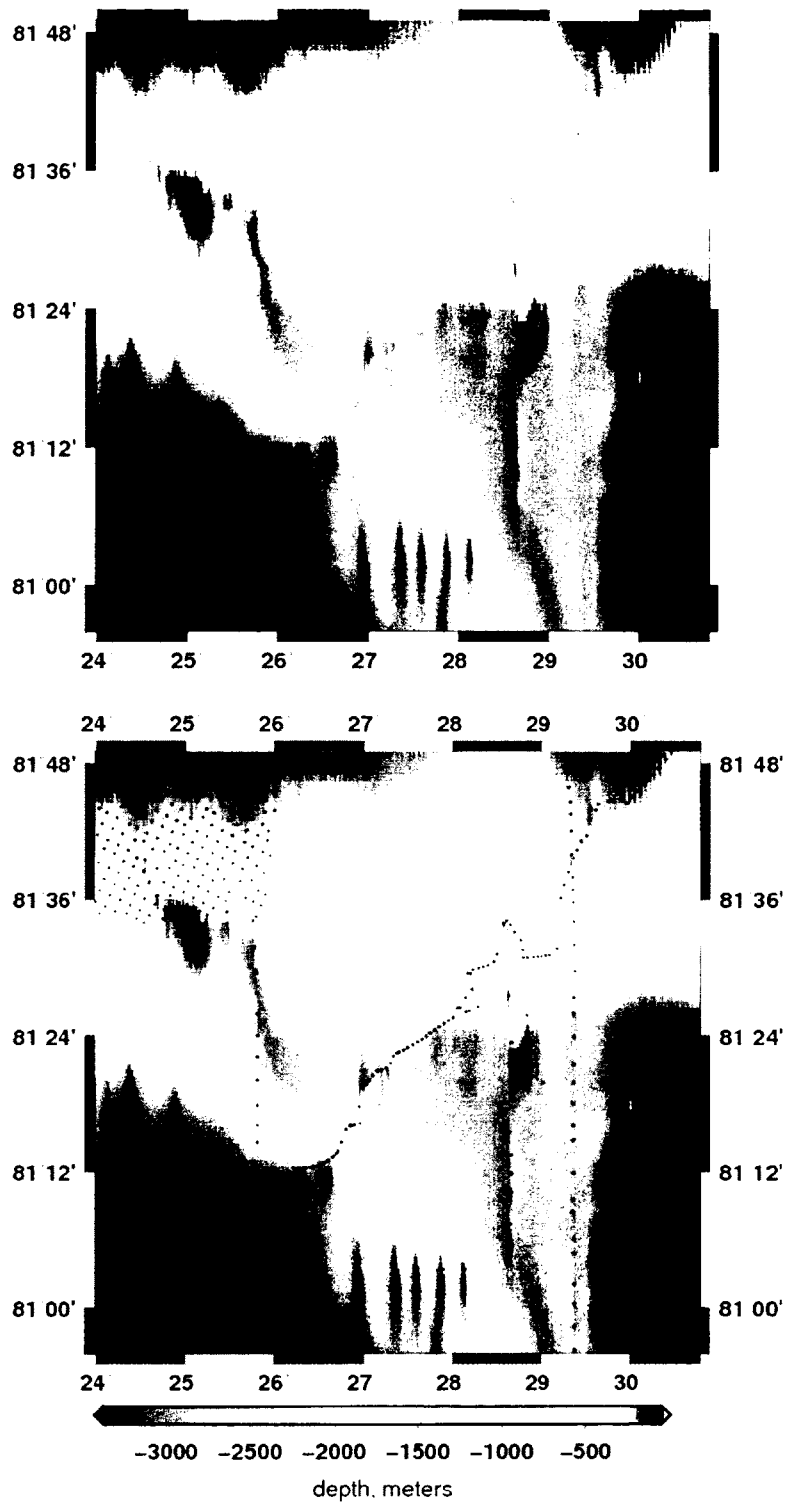
Figure C.8: Bathymetry of S&S overlain by source tracklines and location of GIN RAS multibeam grid (bluescale layer) in polygons 1 (red) and 2 (blue). Coordinates are in Mercator, see real coordinates on GEBCO_08 maps for the corresponding polygon.
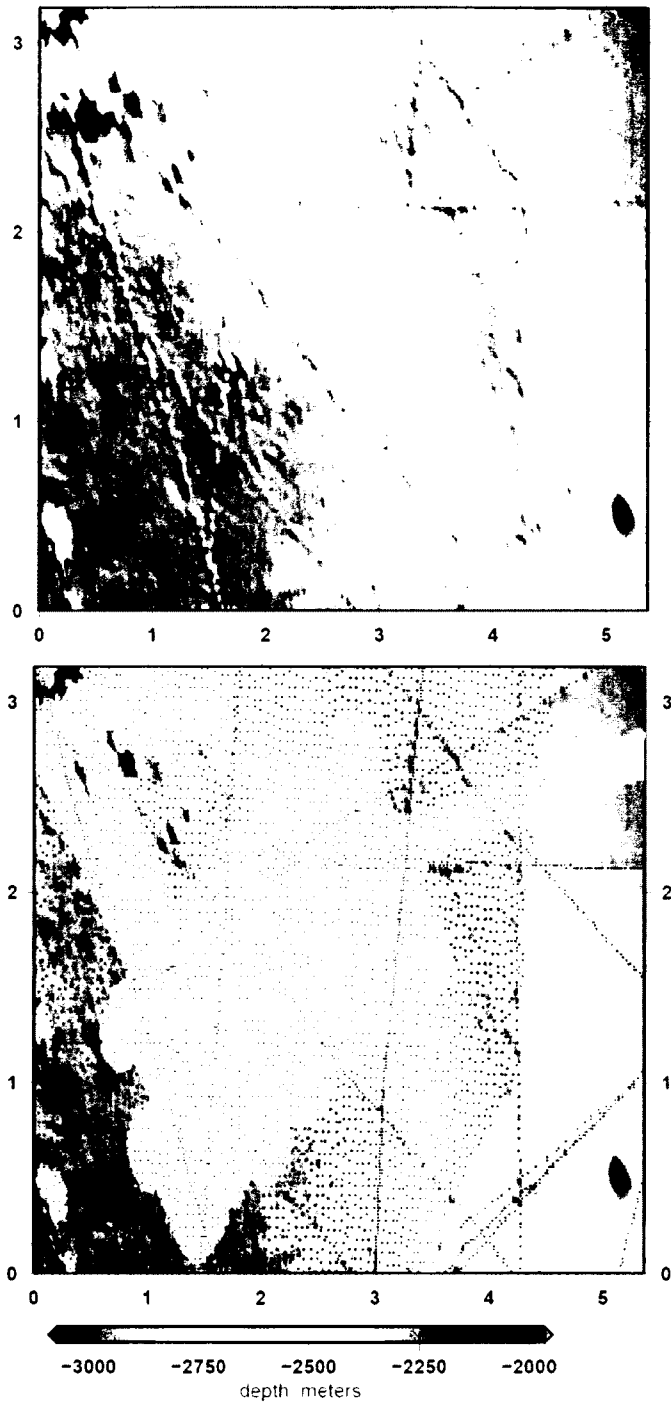
Figure C.9: Bathymetry of S&S overlain by source tracklines and location of GIN RAS multibeam grid (bluescale layer) in polygon 3. Coordinates are in Mercator, see real coordinates on GEBCO_08 maps for the corresponding polygon.

Figure C.10: Bathymetry of S&S overlain by source tracklines and location of GIN RAS multibeam grid (bluescale layer) in polygon 4. Coordinates are in Mercator, see real coordinates on GEBCO_08 maps for the corresponding polygon.

Figure C.11: Bathymetry of S&S overlain by source tracklines and location of GIN RAS multibeam grid (bluescale layer) in polygon 5. In the S&S grid location of source data is encoded as odd depth values. Usually the location of source data can be noticed in S&S bathymetry by "bumps" and "holes". As can be seen from the figure, some of the source data points are not encoded in the bathymetry. These are DNC (Digital Nautical Chart) data points provided by the National Geospatial-Intelligence Agency (NGA), the location of which is not allowed to be revealed due to NGA policy. The fact that source data coverage is not complete prevented the use of this polygon in analyses carried in sections 4.2.2 and 4.4. Coordinates are in Mercator, see real coordinates on GEBCO_08 maps for the corresponding polygon.

126

Figure C.12: Bathymetry of SRTM30_Plus overlain by source tracklines and location of the GIN RAS multibeam grid (bluescale layer) in polygon 6.

APPENDIX D

DIFFERENCE MAPS

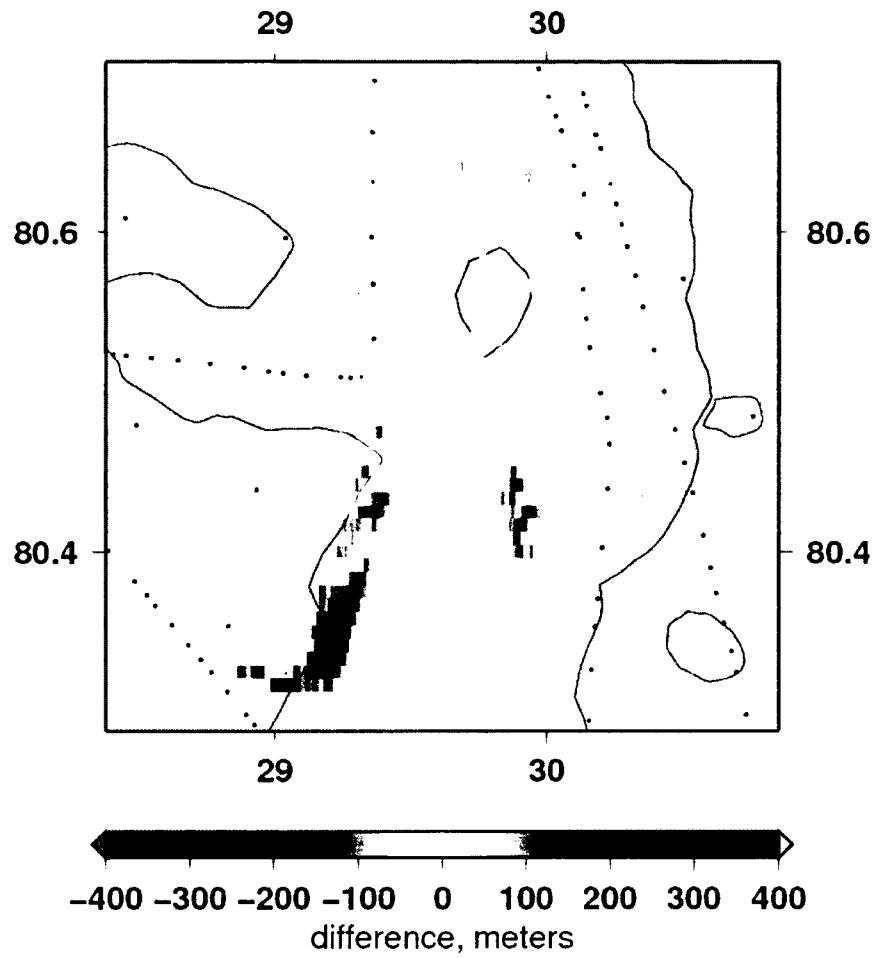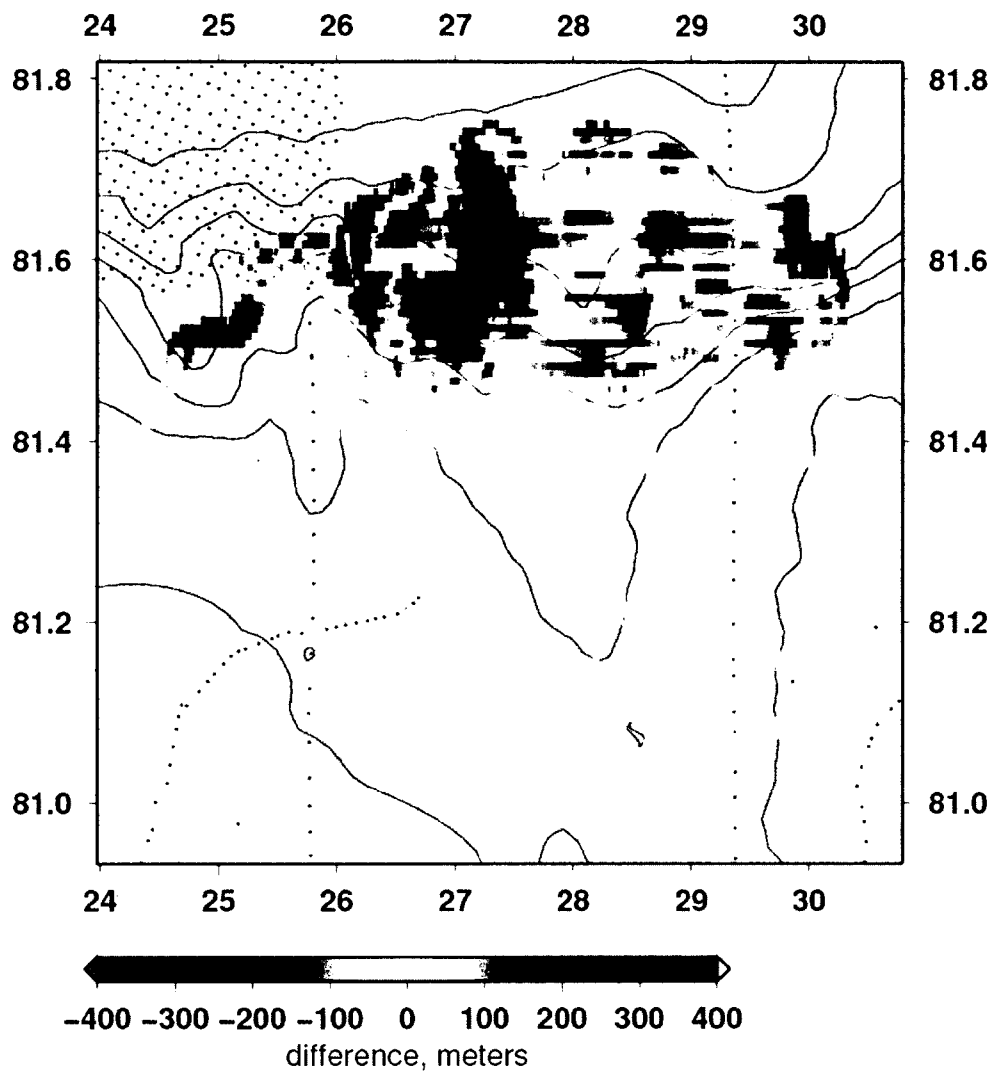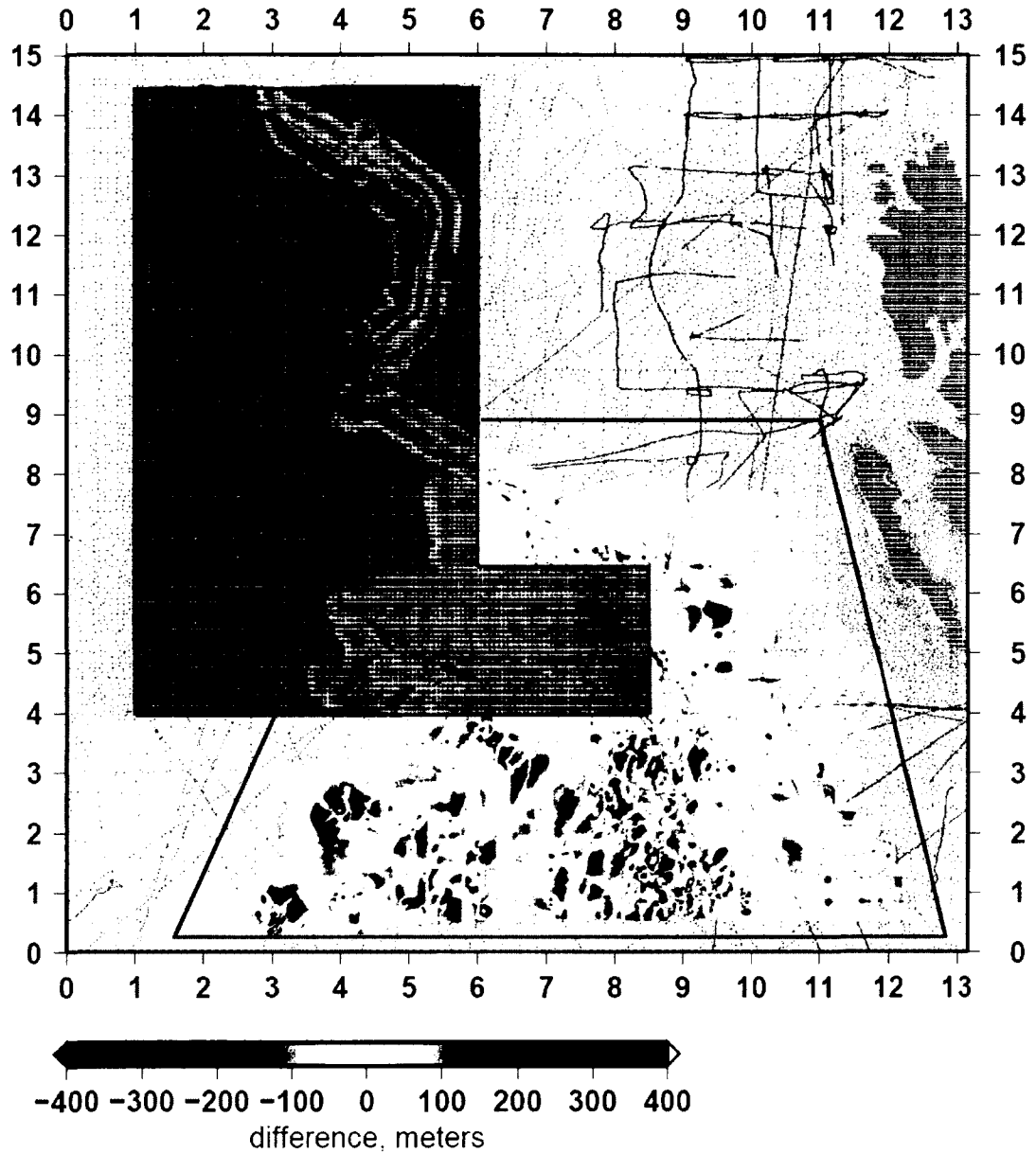### D.1 Difference maps between GEBCO_08 and GIN RAS multibeam
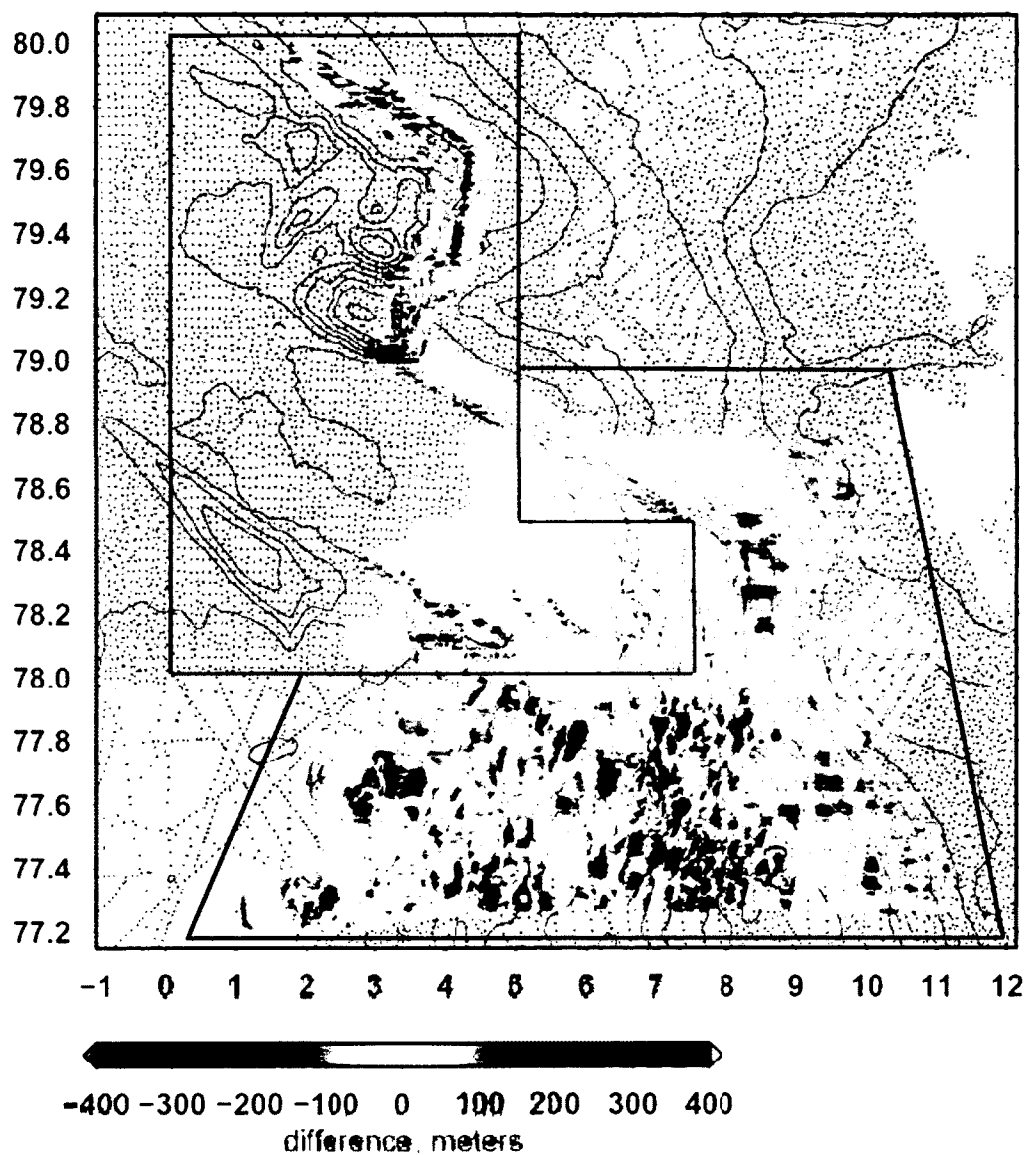
Figure D.1: Map of differences between GIN RAS multibeam grid and GEBCO_08 (GEBCO_08 values are subtracted from GIN RAS) overlain by source tracklines and GEBCO contours in polygons 1 (red) and 2 (blue).
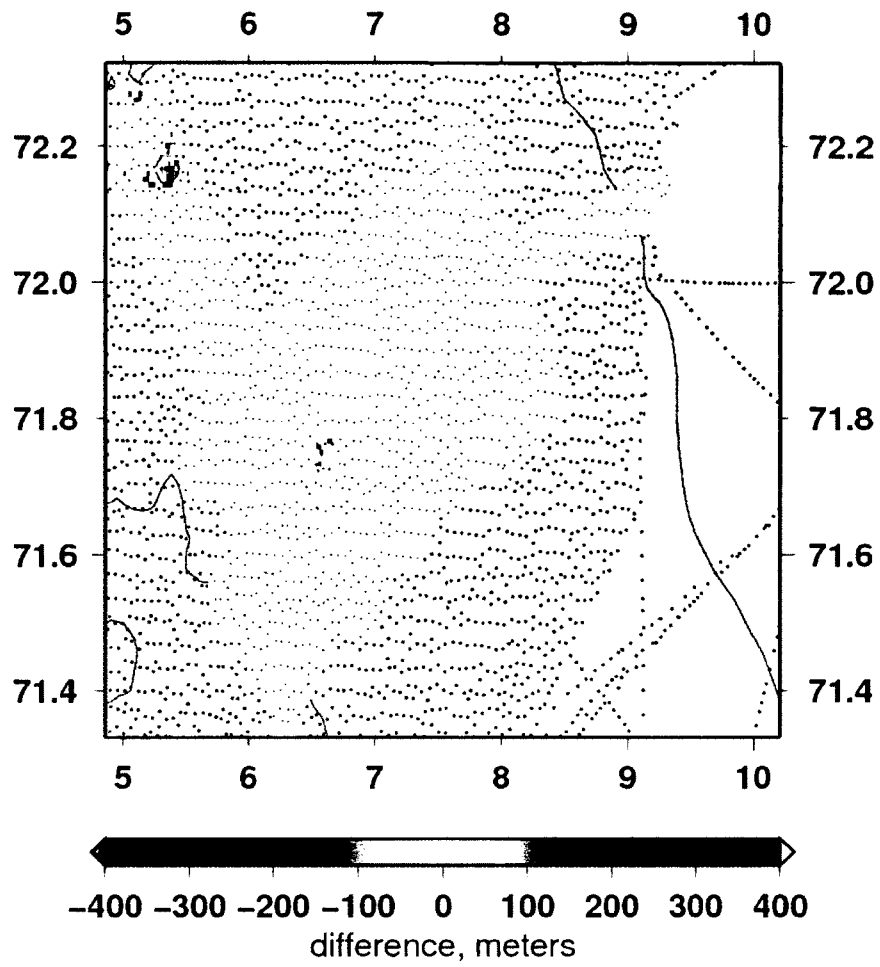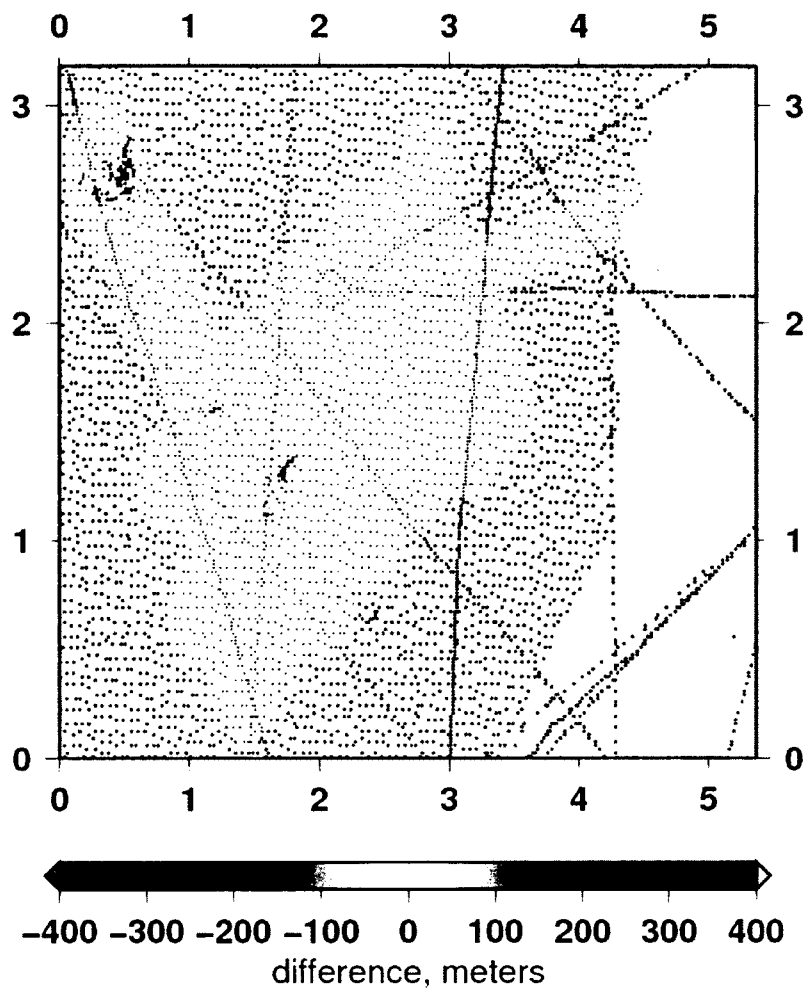
Figure D.2: Map of differences between GIN RAS multibeam grid and GEBCO_08 (GEBCO_08 values are subtracted from GIN RAS) overlain by source tracklines and GEBCO contours in polygon 3.
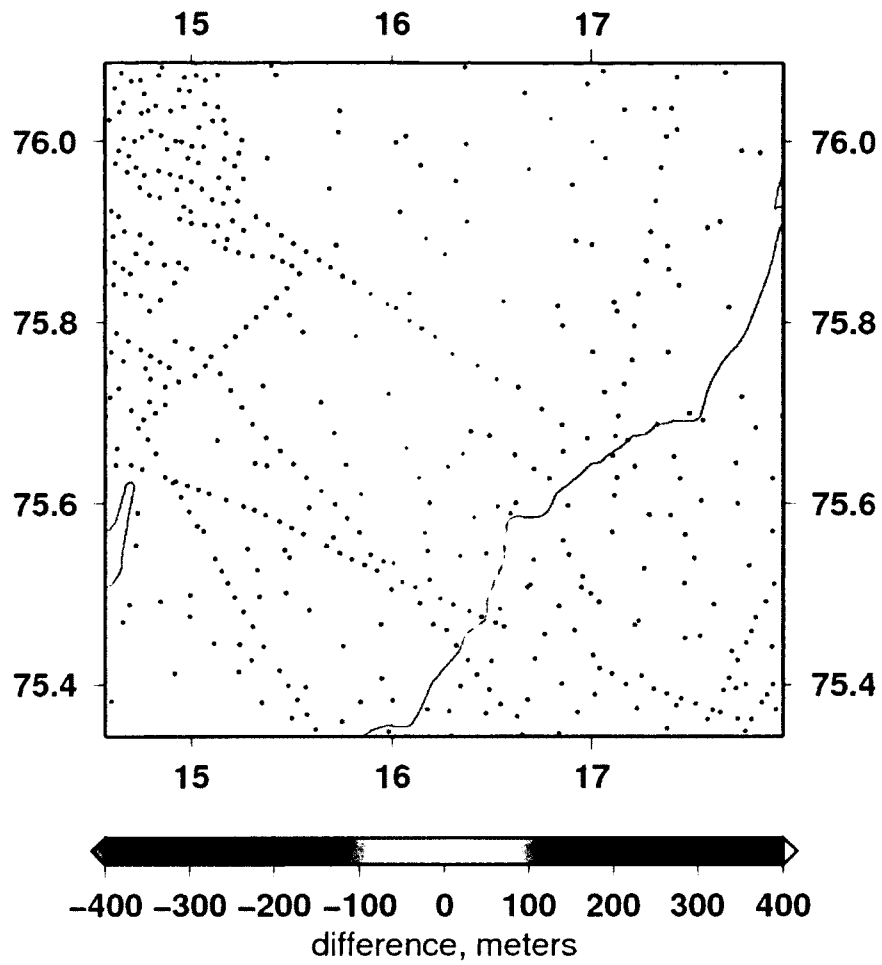
Figure D.3: Map of differences between GIN RAS multibeam grid and GEBCO_08 (GEBCO_08 values are subtracted from GIN RAS) overlain by source tracklines and GEBCO contours in polygon 4.

29 30

80.6 80.6

80.4 80.4

29 30

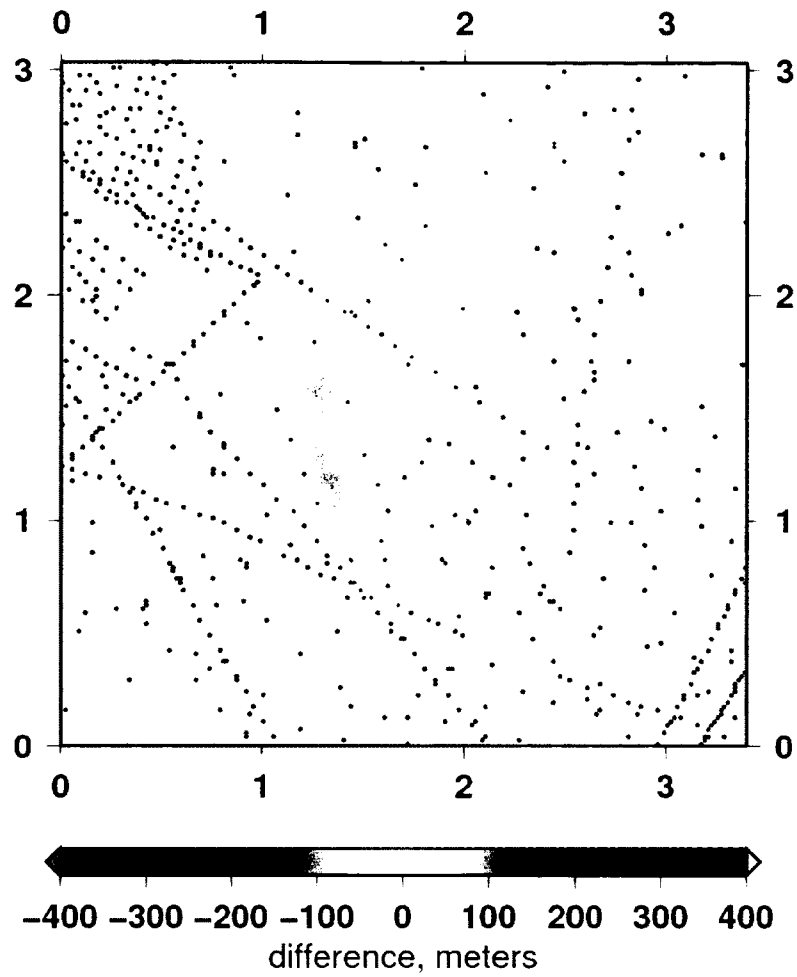-400 -300 -200 -100 0 100 200 300 400
difference, meters

Figure D.4: Map of differences between GIN RAS multibeam grid and GEBCO_08 (GEBCO_08 values are subtracted from GIN RAS) overlain by source tracklines and GEBCO contours in polygon 5.

Figure D.5: Map of differences between GIN RAS multibeam grid and GEBCO_08 (GEBCO_08 values are subtracted from GIN RAS) overlain by source tracklines and GEBCO contours in polygon 6.

D.2 Difference maps between S&S, SRTM30_Plus (polygon 6) and GIN
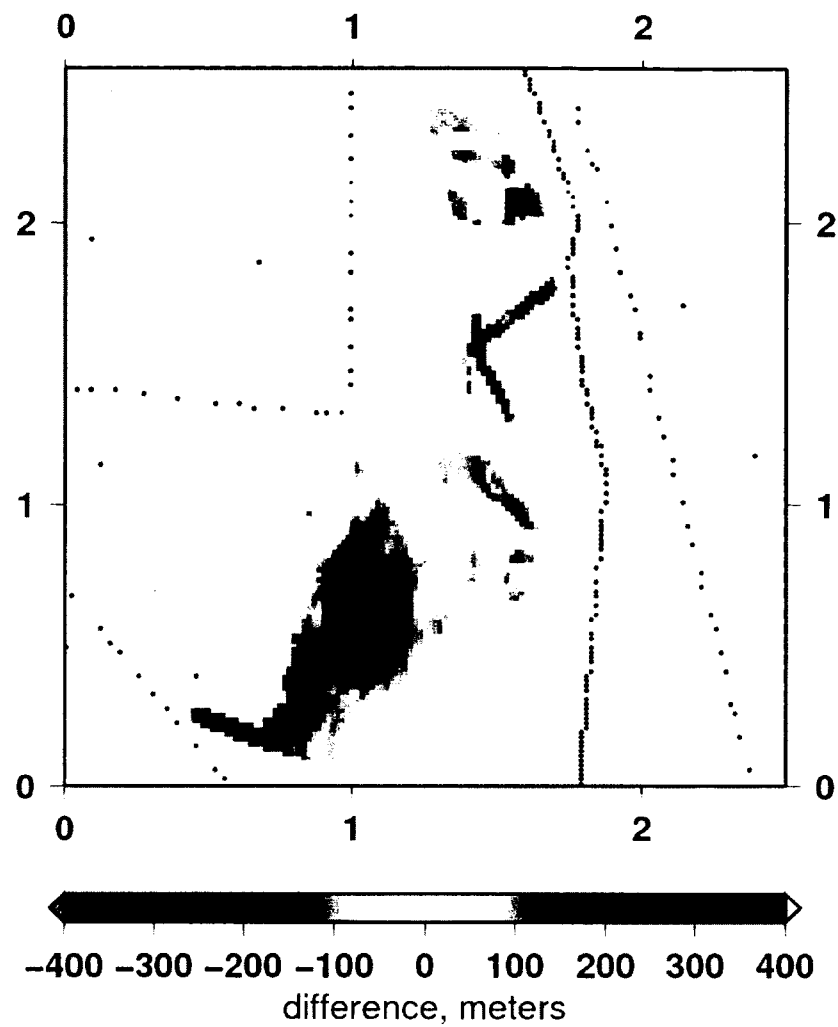
RAS multibeam grids

Figure D.6: Map of differences between GIN RAS multibeam grid and S&S (S&S values are subtracted from GIN RAS) overlain by source tracklines in polygons 1 (red) and 2 (blue). Coordinates are in Mercator, see real coordinates on GEBCO_08 maps for the corresponding polygon.

Figure D.7: Map of differences between GIN RAS multibeam grid and S&S (S&S values are subtracted from GIN RAS) overlain by source tracklines in polygon 3. Coordinates are in Mercator, see real coordinates on GEBCO_08 maps for the corresponding polygon.
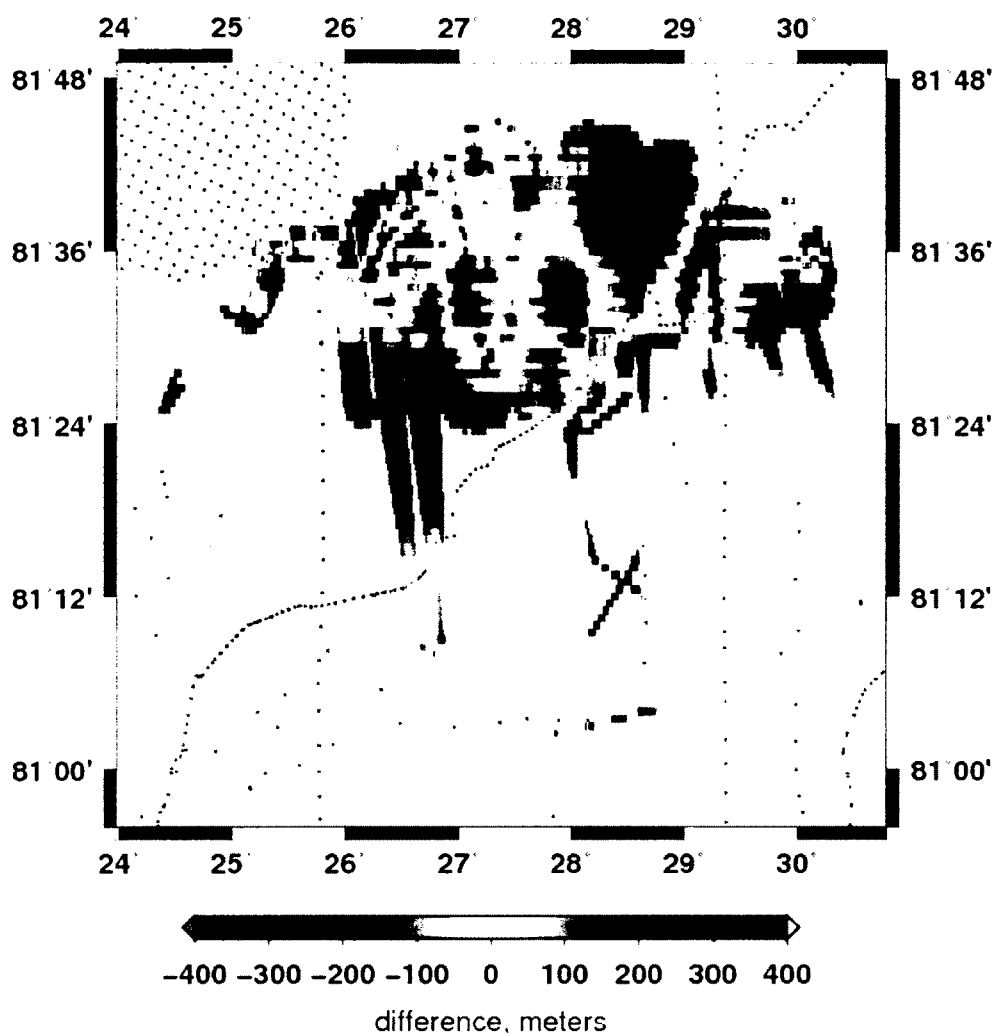
Figure D.8: Map of differences between GIN RAS multibeam grid and S&S (S&S values are subtracted from GIN RAS) overlain by source tracklines in polygon 4. Coordinates are in Mercator, see real coordinates on GEBCO_08 maps for the corresponding polygon.

Figure D.9: Map of differences between GIN RAS multibeam grid and S&S (S&S values are subtracted from GIN RAS) overlain by source tracklines in polygon 5. Coordinates are in Mercator, see real coordinates on GEBCO_08 maps for the corresponding polygon.

Figure D.10: Map of differences between GIN RAS multibeam grid and SRTM30_Plus (SRTM30_Plus values are subtracted from GIN RAS) overlain by source tracklines in polygon 6. S&S grid does not provide coverage north of 80°N.

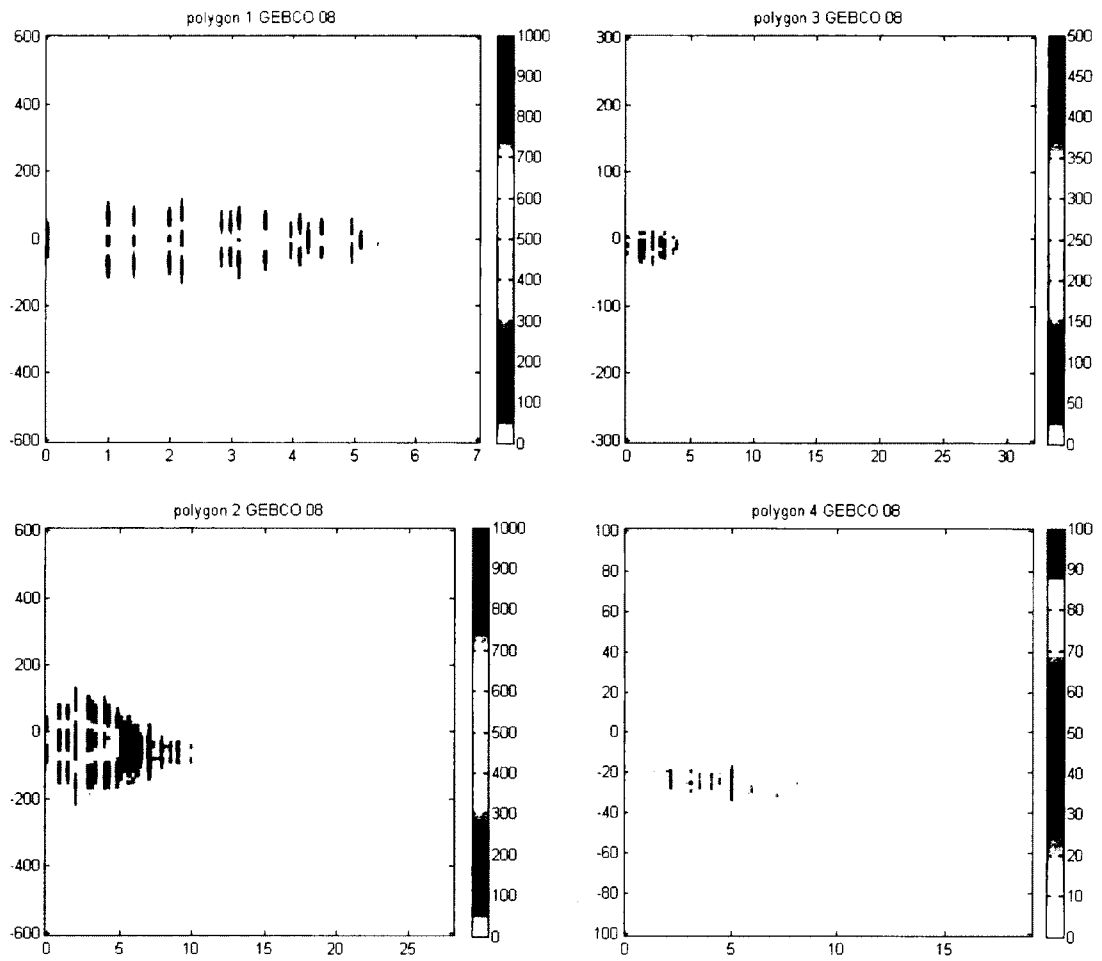# APPENDIX E

ADDITIONAL FIGURES

E.1 Interpolation accuracy
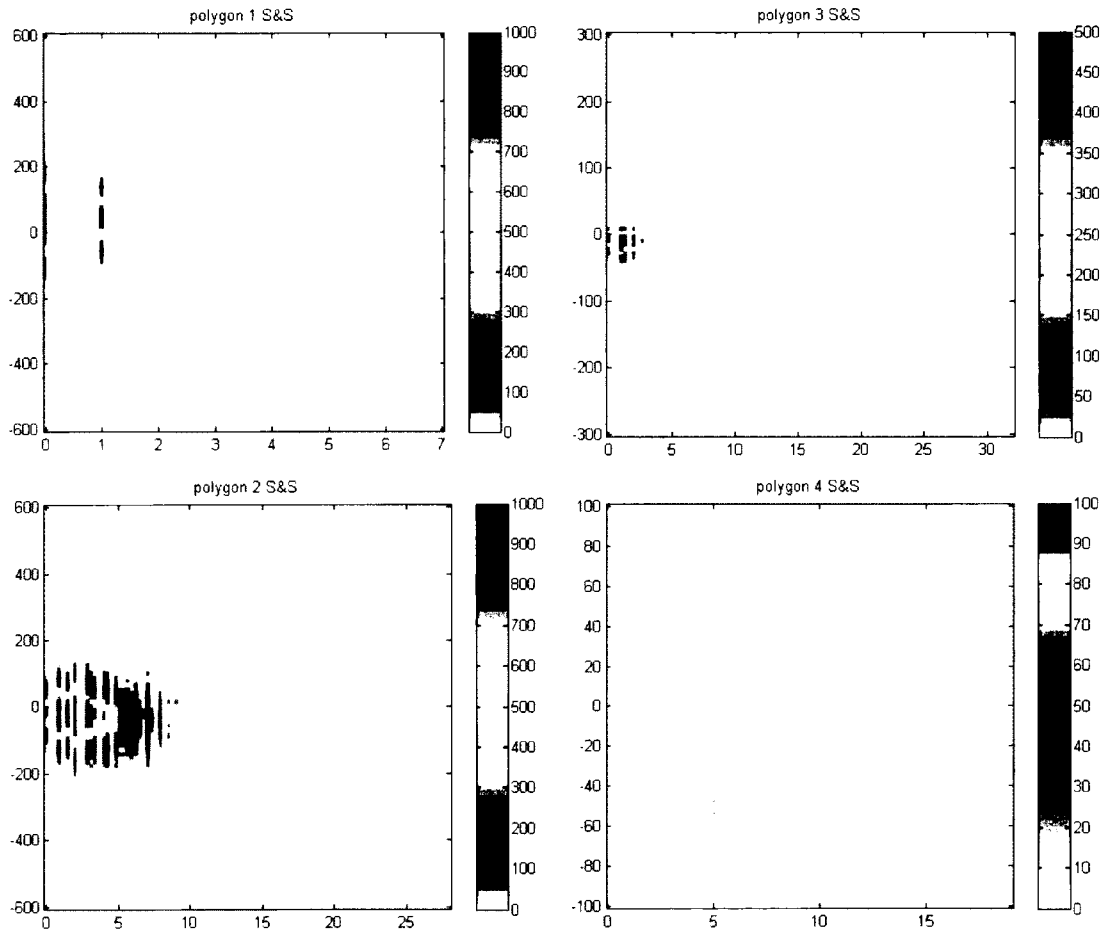
Figure E.1: Two-dimensional histogram of count of events (each axis divided into 100 by100 equal bins) of difference between S&S and GIN RAS multibeam grid values versus distance to nearest source data point (Figure 4-22) in polygons 1, 2, 3 and 4. Y axes: difference (meters), X axes: distance from source, in number of pixels. The observed gaps in the distribution of values in polygon 1 reflects the gaps in the data distribution.

Figure E.2: Two-dimensional histogram of count of events (each axes divided into 100 by100 equal bins) of difference between GEBCO_08 and GIN RAS multibeam grid values versus distance to nearest source data point (Figure 4-22) in polygons 1, 2, 3 and 4. Y axes: difference (meters), X axes: distance from source, in number of pixels. The observed gaps in the distribution of values in polygon 1 reflects the gaps in the data distribution.

E.2 Depth versus difference with GIN RAS multibeam grids plots
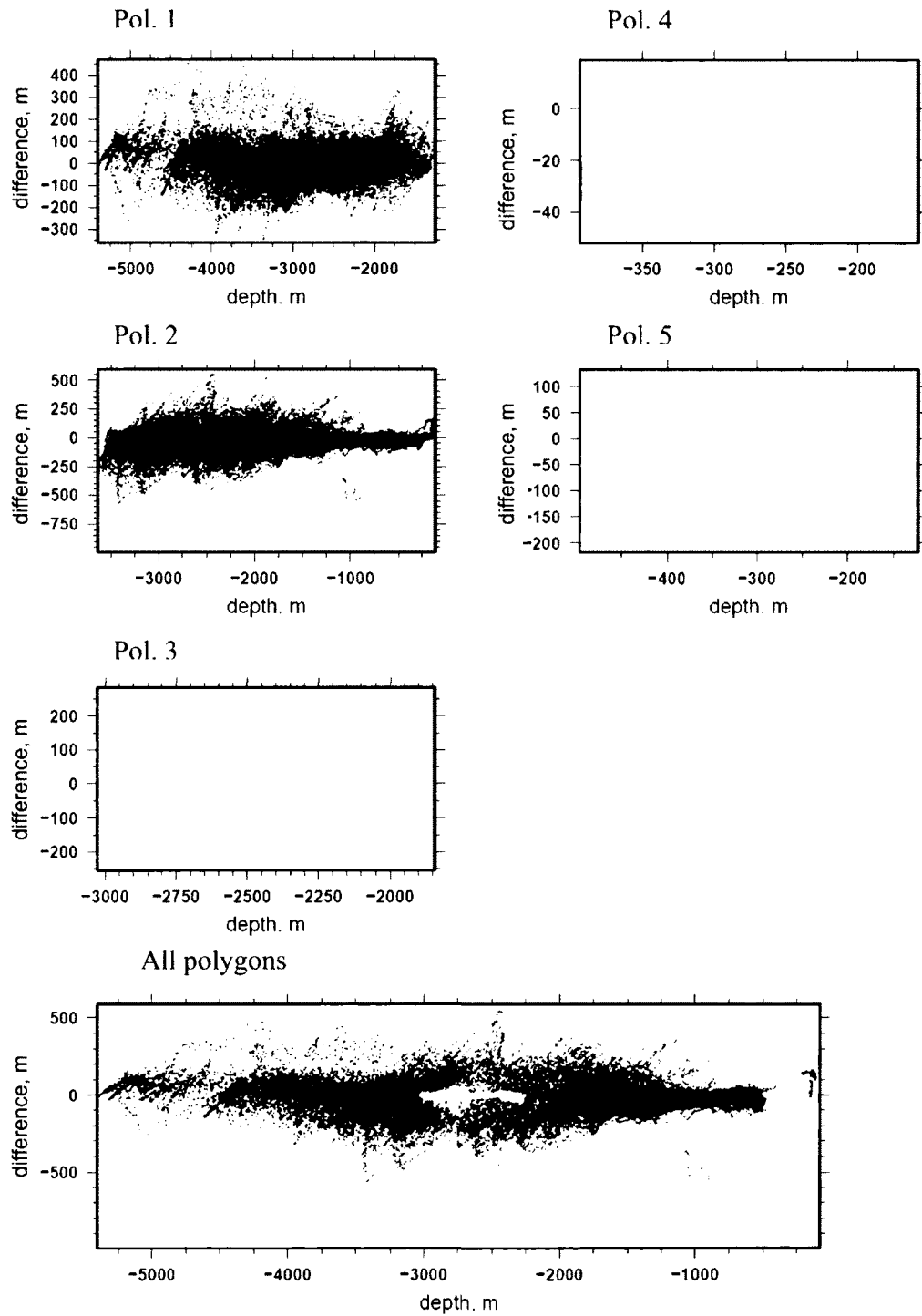
Figure E.3: Depth versus difference with GIN RAS multibeam grids and GEBCO_08 at the location of five polygons and graph for all polygons with data points colored by a polygon.
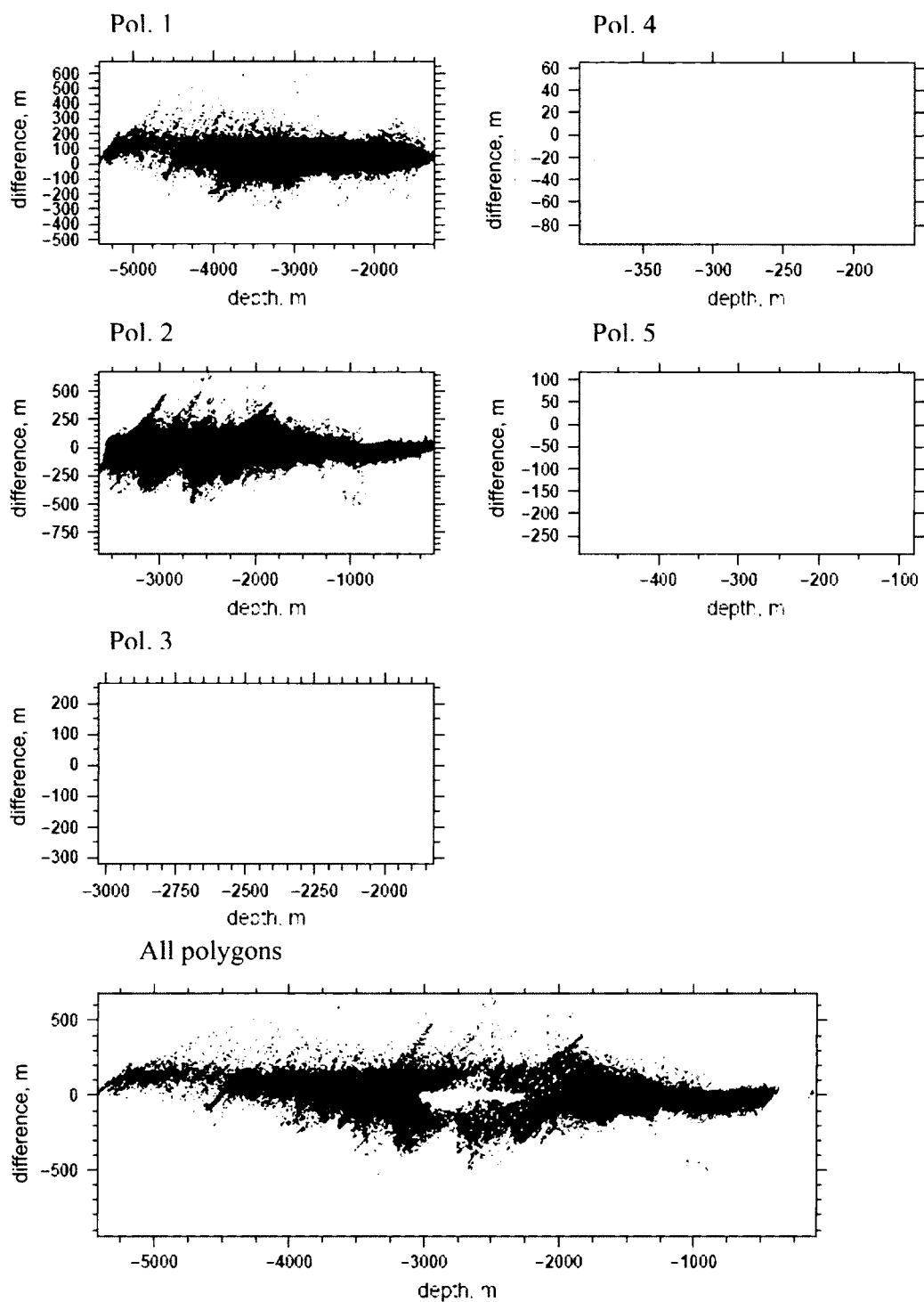
Figure E.4: Depth versus difference with GIN RAS multibeam grids and S&S at the location of five polygons, and graph for all polygons with data points colored by polygon.

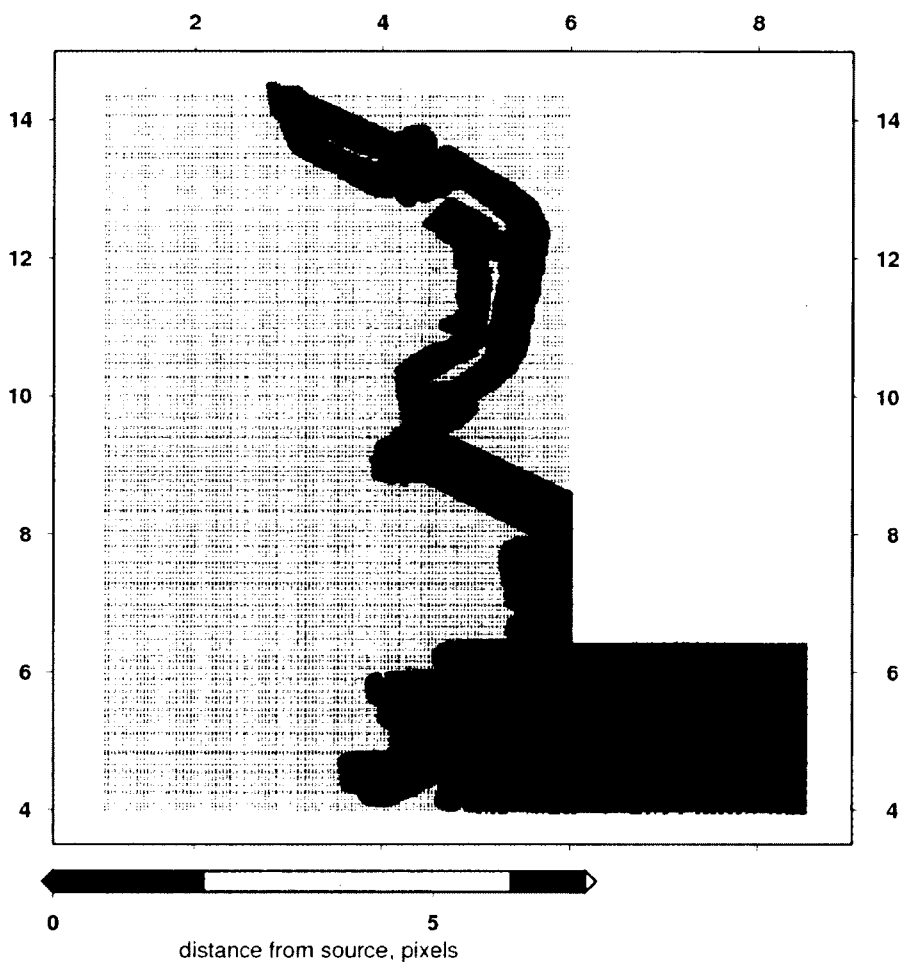# APPENDIX F

DISTANCE TO THE NEAREST SOURCE DATA POINT MAPS

F.1 Distance maps for S&S

distance from source, pixels

Figure F.1: Distance to the nearest source data point map for S&S in polygon 1. Distance is measured in pixels at the same resolution as the S&S grid (GMT spherical Mercator projection used). Source data is extracted from the S&S grid as odd values in bathymetry. Pixel size varies from polygon to polygon. The pixel size corresponds to approximately 0.34 x 0.34 km in the real world at 79.4°N (WGS84) (measured in ArcMap). Coordinates are in Mercator, see real coordinates on GEBCO_08 maps for the corresponding polygon.
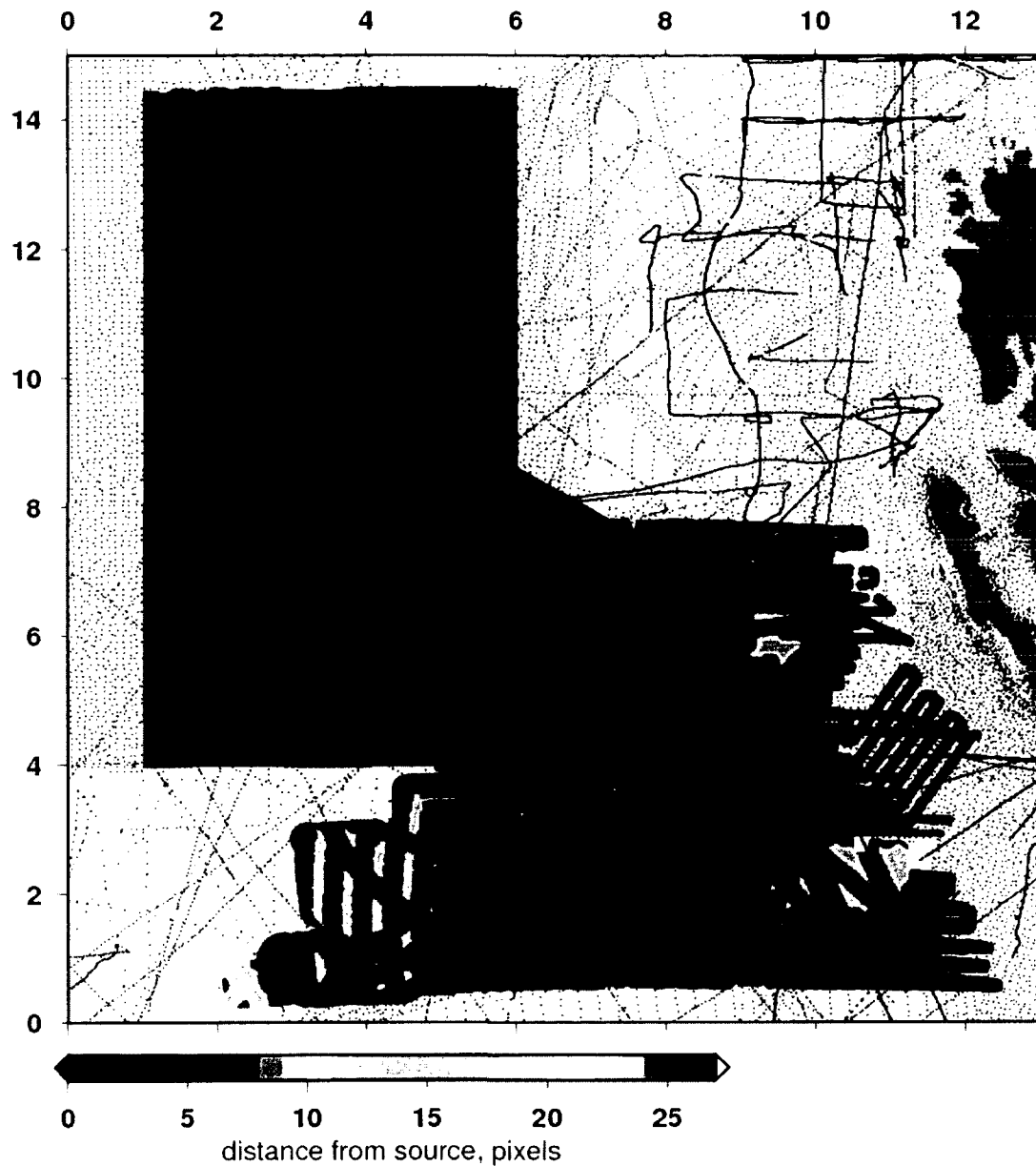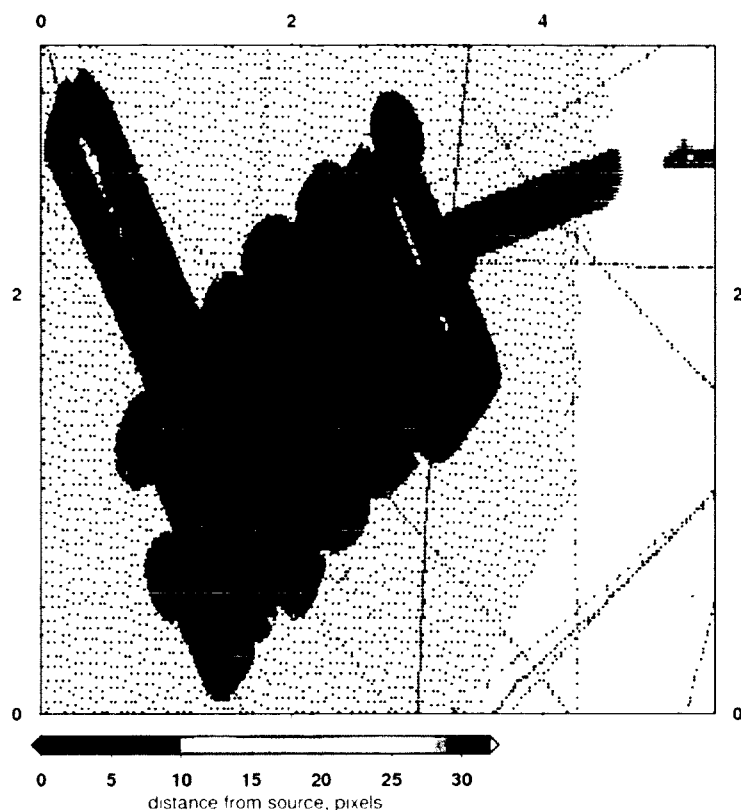
Figure F.2: Distance to the nearest source data point map for S&S in polygon 2. Distance is measured in pixels at the same resolution as the S&S grid (GMT spherical Mercator projection used). Source data is extracted from the S&S grid as odd values in bathymetry. Pixel size varies from polygon to polygon. The pixel size corresponds to approximately 0.34 x 0.34 km in the real world at 77.5°N (WGS84) (measured in ArcMap). Coordinates are in Mercator, see real coordinates on GEBCO_08 maps for the corresponding polygon.
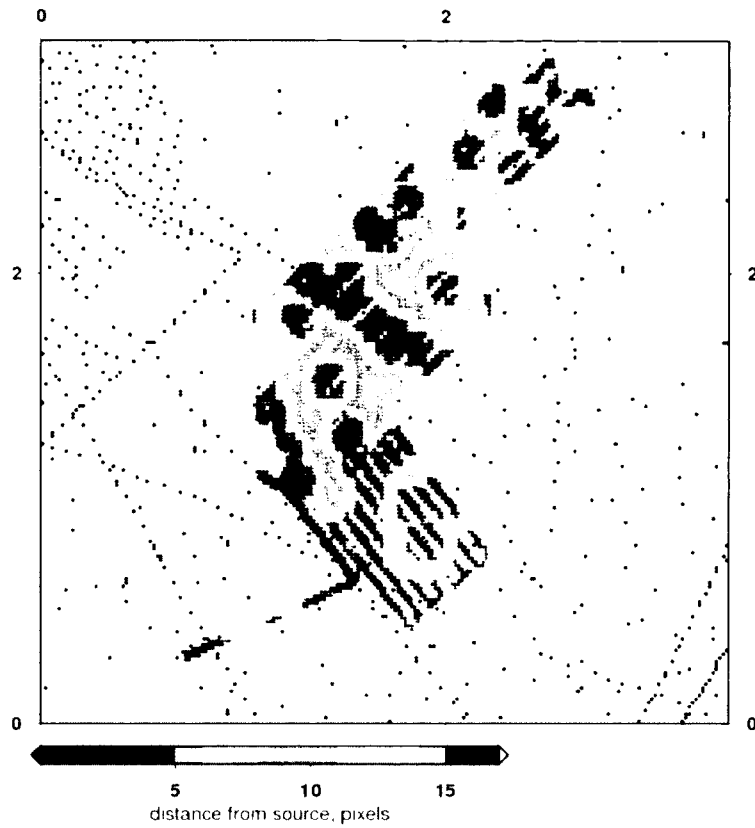
Figure F.3: Distance to the nearest source data point map for S&S in polygon 3. Distance is measured in pixels at the same resolution as the S&S grid (GMT spherical Mercator projection used). Source data is extracted from the S&S grid as odd values in bathymetry. Pixel size varies from polygon to polygon. The pixel size corresponds to approximately 0.57 x 0.57 km in the real world at 71.8°N (WGS84) (measured in ArcMap). Coordinates are in Mercator, see real coordinates on GEBCO_08 maps for the corresponding polygon.

Figure F.4: Distance to the nearest source data point map for S&S in polygon 4. Distance is measured in pixels at the same resolution as the S&S grid (GMT spherical Mercator projection used). Source data is extracted from the S&S grid as odd values in bathymetry. Pixel size varies from polygon to polygon. The pixel size corresponds to approximately 0.46 x 0.46 km in the real world at 75.7°N (WGS84) (measured in ArcMap). Coordinates are in Mercator, see real coordinates on GEBCO_08 maps for the corresponding polygon.
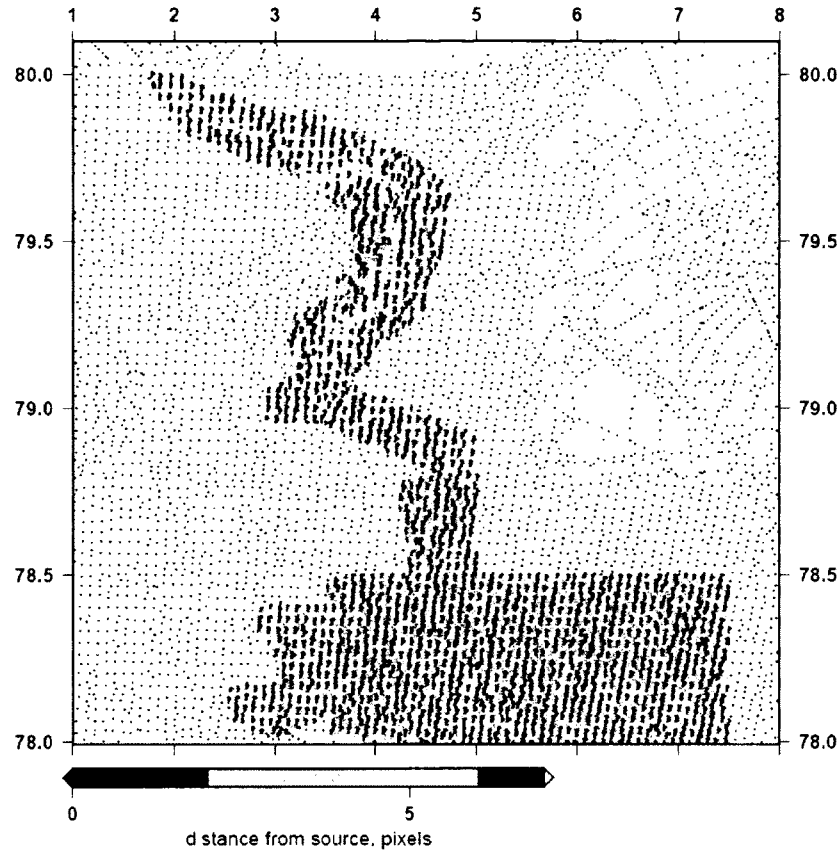
F.2 Distance maps for GEBCO_08

Figure F.5: Distance to the nearest source data point map for GEBCO_08 in polygon 1. Distance is measured in pixels at the same resolution as GEBCO_08 grid (geographic coordinate system). Source data was obtained from Dave Sandwell as IBCAO database used in the construction of SRTM30_Plus. Pixel size varies from polygon to polygon.
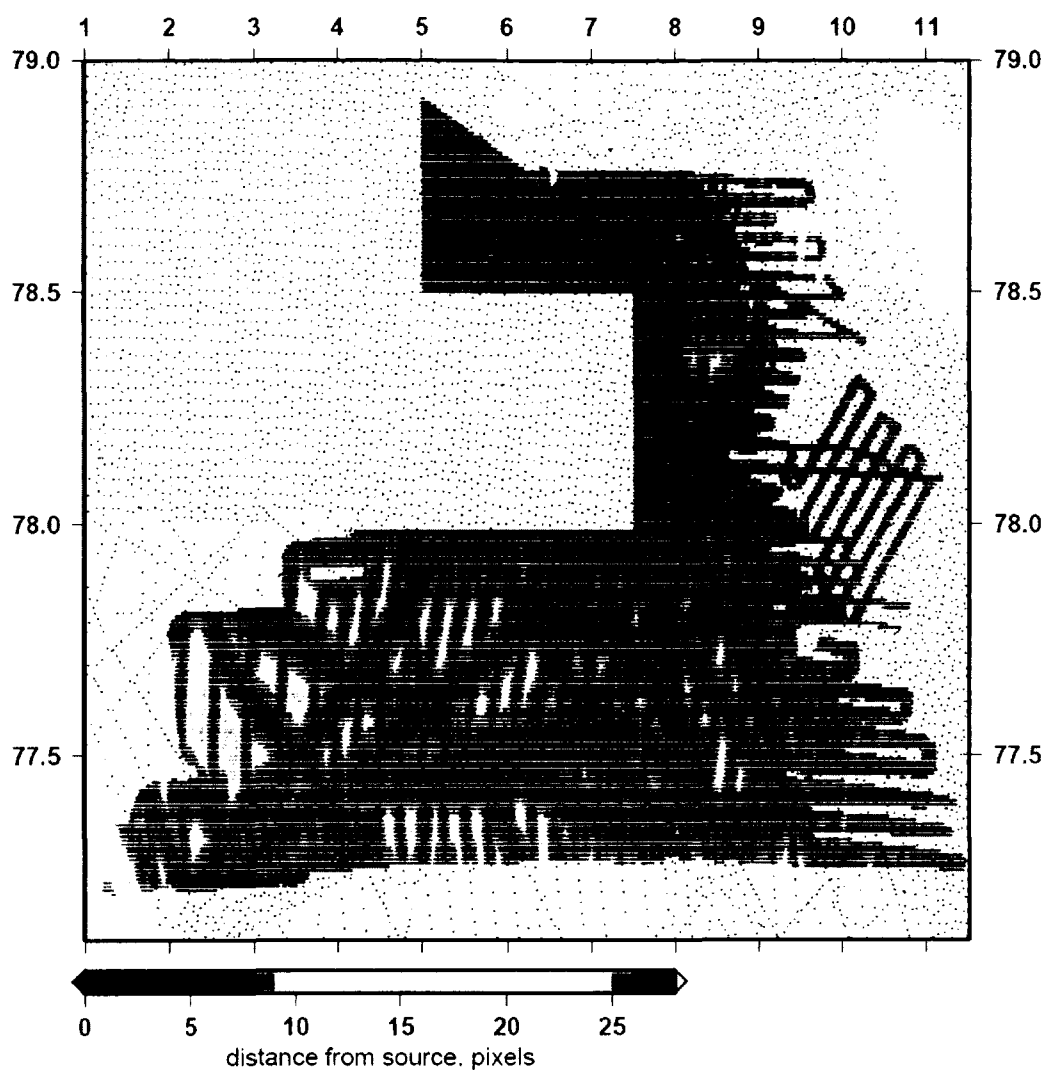
146

Figure F.6: Distance to the nearest source data point map for GEBCO_08 in polygon 2. Distance is measured in pixels at the same resolution as GEBCO_08 grid (geographic coordinate system). Source data was obtained from Dave Sandwell as IBCAO database used in the construction of SRTM30_Plus. Pixel size varies from polygon to polygon.
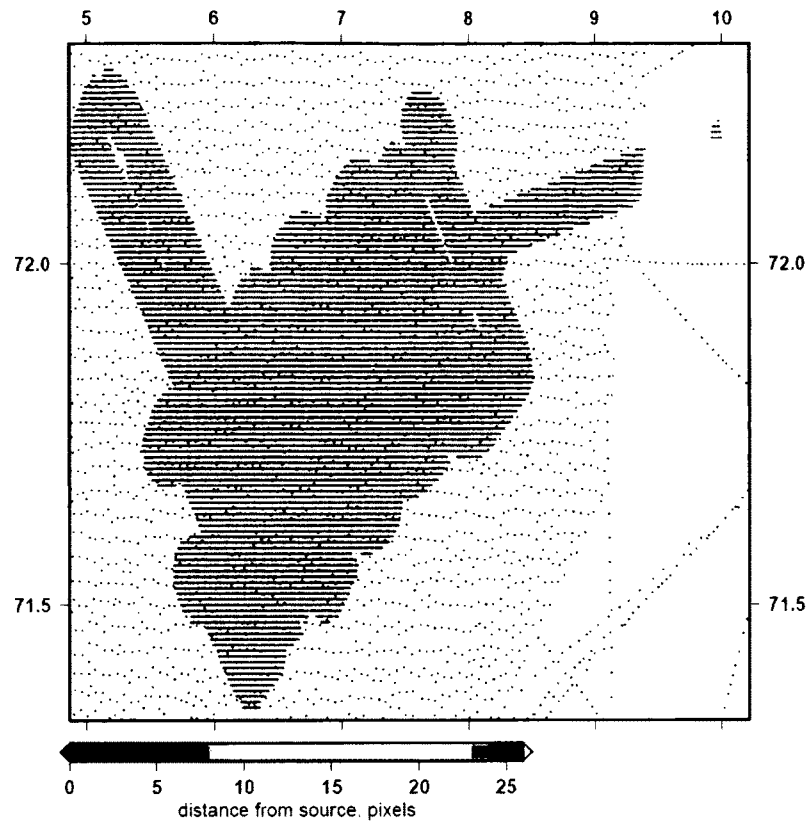
Figure F.7: Distance to the nearest source data point map for GEBCO_08 in polygon 3. Distance is measured in pixels at the same resolution as GEBCO_08 grid (geographic coordinate system). Source data was obtained from Dave Sandwell as IBCAO database used in the construction of SRTM30_Plus. Pixel size varies from polygon to polygon.
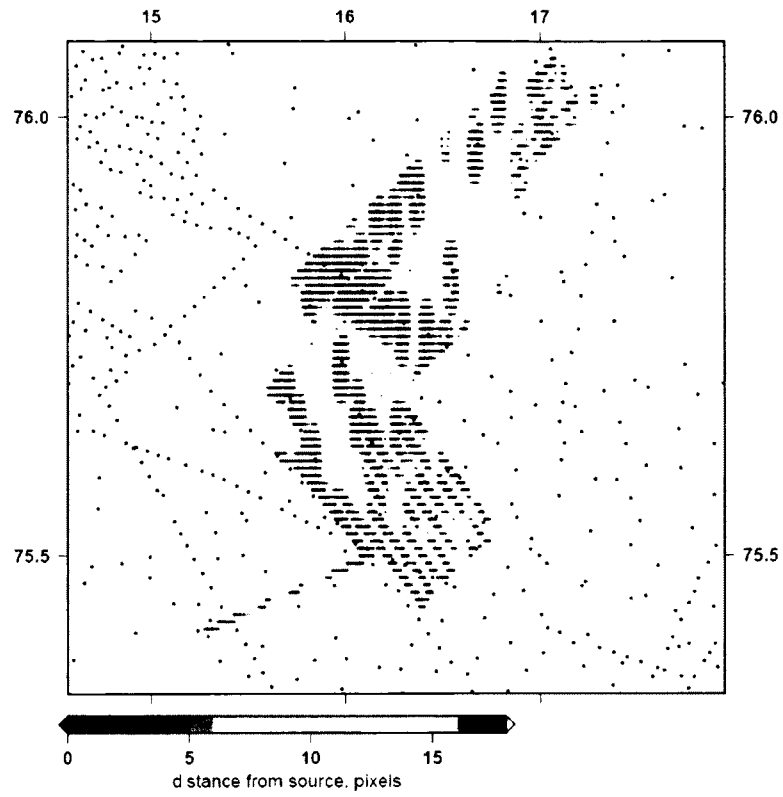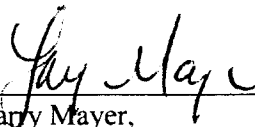
148

Figure F.8: Distance to the nearest source data point map for GEBCO_08 in polygon 4. Distance is measured in pixels at the same resolution as GEBCO_08 grid (geographic coordinate system). Source data was obtained from Dave Sandwell as IBCAO database used in the construction of SRTM30_Plus. Pixel size varies from polygon to polygon.
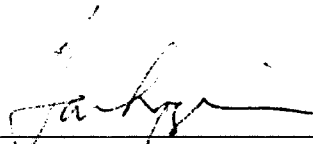
This thesis has been examined and approved.

Thesis Director, Dr. David Monahan,
Adjunct Professor of Geography and Geodesy and Geomatics
Engineering

Dr. Larry Mayer,
Professor of Ocean Engineering and Marine Sciences and Earth
Sciences

Dr. Thomas Lippmann,
Research Associate Professor of Earth Sciences and Ocean
Engineering

Dr. Brian Calder,
Research Associate Professor

07/04/12
Date